# TRACE ELEMENT MOBILITY IN LAYERED OIL SANDS MINE WASTES

A Thesis Submitted to the College of
Graduate and Postdoctoral Studies In
Partial Fulfillment of the
Requirements For the Degree of
Master of Science In the Department
of Geological Sciences
University of Saskatchewan
Saskatoon

By

LAWRENCE A. SWERHONE

## PERMISSION TO USE

In presenting this thesis in partial fulfillment of the requirements for a Postgraduate degree from the University of Saskatchewan, I agree that the Libraries of this University may make it freely available for inspection. I further agree that permission for copying of this thesis in any manner, in whole or in part, for scholarly purposes may be granted by the professor or professors who supervised my thesis work or, in their absence, by the Head of the Department or the Dean of the College in which my thesis work was done. It is understood that any copying or publication or use of this thesis or parts thereof for financial gain shall not be allowed without my written permission. It is also understood that due recognition shall be given to me and to the University of Saskatchewan in any scholarly use which may be made of any material in my thesis.

Requests for permission to copy or to make other uses of materials in this thesis/dissertation in whole or part should be addressed to:

Dean
College of Graduate and Postdoctoral Studies
University of Saskatchewan
116 Thorvaldson Building, 110 Science Place
Saskatoon, Saskatchewan S7N 5C9
Canada

Head of the Department of Geological Sciences
University of Saskatchewan
114 Science Place
Saskatoon, Saskatchewan S7N 5E2
Canada

## ABSTRACT

Potential closure systems consisting of oil sands tailings and upgrading by-products were studied at the Syncrude Mildred Lake Mine in Northern Alberta, Canada. This research aimed to identify the geochemical implications of storing several different mine wastes and by-products together in integrated closure systems, with a specific focus on the behaviour of trace elements in associated porewater. To imitate such systems, layered assemblages of petroleum coke, centrifuged fine tailings (CFT), tailings sand, and peat-mineral mix soil (reclamation material) were placed in large, hydraulically contained lysimeters. Three layering schemes were chosen for the study: one with a reclamation material/petroleum coke cover overlying CFT; one with only petroleum coke overlying CFT; and one with uncovered CFT overlying a tailings sand underdrain layer–each having a duplicate to allow comparisons between fully- and partially-saturated systems. The geochemical behavior of each closure system was monitored with porewater samples obtained by continuous coring and by pumping multi-level piezometers installed throughout the depth of each lysimeter. Field measurements indicated that porewaters were sub-alkaline (7.7 ± 0.29 pH) with elevated specific conductivity (4.9 ± 1.9 mS $cm^{-1}$). Oxidation-reduction potential typically decreased with depth, with fully-saturated systems exhibiting more reduced conditions than their partially-saturated duplicate. Porewater trace element compositions were dominated by Mo (220 ± 350 μg $L^{-1}$), V (110 ± 200 μg $L^{-1}$), As (59 ± 42 μg $L^{-1}$), Ni (7.8 ± 13 μg $L^{-1}$), and Se (4.5 ± 9.0 μg $L^{-1}$). Additional sequential extraction studies showed that porewater elevated in exchangeable cations and inorganic anions produced during the dewatering of CFT could influence the release of trace elements bound to petroleum coke and associated mineral surfaces. The results of this study indicate that the dual-cover closure systems reduced trace element mobility at surface when compared with the single-cover systems, and that coke units in partially-saturated systems can accommodate dewatering of CFT within their pore space and reduce transport of trace elements to surface.

## ACKNOWLEDGEMENTS

I would first like to acknowledge the support and guidance provided by my supervisor Dr. Matt Lindsay throughout the completion of this thesis. Many thanks for your patience through the extended timeline of this project, and for providing both academic and professional development opportunities throughout my time with your group. Thank you to my committee member, Dr. Camille Partin, and my external examiner, Dr. Terry Fonstad, for taking the time to review my thesis and provide comments.

My eternal gratitude to the entire Lindsay lab group, to Jake Nesbitt for providing petroleum coke knowledge, to Mattea Cowell, Noel Galischuk, and Sarah Rudderham for support in the lab and field, and most importantly to Carlo Cilia for working through the entire lysimeter project with me and becoming a very good friend. I would also like to acknowledge the support of the Lindsay lab duck hunting committee, Daniel Francis, James Shulte, and Colton Vessey. Thank you to University of Saskatchewan staff Fina Nelson and Jing Chen for completion of porewater analyses, Tom Bonli for assistance with x-ray diffraction, and Erin Schmeling for completing both surface area and isotope analyses.

Thank you to the Syncrude staff, Jessica Pearcy, Wendy Kline, Janna Lutz, Richard Chao, Lori Cyprien, Mohamed Salem, and the rest of the RCR group for administrative support in the field and lab. Further thanks to the deep cake facility area field leads Kevin Boyer and Kelly Malo for ensuring safe working conditions around the lysimeter field site. My gratitude to the ConeTec staff for their support during the lysimeter coring campaign. Honourable mention to Sweet Basil in Fort McMurray; I recommend the #11.

Many thanks to my family for the support, especially to my Father for his input on electrochemistry. Finally, a special thank you to Alyse for her love and valued input throughout the completion of this thesis.

Funding for this research was provided by Syncrude Canada Limited and the Natural Sciences and Engineering Council of Canada (NSERC) through the NSERC/Syncrude Industrial Research Chair in Mine Closure Geochemistry (Grant No. IRCPJ-463568-13).

## TABLE OF CONTENTS

## LIST OF TABLES

## LIST OF FIGURES

## LIST OF ABBREVIATIONS

| | |
|---|---|
| AER | Alberta Energy Regulator |
| AOSR | Athabasca Oil Sands Region |
| CFT | centrifuged fine tailings |
| EC | electrical conductivity |
| FFT | fluid fine tailings |
| IC | ion chromatography |
| ICP-MS | inductively coupled plasma mass spectrometry |
| ICP-OES | inductively coupled plasma optical emission spectrometry |
| L1 | Lysimeter 1; partially-saturated dual-cover system |
| L2 | Lysimeter 2; partially-saturated single-cover system |
| L3 | Lysimeter 3; partially-saturated uncovered system |
| L4 | Lysimeter 4; fully-saturated dual-cover system |
| L5 | Lysimeter 5; fully-saturated single-cover system |
| L6 | Lysimeter 6; fully-saturated uncovered system |
| LEL | local evaporation line |
| LMWL | local meteoric water line |
| MFT | mature fine tailings |
| NA | naphthenic acid |
| OSPW | oil sands process-affected water |
| $pH_{pzc}$ | pH point of zero charge |
| PVC | polyvinyl chloride |
| SCL | Syncrude Limited |
| SMA | surface mineable area |
| SMP | soil matric potential |
| TDR | time-domain reflectometer |
| v/v | volume per volume (as percent) |
| w/w | weight per weight (as percent) |

# CHAPTER 1: INTRODUCTION

## 1.1 Alberta Oil Sands

The Alberta Oil Sands represents the third largest oil deposit in the world, behind Venezuela and Saudi Arabia, with total initial in-place bitumen reserves estimated at 293.1 billion $m^3$ (Alberta Energy Regulator [AER], 2015). Located in northern Alberta, these deposits are subdivided into 3 distinct regions: The Athabasca oil sands region (AOSR); Cold Lake oil sands region; and Peace River oil sands region (Figure 1-1). Bitumen present in the Cold Lake and Peace River oil sands regions and many areas of the AOSR must be extracted in situ, utilizing conventional and unconventional recovery techniques. However, deposits in some areas of the AOSR reach sufficiently close to surface (<65 meters) to allow for open pit mining (AER, 2015). This surface mineable area (SMA) comprises just over 3% (4800 $km^2$) of the total Alberta Oil Sands footprint, yet as of 2014 surface mining accounted for more than 45% of total daily crude bitumen production in Alberta (AER, 2015). With remaining proven crude bitumen reserves totaling 5.16 billion $m^3$ as of 2014 and production reaching over 164,000 $m^3$ per day as of this same year (AER, 2015), extraction and production operations in the SMA are some of the largest in the world. Production on this scale creates huge volumes of waste, including tailings and upgrading by-products, with roughly five cubic meters of these materials being produced per cubic meter of synthetic crude oil (Luna Wolter & Naeth, 2014). Predicted increase in bitumen production rates (AER, 2015) and new governmental regulations calling for more stringent reclamation timelines (Government of Alberta, 2015) establish mine site closure and the storage of mining wastes as a significant upcoming issue.

## 1.2 Bitumen Extraction

Oil sands consist of unconsolidated deposits containing bitumen, inorganic materials, and water. Surface mineable bitumen in the AOSR is hosted in the Wabiskaw-McMurray deposit, consisting of marine and estuarine clays and sands (Osacky et al., 2013) deposited during the Cretaceous period (145.5–65.5 Ma). This deposit outcrops on the Athabasca River north of Fort McMurray, Alberta and is overlain by Manville group, Quaternary soil, and glacial till units (Hein

et al., 2007). Average ore recovered from the Wabiskaw-McMurray deposit contains 12% bitumen, 3–6% water, and has an 84–86% mineral content by weight (Chalaturnyk et al., 2002). Mineral content is typically dominated by quartz, but also contains considerable amounts of clays present in discontinuous beds and within the water film surrounding the quartz particle surface (Chalaturnyk et al., 2002; Osacky et al., 2013). The clay fraction in this formation includes kaolinite (40–70% [w/w]), illite (28–45% [w/w]) and montmorillonite (1–15% [w/w]; Chalaturnyk et al., 2002). Average ore thickness in the SMA of the AOSR is reported as 25.9 meters, with overburden thickness generally ranging from 25 to 65 meters (Hein et al., 2007; AER, 2015). Large ore and relatively thin overburden thickness make deposits underlying the SMA economical to recover using large scale surface mining techniques.

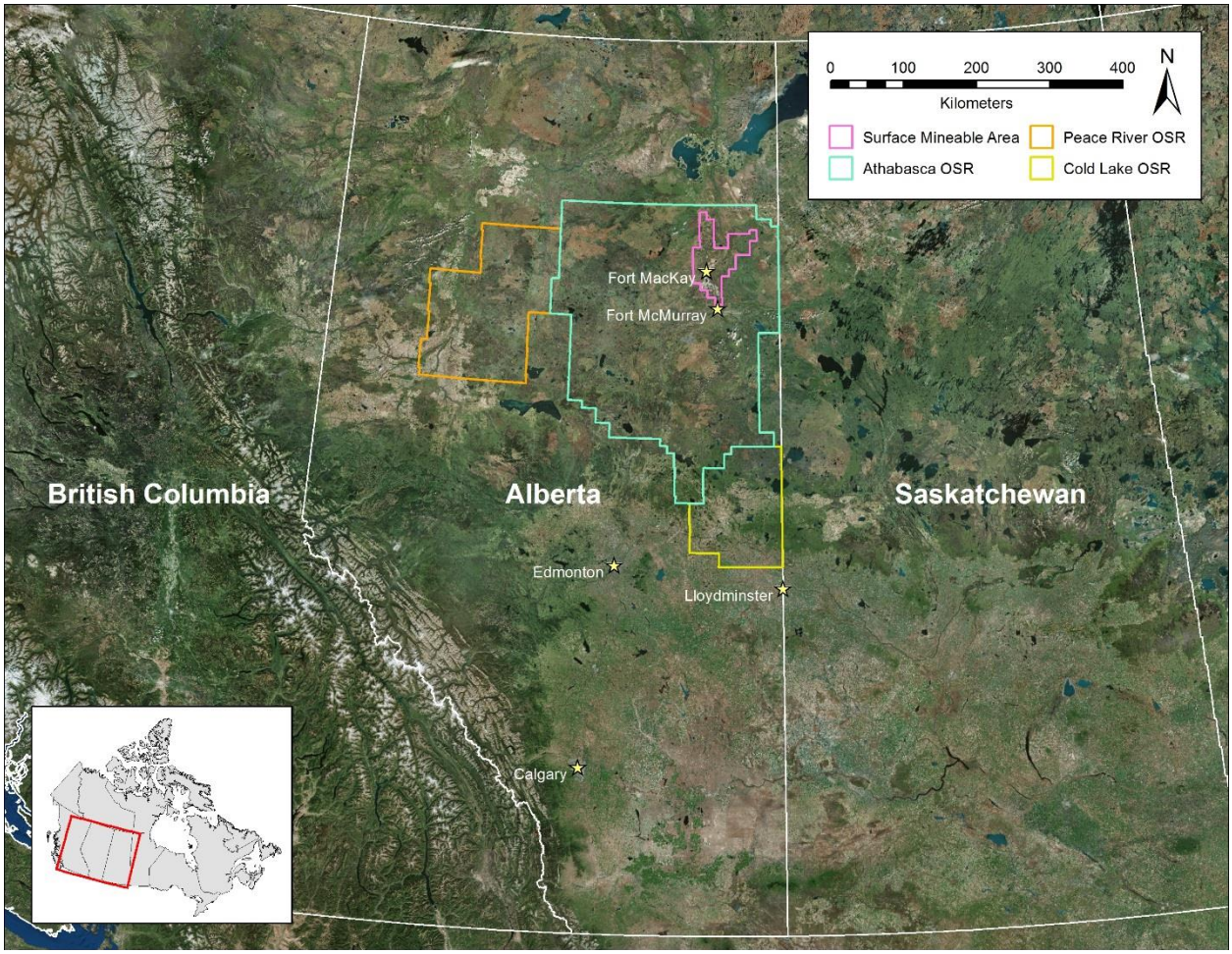


Figure 1-1: Map of the Alberta Oil Sands regions delineated by township. Alberta Energy Regulator, Esri, DigitalGlobe, GeoEye, Earthstar Geographics, CNES/Airbus DS, USDA, USGS, AeroGRID, IGN, and the GIS User Community.

Mining in the AOSR takes place in open pits where overburden material is stripped from the land surface and bitumen ore is extracted and transported using large power shovels and dump trucks. Recovered bitumen ore is crushed and mixed with water to create a slurry that is moved through hydro-transport pipelines and tumblers where size reduction of the ore takes place, improving transportability (Masliyah et al., 2004). This slurry is then transported to facilities where bitumen extraction begins.

Bitumen is a high-molecular weight, highly-viscous hydrocarbon found in the pore spaces of oil sands ore (Chalaturnyk et al., 2002; Masliyah et al., 2004; Liu et al., 2005). To extract bitumen from the ore, the bond holding bitumen to the sands and clays must be broken. In the AOSR this is accomplished using a caustic (NaOH) hot water method based on the Clark Hot Water Process. High water temperatures (~85°C) are maintained and controlled throughout this process through varying inputs of steam and act to decrease bitumen viscosity (Chalaturnyk et al., 2002). Addition of NaOH to the bitumen ore slurry causes asphaltic acids present in the ore to become water soluble and act as surfactants, while the concomitant rise in pH (~8.5) reduces surface and interfacial tensions, resulting in ore structure disintegration and increased bitumen recovery (Chalaturnyk et al., 2002). Air introduced during transport binds with bitumen to form a froth that promotes floatation in large gravity separation vessels (Liu et al., 2005), leaving behind solids destined for tailings processing. Recovered froth normally contains approximately 60% bitumen, 30% water, and 10% solids by weight (Masliyah et al., 2004), however deaeration and addition of naptha can act to remove solids and further improve bitumen recovery (Masliyah et al., 2004; Liu et al. 2005). During froth treatment and solvent recovery two material streams are produced: (1) the tailings stream, which consists of coarse (sand), fine (clay and silt), and heavy (froth treatment) material sent to tailings facilities for water-solid separation; and (2) the processed bitumen stream, which is sent to upgrading facilities such as cokers. Overall bitumen recovery achieved during the extraction process ranges from 88–95% (Chalaturnyk et al., 2002; Masliyah et al., 2004; Liu et al., 2005).

### 1.3 Oil Sands Process-Affected Water

During the bitumen extraction process, water is withdrawn from nearby freshwater sources and on-site tailings ponds. In 2014, two major operators in the oil sands reported fresh water usage of 27.4 $Mm^3$ (Suncor) and 38.8 $Mm^3$ (Syncrude), or 1.60 and 2.55 $m^3$ per cubic meter of synthetic crude oil produced, respectively (Suncor Energy Inc., 2015; Syncrude Canada Ltd., 2015). Once

freshwater is used in the extraction process and has undergone solid-water separation it is termed oil sands process-affected water (OSPW; Allen, 2008; Gamal El-Din et al., 2011; Holden et al., 2011; Zubot et al., 2012; Abolfazlzadehdoshanbehbazari et al., 2013). To reduce freshwater consumption, oil sands operators in the AOSR recycle OSPW for re-use in the extraction process. In 2014, one operator used around 85% recycled water during the extraction process, or about 14.5 $m^3$ per cubic meter of synthetic crude oil produced (Syncrude Canada Ltd., 2015). This recycling of OSPW has allowed operators to stay below their licensed freshwater consumption limit (Suncor Energy Inc., 2015; Syncrude Canada Ltd., 2015). Long term continuous recycling, however, has led to a sustained increase of problem contaminant concentrations over time (Allen, 2008; Gamal El-Din et al., 2011; Holden et al., 2011; Zubot et al., 2012; Abolfazlzadehdoshanbehbazari et al., 2013). Oil sands process-affected water in oil sands tailings ponds typically contain elevated concentrations of sodium ($Na^+$), chloride ($Cl^-$), and bicarbonate ($HCO_3^-$; Allen, 2008; Holden et al., 2011; Zubot et al., 2012). Other constituents present in OSPW at elevated concentrations include sulfate ($SO_4^{2-}$), ammonia ($NH_3$), and naphthenic acids (NAs; Allen, 2008; Holden et al., 2011; Gamal El-Din et al., 2011; Zubot et al., 2012). Continuous increase of potential contaminants poses issues for the successful reclamation of mined areas in the AOSR; specifically, with respect to contaminant fate when integrating OSPW in closure landscapes.

### 1.4 Tailings

Bitumen extraction produces large volumes of tailings that must be stored on site due to zero-discharge policies followed by operators in the AOSR. Current estimates stand at 2.5 $m^3$ of tailings waste produced per cubic meter of synthetic crude oil (Luna Wolter & Naeth, 2014). As of 2013, approximately 975.6 million $m^3$ of tailings have accumulated in tailings ponds present in the AOSR, occupying a total area of 220 $km^2$ (AER, 2015). As a result, the accumulation of fluid tailings is a major problem facing operators. Factors that increase the settling rate of tailings are of great interest to operators, as increased consolidation will release larger quantities of process-affected water to be reused and increase reclamation timelines.

After the bitumen extraction process, tailings consist of 20–30% solids and around 3% bitumen by weight, suspended in alkaline OSPW (Chen et al., 2013). Following deposition into tailings ponds, coarse solids (>44 µm diameter) settle out quickly under the force of gravity, leaving dispersed fine solids (<44 µm diameter) in suspension (Mikula et al., 2009). This

suspension is allowed to dewater further under gravity, forming high water content tailings termed fluid fine tailings (FFT; Chen et al., 2013). Fluid fine tailings consists of dispersed clay, silt, and bitumen particles, typically around 10% (w/w) solids, suspended in the OSPW matrix (Holden et al., 2011; Siddique et al., 2014). The solids present in FFT gradually settle over several years until they reach 30–40% (w/w) solids, at which point they are termed mature fine tailings (MFT; Allen, 2008; Holden et al., 2011; Kasperski & Mikula, 2011; Proskin et al., 2012; Siddique et al., 2014). Mature fine tailings analyzed in a study by Siddique et al. (2014) contained an average of 75% water, 23.5% solids and 1.5% bitumen by weight. The solid particle size range in this same study consisted of 25.6% clay, 70.9% silt, and 3.5% fine sand (Siddique et al., 2014). Electrostatic interactions occurring at the fine particle surfaces within MFT cause this material to take anywhere from decades to centuries to consolidate to a density suitable for reclamation.

### *1.4.1 Centrifuged Fine Tailings*

In 2009 the AER established Directive 074, which set out requirements for the reduction of fluid tailings volumes and called for the formation of more trafficable tailings deposits (AER, 2015). This directive initiated a substantial amount of research that focused on the creation and implementation of a dry stackable tailings stream that could be incorporated into terrestrial reclamation landscapes. One technology used to increase tailings reclamation is the large-scale centrifugation of fine tailings, creating a more trafficable deposit termed centrifuged fine tailings (CFT). In this method, MFT is amended with gypsum ($CaSO_4 \bullet H_2O$) and anionic polyacrylamide and centrifuged at several times the force of gravity. This process has been shown to achieve a tailings product with a solids content of up to 70% (w/w) in laboratory-scale studies (Rima & Azam, 2015). Currently, very little is known about the geochemical behaviour of CFT, however recent studies suggest that water released from CFT contains elevated concentrations of $Na^+$, $Cl^-$, $HCO_3^-$, $SO_4^{2-}$, NAs, and hydrogen sulfide ($H_2S$; Heaton, 2015). Trace elements of concern elevated in these waters include arsenic (As), molybdenum (Mo), and selenium (Se; Heaton, 2015). A number of these constituents could pose problems when CFT is incorporated into reclamation landscapes, as they can have toxic effects on flora and fauna (Rogers et al., 2002; Anderson et al., 2011).

As of March 2015, Directive 074 has been suspended and replaced with the Lower Athabasca Region Tailings Management Framework (TMF) by the Government of Alberta (Government of Alberta, 2015). Similar to Directive 074, the TMF limits the volume of tailings

that can be accumulated and ensures that tailings ponds are progressively treated and reclaimed within 10 years of mine closure (Government of Alberta, 2015; AER, 2015; Syncrude Canada Ltd., 2015).

### 1.5 Petroleum Coke

Following extraction, the processed bitumen stream is piped to upgrading facilities on site where heavy hydrocarbons are refined to a lighter, more marketable crude material. In the AOSR upgrading is commonly carried out using either fluid, flexi-, or delayed coking methods. These coking processes involve the use of high temperatures (typically 350–550°C, dependent on the coking method) to break down long-chain hydrocarbons present in the heavy oil feed into shorter-chain hydrocarbons, producing petroleum coke as a by-product (Gray, 2015). Petroleum coke is commonly enriched in carbon (C; ~84%), sulfur (S; ~7%), metal oxides (~5%) and other minor elemental constituents (~4%; Zubot et al., 2012), with variability in chemical structure depending on the bitumen feed (Kessler & Hendry, 2006). Minor elemental constituents in petroleum coke include vanadium (V), zirconium (Zr), barium (Ba), strontium (Sr), nickel (Ni), cerium (Ce), lanthanum (La), Mo, neodymium (Nd), yttrium (Y), and cobalt (Co; Zubot et al., 2012). Several of these constituents including Mo, Ni, and V are of potential concern as they can exceed environmental guidelines in leachate derived from petroleum coke material (Kessler & Hendry, 2006; Puttaswamy et al., 2010; Nakata et al., 2011; Puttaswamy & Liber, 2012; Zubot et al., 2012; Nesbitt, 2016).

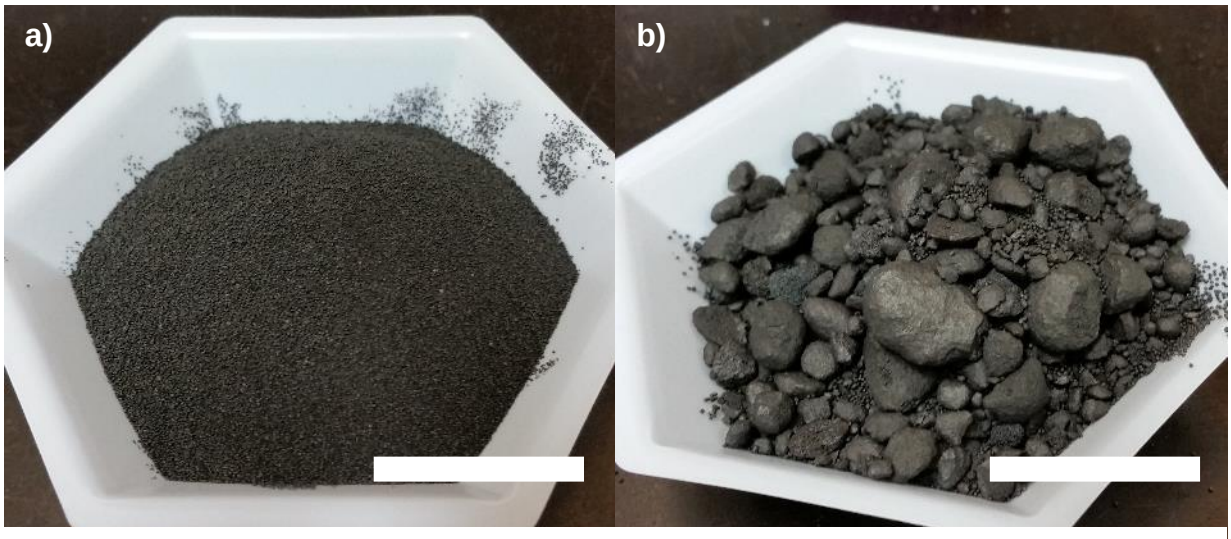


Figure 1-2: Photographs of a) fine-grained, and b) coarse-grained Syncrude fluid petroleum coke, displaying the wide range of possible particle size. Scale bars are 3 cm.

The leachability of elements in petroleum coke differs drastically depending on the type of coke (fluid/flexi- or delayed) and the age of the material (Kessler & Hendry, 2006). Variability in the leachable fraction with age is attributed to finite sources of the constituent of interest in the petroleum coke, while variability with the type of petroleum coke is likely due to differences brought about during the different coking methods (e.g. textural differences, proportion of fly-ash, etc.). In the fluid- and flexi- coking processes, a hot bitumen feed is sprayed into a circulating fluidized particle reactor bed where coking takes place at the particle surface (Gray, 2015). This method creates a dense, fine sand textured material with round smooth particles that exhibit an onion-skin like structure (Kessler & Hendry, 2006; Sobkowicz et al., 2012; Gray, 2015; Nesbitt, 2016). During the delayed coking process, the heavy oil feed is heated in large coking drums and petroleum coke is allowed to accumulate where it is subsequently recovered using a hydraulic cutting procedure (Gray, 2015). Delayed coke is typically more porous than fluid coke (Sobkowicz et al., 2012) and exhibits coarse sand to gravel texture (Kessler & Hendry, 2006), dependent on the degree of hydraulic cutting. Although texturally different, these two coke types exhibit similar bulk chemical composition (Kessler & Hendry, 2006).

In the AOSR petroleum coke is either stockpiled or used as a fuel source by operators, however stockpiling rates greatly exceed fuel usage (Sobkowicz et al., 2012; AER, 2015). High sulfur content as well as transportation costs from northern Alberta limit the commercial appeal of oil sands petroleum coke as a viable fuel source (Sobkowicz et al., 2012). As a result, on-site inventories of petroleum coke rose to more than 90 million tonnes during 2014 (AER, 2015; Figure 1-3). Expected increases in inventory volume (AER, 2015) make petroleum coke a potential problem for operators come mine closure. Petroleum coke, however, shows promise as a reclamation material, where it can act as a low density, high permeability aggregate for a light capping fill on soft tailings materials (Sobkowicz et al., 2012; Simhayov et al., 2017). Several studies have also used petroleum coke as a contaminant adsorption option for OSPW management (Gamal El-Din et al., 2011; Small, 2011; Zubot et al., 2012); however, potential leachability of certain trace elements may limit its implementation.

## 1.6 Reclamation Considerations

Impending mine site closure, as well as regulations put forth in the TMF place reclamation as a major upcoming issue in the Alberta oil sands. During the end-of-life mine closure process, large volumes of tailings and upgrading by-products require efficient and effective storage before

the land is returned to government control. Successful reclamation will require substantial amounts of research before large-scale implementation of these systems can be put in place. In the AOSR, tailings (FFT, CFT, tailings sand, etc.), petroleum coke, and overburden will likely be stored together in terrestrial or subaqueous closure landscapes. A major concern regarding this strategy is the interactions that will occur between these materials of differing chemical and physical composition, as well as the potential effects of these interactions on the overall success of a closure system.

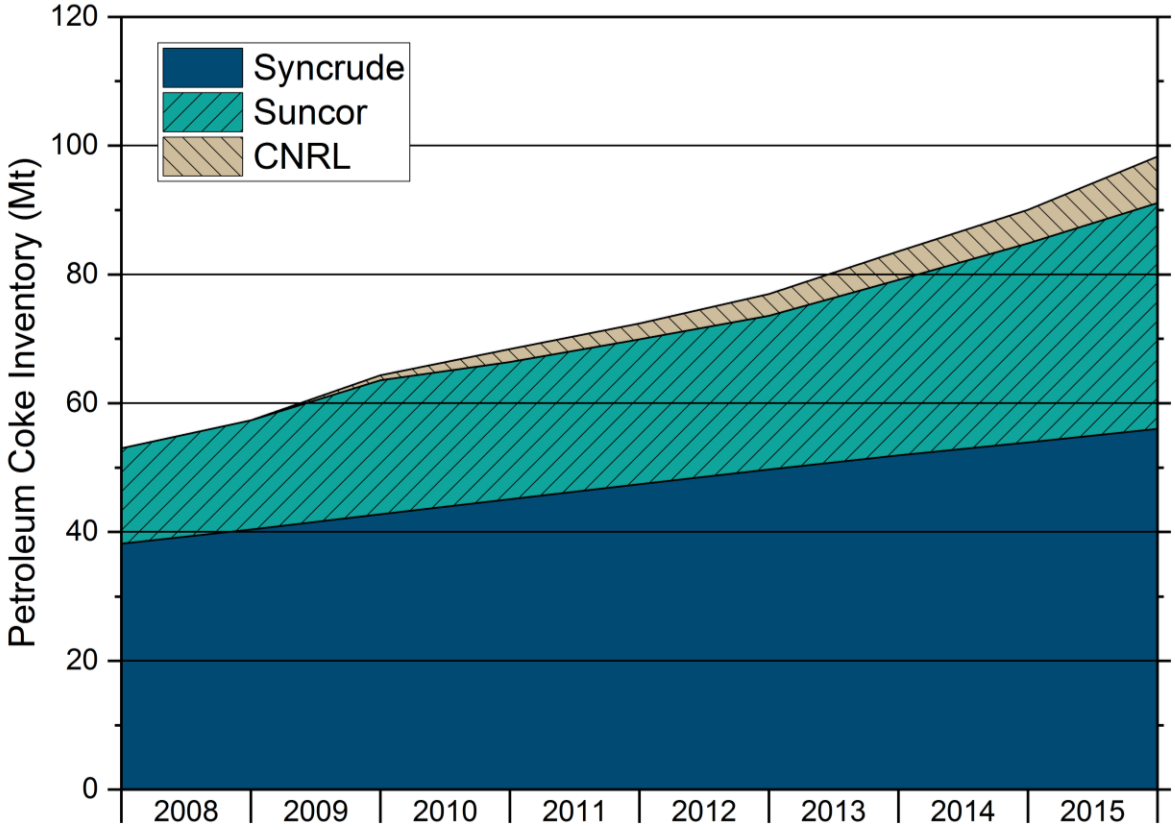


Figure 1-3: Petroleum coke inventory from 2008 through 2015 (AER, 2015).

Major controls on the transport of contaminants in these systems is expected to be advective-diffusive fluxes, adsorption-desorption processes, and mineral precipitation-dissolution dynamics. Porewater released from CFT is highly enriched in inorganic anions ($Cl^-$, $HCO_3^-$ and $SO_4^{2-}$) and exchangeable cations ($Na^+$, $Ca^{2+}$), which will move into adjacent layers within a closure system. Interaction between petroleum coke and elevated concentrations of inorganic ions will influence both the release of trace elements from this material and their mobility in the closure systems (Puttaswamy & Liber, 2010). Trace element fate will be influenced by adsorption-

desorption processes, and precipitation-dissolution reactions. Adsorption-desorption and precipitation-dissolution reactions depend on the pH and reduction-oxidation (redox) conditions of the system. These parameters influence the oxidation state of elements, and both the surface charge and solubility of minerals. Porewater associated with CFT and petroleum coke is generally sub-alkaline (Zubot et al., 2012; Heaton, 2015; Nesbitt, 2016), which presents poor conditions for the sorption of oxyanion forming trace elements, but promotes precipitation and sorption of certain cationic trace elements from solution. Furthermore, increased loading of exchangeable cations will compromise the sorptive capacity of clay and petroleum coke surfaces, leading to a greater role of advective and diffusive transport of trace elements throughout the closure systems.

# CHAPTER 2: RESEARCH MOTIVATION, SCOPE, & HYPOTHESES

## 2.1 Research Motivation

The current surface mining disturbance footprint in the Athabasca oil sands region (AOSR) currently exceeds 950 $km^2$ (Government of Alberta, 2017). An area of approximately 63 $km^2$ has undergone permanent terrestrial or aquatic reclamation, but to date only 1.04 $km^2$ has received government certification (Government of Alberta, 2017). During mine closure, disturbed land in the AOSR will have to be reclaimed using materials produced during the mining process, and handed back to government control. These materials have a wide range of chemical and physical properties, and include tailings and by-products of the bitumen extraction and upgrading processes. Currently, tailings and by-products of concern for remediation efforts in the oil sands include fluid fine tailings (FFT), centrifuged fine tailings (CFT), and petroleum coke. These materials will have to be stored together in mine closure systems, where understanding of their geochemical behaviour is limited.

## 2.2 Project Scope

This study is part of the NSERC-Syncrude Industrial Research Chair in Mine Closure Geochemistry, which is aimed at advancing the understanding of geochemical characteristics and behaviour of oil sands mine closure landscapes. This specific Master of Science thesis project is focused on understanding the geochemical controls on the transport and mobility of trace elements of concern in potential mine closure scenarios. Of particular interest in this study is the interactions occurring between mining wastes and by-products of differing physical and chemical compositions, and the impact of these interactions on the success of a mine closure landscape.

Field-scale lysimeter experiments were implemented on the Mildred Lake mine, operated by Syncrude Canada Limited. Lysimeters were layered with varying assemblages of petroleum coke, CFT, reclamation soil, and tailings sand. Each lysimeter was instrumented with multi-level wells and sensors connected to datalogger units collecting variables of interest. Sensor measurements were collected at 4-hour intervals and included temperature, water content, matric potential, and electrical conductivity (EC).

Core and pore water sampling campaigns were completed at the lysimeter field site with samples subject to detailed geochemical analyses. Measurements included pH, $E_h$, electrical conductivity (EC), alkalinity, total dissolved sulfide ($S^{2-}$), ammonium (measured as $NH_3$-N), major cations, inorganic anions, trace elements, NAs, and stable isotopes of water.

Supplementary studies on petroleum coke included solid-phase analysis and sequential extraction on discrete grain sizes from petroleum coke deposits of varying age and depth of storage. These studies further solidify understanding of the release of trace elements from this material, and will provide evidence regarding the behaviour of these constituents in the lysimeter systems.

## 2.3 Research Hypotheses

This research will help to constrain the geochemical implications of potential closure scenarios with respect to trace element mobility, as well as identify processes and conditions controlling water quality within these systems.

Hypothesis 1: Petroleum coke and CFT will act as a source of trace elements within mine closure landscapes.

- Objective 1a: Define the geochemical behavior of petroleum coke and CFT in potential mine closure landscapes with respect to trace element release, transport and mobility;
- Objective 1b: Assess the variability of these properties within different potential mine closure landscapes;
- Objective 1c: Develop conceptual models of the geochemical evolution of closure landscapes with respect to trace element release, transport and mobility.

Hypothesis 2: Petroleum coke will act as a capillary break in partially-saturated closure systems, reducing the transport of trace elements to overlying reclaimed and vegetated areas.

- Objective 2a: Assess transport capability of constituents of interest through petroleum coke into overlying reclamation analogs.

Hypothesis 3: Soil covers will promote attenuation of trace elements, reducing the potential for water with elevated concentrations reaching surface in fully-saturated closure systems.

- Objective 3a: Compare porewater chemistry between covered and uncovered systems with respect to trace element concentrations at surface.

# CHAPTER 3: MATERIALS & METHODS

## 3.1 Field Methods

### *3.1.1 Site Description and Setup*

The Syncrude Mildred Lake mine is located approximately 35 km north of Fort McMurray, Alberta and has been in operation since 1978. The local climate is sub-arctic, characterized by long cold winters and short cool summers (Peel et al., 2007). Regional hydrologic conditions are sub-humid–where annual evapotranspiration exceeds precipitation–with pronounced seasonal and decadal cycles of water availability (Devito et al., 2012). The Mildred Lake weather station adjacent to the mine reported maximum and minimum mean monthly temperatures of -15.9ºC (January) and 18.9ºC (July), respectively, from 2005 to 2017 (Environment Canada, 2017). Mean annual precipitation over this same period was 408 mm (Environment Canada, 2017).

The study site (57°00′42″ N, 111°46′38″ W) lies north of the South West Sand Storage (SWSS) facility on the south-west corner of the Mildred Lake mine site (Figure 3-1). In the Fall of 2015, six lysimeters were constructed of 2.92 m diameter and 15 mm wall thickness polyethylene tanks cut to an internal height of 3 m. Tank bottoms were left intact and no under drain was installed. As a result of this design decision, porewater is expected to move upward during material consolidation. Lysimeters were placed in the subsurface to a depth of 2.2 m to maintain the local temperature-depth gradient.

Following construction, lysimeters were filled with varying layers of CFT, petroleum coke, reclamation material, and tailings sand as follows (Figure 3-2):

- Lysimeters 1 and 4 (L1 and L4): a dual-cover scheme consisting of 1.5 m of CFT, overlain by 1 m of petroleum coke and 0.5 m of reclamation material;
- Lysimeters 2 and 5 (L2 and L5): a single coke layer cover scheme consisting of 2 m of CFT overlain by 1 m of petroleum coke;
- Lysimeters 3 and 6 (L3 and L6): an uncovered scheme consisting of 1 m of tailings sand overlain by 2 m of CFT.

Following material placement, lysimeters 4, 5 and 6 were saturated with water acquired from the potable water storage on site. A fill-water tank was also brought on site, allowing for convenient re-saturation of the systems as required.

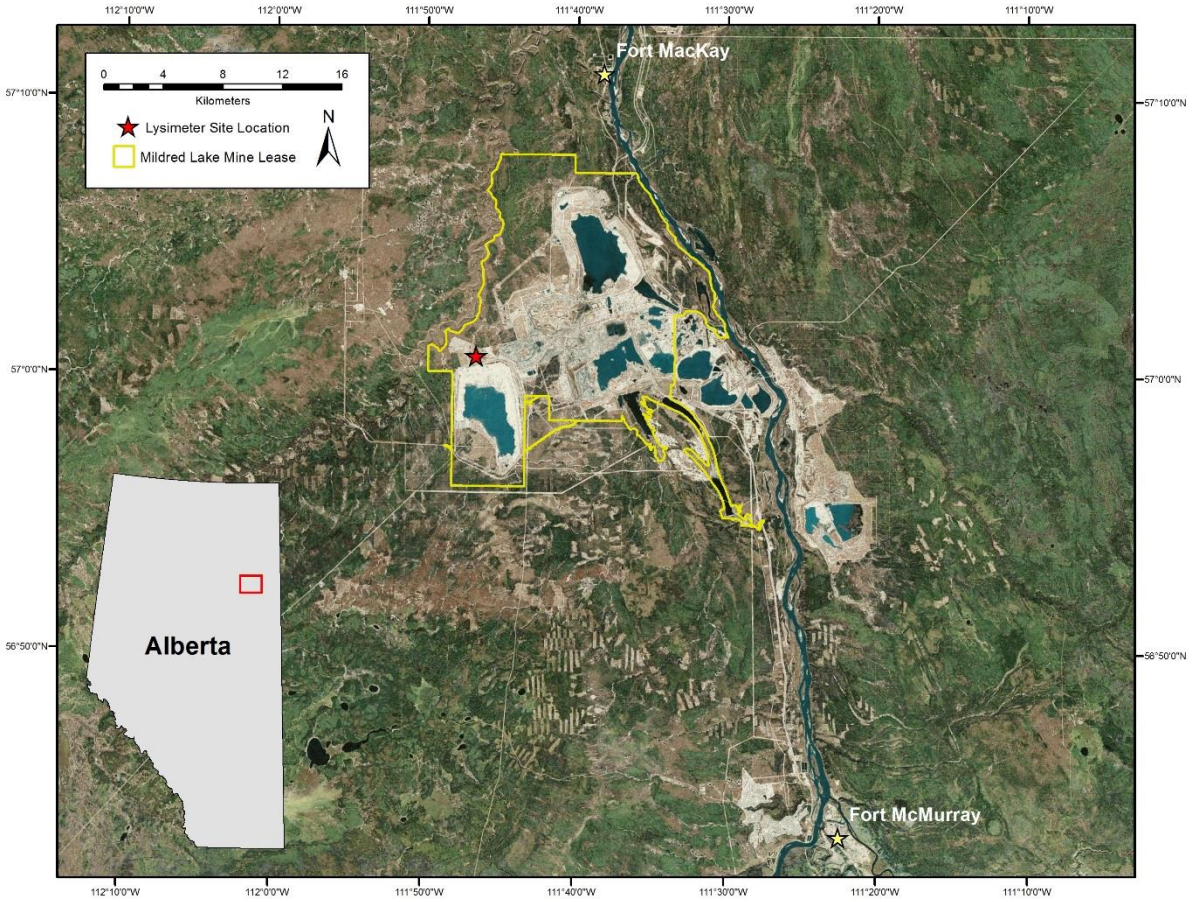


Figure 3-1: Location of the lysimeter field site on the Mildred Lake mine. Source: Regional Aquatics Monitoring Program, Esri, Digital Globe, GeoEye, Earthstar Geographics, CNES/Airbus DS, USDA, USGS, AeroGRID, IGN, and the GIS User Community.

Prior to filling with material, multi-level sampling wells were installed in the center of each lysimeter. Sampling wells were constructed of multiple 3.175 mm inner diameter, 6.35 mm outer diameter polyethylene tubing, supported by 12.7 mm polyvinyl chloride (PVC) rigid conduit. Wells were screened with 125 µm Nitex screen for 10 cm at the base and spaced at 25 cm intervals along the PVC conduit, allowing for detailed sample collection.

During the infilling process sensors were installed at intervals of interest within the material. Each lysimeter was instrumented with six time domain reflectometry (TDR) probes (CS655 & CS655-L; Campbell Scientific, USA), providing water content, electrical conductivity

and temperature data of the material; and four soil matric potential (SMP) sensors (229-L; Campbell Scientific, USA), which provide soil suction data. Sensors and probes were placed toward the centre of the lysimeters to avoid differences in temperature and fluid flow occurring at the tank walls. These instruments were individually calibrated prior to installation by O'Kane Consultants (Saskatoon, SK). All probes and sensors were connected to CR1000 model dataloggers (Campbell Scientific, USA) set to collect the average of hourly readings at four-hour intervals to reduce the overall volume of data while still monitoring diurnal variations in readings. Dataloggers were placed in a sealed enclosure and mounted on a tripod equipped with a solar panel and a 12V sealed rechargeable battery. A modem connected to each datalogger system allows for reliable year-round data collection through a wireless network.

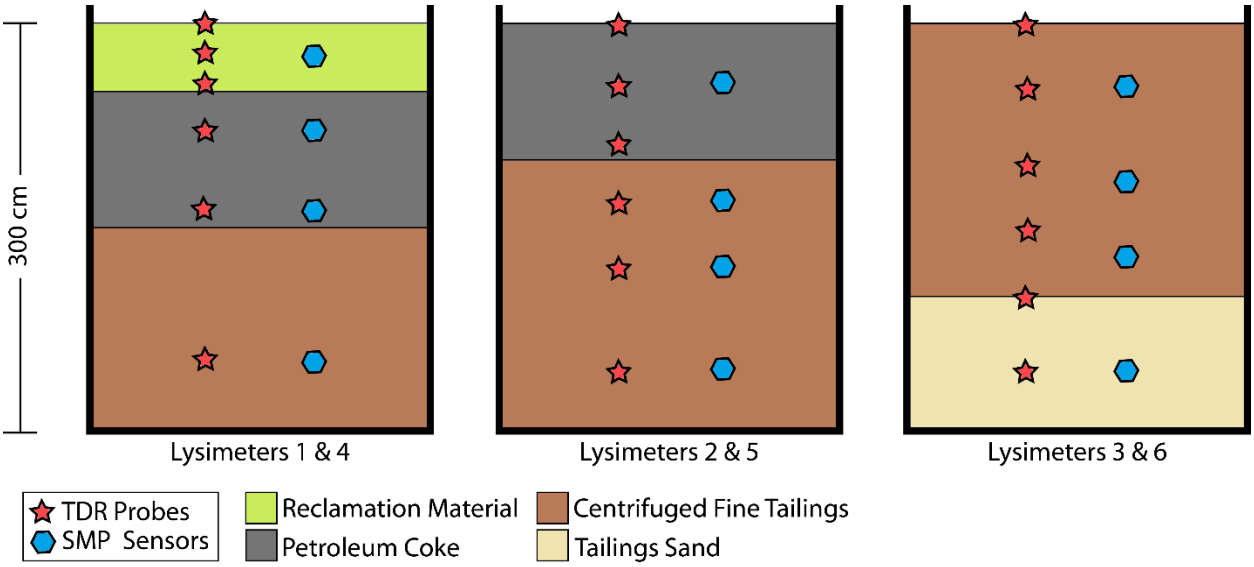


Figure 3-2: Schematic diagram of the three layering schemes implemented in the lysimeter field study.

### *3.1.2 Lysimeter Porewater Sample Collection*

One objective of this study was to gather porewater samples from discrete depths throughout the lysimeter systems. Sample collection was attempted from each of the multi-level wells using clean 6.35 mm diameter silicone tubing (Masterflex; Cole-Parmer Instrument Company, LLC, USA) routed through a peristaltic pump head (Geopump; Geotech Environmental Equipment, Inc., USA). Wells were purged by three well volumes prior to sample collection at each depth to avoid collection of stagnant fluid that may have been exposed to the well casing and atmosphere for an extended period. Immediately following sample collection, measurements of pH, redox ($E_h$ corrected to the standard hydrogen electrode), EC, alkalinity, $NH_4^+$, and $S^{2-}$ (reported

as $\Sigma H_2S$) were recorded. Samples of trace elements, major cations, major anions, isotopes of water, and naphthenic acids (NAs) were collected and preserved for laboratory analysis (Section 3.2.1). A flow through cell was not used during porewater sampling due to the low volume of porewater available in the systems. Most wells screened in CFT intervals in each lysimeter produced very little pore water due to the low hydraulic conductivity of the material. Therefore, samples collected from wells in this study are mainly representative of the pore water present in the petroleum coke, reclamation material, and tailings sand.

Figure 3-3: Photograph of the lysimeter field site taken in the summer of 2016. Lysimeter 1 is in the foreground and lysimeter number increases sequentially toward Lysimeter 6 in the background.

### *3.1.3 Lysimeter Core Sample Collection*

Continuous coring of the lysimeter field experiments took place in late November 2016. A portable ramset deployed by a hand crank system was placed on a wooden platform constructed over top of each lysimeter. The sampler consisted of a Shelby tube with an independently-operated internal piston. The Shelby tube is a 76.2 cm length by 7.62 cm diameter thin walled hollow aluminum tube with a chamfer on the leading end to form a cutting edge. Samples were taken at 0.6 meter intervals throughout the depth of each lysimeter. Following recovery of each interval, the Shelby tube was capped, labelled, and frozen until shipment to the University of Saskatchewan.

## 3.2 Laboratory Methods

### *3.2.1 Core Porewater Extraction*

To collect samples necessary to create a depth profile, Shelby tubes were cut to intervals of interest using a reciprocating saw equipped with a bi-metal blade. Due to compaction of some

intervals during coring a compaction factor was calculated to estimate the actual depth of each interval. The compaction factor was calculated as the quotient of the recovered length and the total push length, assuming linear compaction across the depth interval. This factor was multiplied by the interval of interest (15 cm) to give the required cut length interval for each Shelby tube. Immediately following the cutting of each interval of interest, the tubes were capped, labelled, and stored at -20°C until analysis.

Prior to analysis, frozen core samples were placed in an anaerobic chamber (<5% [v/v] Hydrogen gas [$H_2$], balance nitrogen gas [$N_2$]), and allowed to thaw at room temperature. The sample was extruded from the core casing and any material in direct contact with the casing or cutting surface was removed. Following this step, sub-samples were collected, transferred to 50 mL centrifuge tubes, and centrifuged at 10,000 rpm (13,750 g) for 30 minutes. Supernatant from the sub-samples were combined for each depth interval and subjected to a detailed geochemical analysis (Section 3.2.2).

### *3.2.2 Water Sample Chemistry*

Measurements of pH, $E_h$, and EC were taken on unfiltered samples immediately following collection. The pH electrode (Orion 8156BNUWP ROSS Ultra) was regularly calibrated using pH 4, 7, and 10 NIST-traceable buffer solutions (Thermo Scientific), while ZoBell's (Nordstrom, 1977) and Light's (Light, 1972) solutions (RICCA Chemical) were used to evaluate the accuracy of the redox electrode (Orion 9678BNWP Sureflow). Measured redox potential values were corrected to the standard hydrogen electrode and reported as $E_h$. The EC cell (Thermo ORION, model 011050MD) was regularly calibrated to standard conditions using a 1413 μS $cm^{-1}$ standard solution (Thermo Scientific).

Measurements of alkalinity, $\Sigma H_2S$, and $NH_4^+$ were taken using sample passed through a sterile 0.45 μm polyesthersulfone (PES) syringe filter membrane (Acrodisc; Pall Corporation, USA) connected to a sterile syringe (30 mL HSW NORM-JECT; Henke-Sass Wolf, Germany). Alkalinity was measured by titrating to the bromocresol green-methyl red endpoint using either 1.6 or 0.16 N sulfuric acid. Hydrogen sulfide was measured by spectrophotometry (DR2800; Hach Company, USA) using the methylene blue method (HACH Method 8131). Ammonium was also measured by spectrophotometry using the salicylate method (HACH Method 10031).

Samples for inorganic anions and stable isotopes of water were passed through a 0.45 μm PES membrane and stored in high-density polyethylene (HDPE) bottles at 4°C prior to analysis.

Inorganic ions were quantified using ion chromatography (IC; EPA Method 300.0), while stable isotopes of water were measured using a Picarro 2130 cavity ringdown spectrometer coupled to a CTC LC-PAL liquid autosampler using the method described in Lis et al. (2008). Samples for major cations and trace elements were passed through a 0.1 μm PES membrane filter, acidified to pH < 2 using trace metal grade nitric acid (Omnitrace, EMD Millipore), and stored in HDPE bottles at 4°C until analysis. Major cations were measured using inductively-coupled plasma optical emission spectrometry (ICP-OES; EPA Method 200.7), while trace elements were quantified using inductively-coupled plasma mass spectrometry (ICP-MS; EPA Method 200.8).

### *3.2.3 X-ray Diffraction*

CFT mineralogy was characterized by X-ray diffraction (XRD) on a number of core samples of varying depth within each lysimeter. XRD was performed using a PANalytical Empyrean diffractometer operated at 45 kV and 40 mA with a Cobalt Kα source. Diffraction patterns were obtained for randomly oriented bulk and preferentially oriented clay samples. Bulk CFT samples were transferred to a glove box, placed in clean polystyrene weighing trays (Fisher Brand; Thermo Fisher Scientific, USA), and allowed to air-dry under a gas-mix atmosphere (5% [v/v] $H_2$, balance $N_2$) for 24-hours. These samples were then ground up using an agate mortar and pestle, slurried with methanol, and mounted on a glass plate for analysis. Preferentially oriented clay samples were produced by mixing each CFT sample with deionized water using a bench-top agitator, and allowing the resulting slurry to settle for approximately 10 minutes. A 1 mL aliquot was then pipetted from the resulting particle suspension, placed on a glass plate, and allowed to air-dry. Samples were then placed in an ethylene glycol atmosphere and allowed to glycolate for 24 hours before analysis. All scans were collected over the range of 5–80º 2θ with a 2θ resolution of 0.017º. Phase identification was performed using X'Pert HighScore Plus software (Version 3.0.0; PANalytical B.V.).

### *3.2.4 Geochemical Modeling*

The geochemical model PHREEQCi (Version 3.3.8.11728; Parkhurst & Appelo, 2013) using the MINTEQA2 Version 4.0 (USEPA, 1998) database was used to investigate mineral phases and trace element speciation occurring in the porewater. PHREEQC is an equilibrium and mass-transfer model that provides saturation indices for discrete mineral phases, as well as speciation calculations for various elements.

### *3.2.5 Sequential Extractions*

The purpose of the sequential extraction study was to investigate the relationship between fluid petroleum coke grain size and the overall leachability and potential availability of trace elements. Petroleum coke was selected from several sites and depths to vary both the age and conditions of storage of the material. Following sample selection, petroleum coke was separated into several grain size fractions of interest and subjected to a detailed sequential extraction analysis.

*Sample and Site Description*

Petroleum coke produced at the Mildred Lake mine upgrading facility is subsequently stockpiled in several deposits on site. Coke Cell 5 (CC5), Coke Watershed (CW) and Coke Beach (CB) have been utilized as coke storage areas in varying capacities over the production lifetime. Coke Cell 5 (1985–1999) represents an aged deposit that has been capped with reclamation soil cover and left partially saturated since deposition. Samples collected from CC5 and used in this study include: DM050, collected from the near surface; DM550, collected from the surface of the water table; and DM950 collected from deep below the water table. Coke Watershed (2000–2003) represents a relatively recent deposit that, similar to CC5, has been capped with a vegetated soil cover and left partially saturated since deposition. Samples collected from CW and used in this study include: CX050, collected from the near surface; and CX300 collected from the surface of the water table. Samples from deep below the water table were also collected, however high hydrocarbon content limited their use in this study. Coke Beach (2000–present) represents an active deposit with no reclamation activities occurring at surface. Samples collected from CB and used in this study include: AB000 and AM200, collected from the near surface; AB250 and AM350, collected from just below the water table; and AB750 and AM650, collected from deep below the water table. Together, these samples cover the wide range of deposit ages and storage conditions found on site at the Mildred Lake mine.

*Sample Collection*

Samples were collected using an amphibious track-mounted sonic drill rig in July of 2014 and transported to the laboratory where they were frozen at -18°C until analysis (Nesbitt, 2016). Samples ($n$ = 11) were selected from four sites with three depths chosen from each site, representing petroleum coke stored above, below and deep below the water table. Frozen samples were thawed in a glove box under anoxic atmosphere (5% $H_2$, balance $N_2$) and vacuum filtered

(47mm Millipore; EMD Millipore, Canada) to remove pore water. The filtered samples were then air dried in polystyrene weighing trays (Fisher Brand; Thermo Fisher Scientific, USA) within the glove box. These samples were then placed in high-density polyethylene (HDPE) sample bottles (Nalgene; Thermo Fisher Scientific, USA) and stored under the gas-mix atmosphere until sieving.

After consulting the available literature with respect to fluid coke grain size distribution, six size fractions were selected for sieving. Dry sieving was conducted using standard soil sieves (Canadian Standard Sieves, Canada) mounted on a rotary sieve shaker (Ro-Tap; Tyler, USA) operating at approximately 200 RPM for 15 minutes, producing seven definite size fractions ($p$; 2000 μm < $p$; 350 μm < $p \leq$ 2000 μm; 212 μm < $p \leq$ 350 μm; 149 μm < $p \leq$ 212 μm; 124 μm < $p \leq$ 149 μm; 63 μm < $p \leq$ 124 μm; $p \leq$ 63 μm). After sieving, the split samples were combined into three grain fractions ($f$; $f_1 \leq$ 149 μm; 149 μm < $f_2 \leq$ 350 μm; 350 μm < $f_3$). Selection for grain size fractions was based on the resulting average grain size distribution of all samples. This produced samples ($n$ = 33) that varied in location, depth and grain size. Fractioned samples were stored in HDPE sample bottles (Nalgene; Thermo Fisher Scientific, USA) under the gas-mix atmosphere until extraction.

*Sequential Extraction Protocol*

Each sample fraction was subsampled in triplicate and subjected to a sequential extraction protocol created to partition trace elements into five fractions (Table 3-1). A sub-alkaline Milli-Q (18.2 MΩ·cm) extractant quantified the potential for trace element release under conditions similar to flushing by precipitation (Jack et al., 1979; Kessler & Hendry, 2006; Nesbitt, 2016). Trace elements associated with clay and (oxy)(hydr)oxide mineral surfaces or adsorbed directly on the petroleum coke particle surface are mobilized in the exchangeable fraction by a high ionic strength solution at near-neutral pH (Nesbitt, 2016). The reducible fraction utilized a moderate reductant solution at neutral pH to examine trace elements bound in the chemical structure of (oxy)(hydr)oxides present in the coke matrix (Blackmore et al., 1996; Zubot et al., 2012; Nesbitt, 2016). Trace elements bound in carbonates and other acid soluble minerals were brought into solution in the acid soluble extraction using a relatively weak acid extractant at low pH. During the oxidizable extraction, trace elements associated with organic matter were brought into solution by a highly oxidizing extractant at sub-neutral pH, similar to that used by Kessler & Hendry (2006). At each extraction step, 1.0 g of sample was combined with 40 mL of the extractant in an acid washed 50 mL polypropylene centrifuge tube (SuperClear™ Ultra-High Performance; VWR,

USA). Samples from extraction steps 1 through 4 were shaken horizontally on a mechanical platform shaker (Innova 2100; New Brunswick Scientific, USA) at 80 RPM for 16 hours, while samples undergoing the oxidizable extraction were shaken upright with a loosened cap at 120 RPM for 16 hours to avoid gas build up and leaking. Following shaking, samples were centrifuged (5804R; Eppendorf, Germany) at 4000 RPM (2934 g) for 40 minutes. The supernatant was then collected using a syringe (30 mL HSW NORM-JECT; Henke-Sass Wolf, Germany) and filtered using a 0.45 µm membrane syringe filter (Acrodisc® 25mm; Pall Corporation, USA). All samples were acidified with $HNO_3$ to below pH 2 and promptly stored at 4°C until analysis by ICP-MS. Between each extraction step, petroleum coke samples were washed with 20 mL Milli-Q (18 Ω), shaken horizontally for 20 minutes and centrifuged at 4000 RPM for 20 minutes, after which the supernatant was collected using a pipette and discarded.

Table 3-1: Description of extractants used in the petroleum coke extraction study.

| Fraction | Extractant | Preparation |
|---|---|---|
| 1. Water Soluble | Milli-Q (18.2 MΩ·cm) | ~ pH 7.5 |
| 2. Exchangeable | $Na_2HPO_4 \cdot 7H_2O$ (0.58 M)[1]<br>$NaH_2PO4 \cdot H_2O$ (0.42 M)[2] | pH 6.7 |
| 3. Reducible | Na-Ascorbate (0.12 M)[3]<br>$Na_3$-Citrate (0.17 M)[4]<br>$NaHCO_3$ (0.60 M)[5] | pH 7.0 |
| 4. Acid Soluble | Acetic Acid (0.11 M)[6] | pH 2.8 |
| 5. Oxidizable | Ammonium Acetate (1.0 M)[7]<br>$H_2O_2$ (30 wt%)[8] | 2:1 (volume) AmAce:$H_2O_2$ at pH 6.8 |

[1]ACS Reagent (98.0–102.0% assay), ≤0.001% metals; [2]BioXtra, for molecular biology (T) (≥99.5% assay), ≤5 mg $kg^{-1}$ metals; [3]BioXtra, for molecular biology (NT) (≥99.0% assay), ≤5 mg $kg^{-1}$ metals; [4]BioUltra, for molecular biology (NT) (≥99.5% assay), ≤5 mg $kg^{-1}$ metals; [5]ACS Reagent (99.7–100.3% assay); [6]Certified ACS Glacial Acetic Acid, <0.05 ppm metals; [7]Ultra Pure, <0.0005% metals; [8]ACS Reagent), ≤1 ppm metals.

*Data Corrections*

Before evaluation of the data could take place, extraction concentrations first required correction to subtract minor contributions of trace elements present in the extractant solutions. Samples of each extractant were taken as blanks and analyzed by ICP-MS to characterize the degree of trace element contribution. Corrections were performed by subtracting the contribution of each element in the blank from the concentrations in each sample. For some extractions (exchangeable, reducible and oxidizable), it was necessary to dilute the sample with concentrated $HNO_3$ to achieve a pH suitable for preservation. In these cases, the corrected concentrations were multiplied by the inverse of the fraction of extractant in each sample.

Following this step, the leachability of the coke used in each sample was calculated using the equation:

$$Leachability = \frac{C_i \times V}{m_s} \quad (3.1)$$

where: $C_i$ is the corrected concentration of the element in the sample; V is the volume of extractant used; and $m_s$ is the mass of coke used in the extraction.

This produces a value for the leachability of the coke sample in mg $kg^{-1}$.

### *3.2.6 Petroleum Coke Surface Area*

Select petroleum coke samples were subject to specific surface area analysis to compare the surface area of the different grain size fractions, as well as to compare the surface area of samples to the magnitude of leachability. Specific surface areas measurements were performed on a Quantachrome Nova 2200e surface area and pore size analyzer with an adsorption isotherm in a $p/p_0$ range of 0.05-0.3. Measurements were collected using a 10-pt BET nitrogen isotherm for three whole grain samples and nine fractioned samples to observe the dependence of surface area on grain size. Each sample was vacuum degassed for 6 hours and backfilled with helium prior to measurement. Analysis was performed using liquid nitrogen as the coolant.

# CHAPTER 4: RESULTS

## 4.1 Lysimeter Experiments

### *4.1.1 Pore-water chemistry*

*pH, $E_h$, EC, alkalinity, and temperature*

Porewater pH in all lysimeters are generally circum-neutral to mildly alkaline, ranging from 6.80 to 8.73, and averaging 7.70 ± 0.29 ($n$=59; note that this and all future statistical calculations are global averages of all samples collected in the lysimeter systems unless otherwise stated, and that any variability reported is one standard deviation from the mean). The porewater present in the CFT layers generally remain more consistent with depth and are more alkaline, averaging 7.88 ± 0.11 ($n$=37). These values are in agreeance with findings by Heaton (2015), who noted similar trends and values with pH and depth in a number of full-scale CFT deposits. Porewater pH in petroleum coke layers overlying CFT generally become less alkaline moving upward toward the surface, with pH in L4 and L5 decreasing to a minimum of ~7.25. Porewater becomes slightly acidic moving upward into the reclamation material of L4, where pH dips to 6.80, but promptly returns to 7.5 at the surface. In L3 and L6, pH decreases downward into the tailings sand, reaching a pH of around 7.25 at and near the bottom. Porewater pH in both L3 and L6 exhibit comparable values and trends with depth.

Porewater redox potential ranged from -81.6 to +387.4 mV, averaging +161 ± 158 mV ($n$=44). Redox potential in in the CFT layers varied based on the saturation conditions and layering scheme of each lysimeter. In the L4 and L5 layering schemes, conditions were generally <+200 mV. Values decreased with depth, reaching minimum values of −81.6 and −79.4 mV in L4 and L5, respectively. Moving upward into the petroleum coke in these layering schemes, there is a notable decrease in $E_h$ at the coke-CFT interface, after which conditions become more oxic toward the surface. Redox potentials reach values of +387.4 and +230.8 mV at the surfaces of the petroleum coke in L4 and L5, respectively. Conditions become slightly less oxic after the reclamation material-coke interface in L4, but return to ~300 mV at surface. Redox potentials are typically higher in the partially-saturated systems compared to the fully-saturated systems. Redox

conditions in the CFT in L3 and L6 are generally oxic, averaging +335.6 ± 33.0 mV ($n$=11) and remaining relatively constant with depth. Redox potential below the CFT-tailings sand interface become slightly less oxic, but return to values similar to the CFT near the base of the tailings sand.

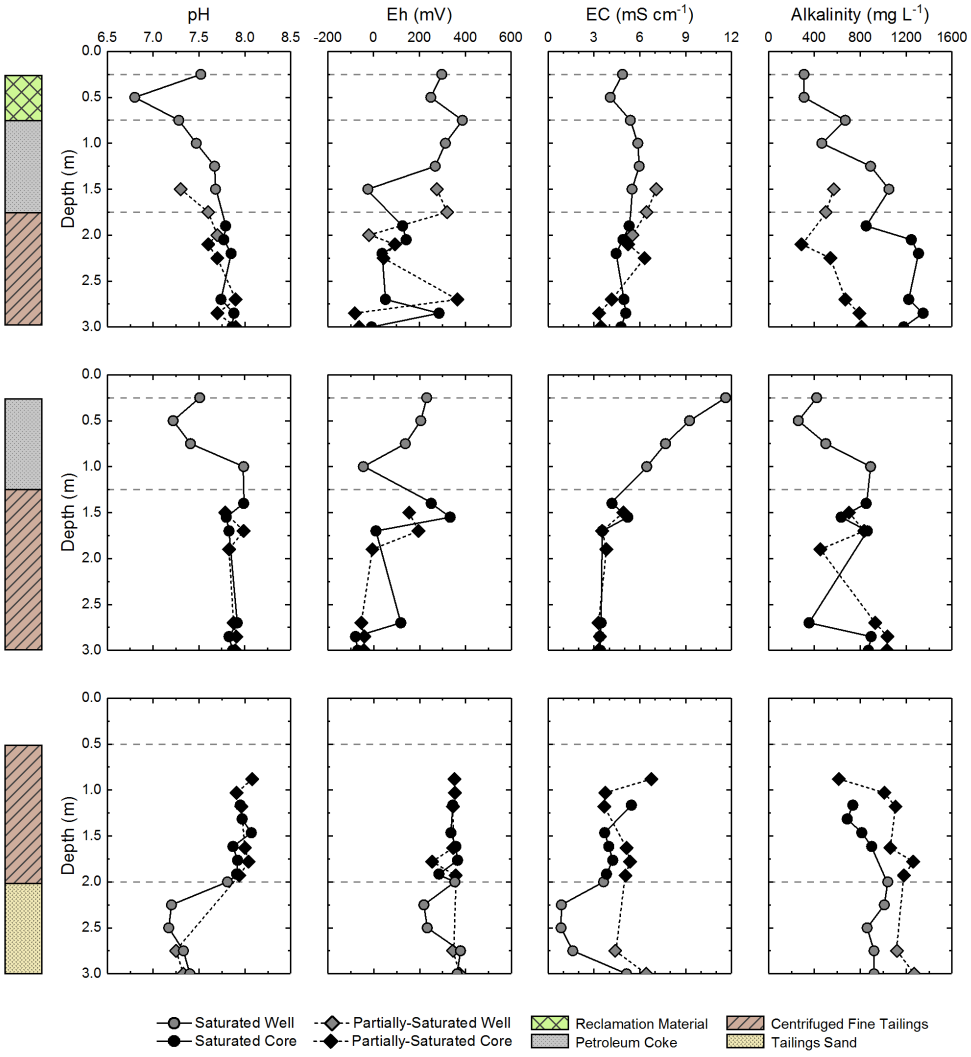


Figure 4-1: Well and core porewater pH, $E_h$, EC, and alkalinity with depth for all lysimeters. The bars along the left-hand side of the graphs designate the material within the three layering schemes.

Electrical conductivity ranged from 0.85 to 11.6 mS cm$^{-1}$, averaging 4.9 ± 1.9 mS cm$^{-1}$ ($n$=58). Conductivity generally increased toward the surface in the L4 and L5, but remained relatively stable with depth in L4. Conductivity in the CFT units in each layering scheme averaged 4.4 ± 0.91 mS cm$^{-1}$ ($n$=34), which is within the range observed by Heaton (2015) in several full scale CFT deposits. In petroleum coke layers, EC was typically elevated above values seen in the CFT below; however, there are notable differences between the systems with and without a soil cover. In L4, EC generally remains similar to those found in the CFT below, at around 4–

5 mS $cm^{-1}$. There is a decrease in EC as you move into the reclamation material in this system, with a slight increase at surface. In L5, there is a sharp increase moving upward in the petroleum coke layers, increasing from 4.18 mS $cm^{-1}$ at just below the coke-CFT interface, to 11.61 mS $cm^{-1}$ at surface. In tailings sand layers in L3 and L6, EC decreases with depth and then increases slightly at the bottom. Differences between fully- and partially-saturated layering schemes over time are observed in the datalogger data (Appendix B). In the saturated systems, EC is typically highest at the surface, while the partially-saturated systems exhibit highest EC at just above the petroleum coke-CFT interface (the water table) in L1 and L2. In L3 and L6, EC is highest around 50 cm below the surface of the CFT. Electrical conductivity is typically higher in partially-saturated systems when compared with their fully-saturated counterparts.

Alkalinity ranges between 260 to 1560 mg $L^{-1}$ $CaCO_3$, averaging 823 ± 302 mg $L^{-1}$ ($n$=57). Alkalinity in the CFT averages 881 ± 267 mg $L^{-1}$ ($n$=33), and generally increases with depth in these layers. These values are elevated when compared with average values reported by Heaton (2015), but are still within a similar range compared to a number of the deposits. Alkalinity decreases at the coke-CFT interface in L4 and L5, and decreases toward the surface of the coke layers. Alkalinity in the coke follows similar trends with depth observed by Nesbitt (2016), however values in this study are ~400 – 800 mg $L^{-1}$ higher in most cases. There is a small decrease in alkalinity at the reclamation material-coke interface in the L4, which decreases values to ~300 mg $L^{-1}$ $CaCO_3$ at surface. In the tailings sand underlying CFT in L3 and L6, alkalinity concentrations remain relatively constant with those observed in the overlying unit, and are more highly elevated in the partially-saturated unit. In general, alkalinity follows similar trends observed for pH; exhibiting decreased values at lower pH and increased values in locations where pH is more alkaline.

Temperature variation is similar across all layering schemes (Appendix B). In the summer, temperatures are warmest at the surface and decrease with depth. In the winter, temperatures are coldest at the surface and increase with depth. Surface temperatures exhibit the greatest fluctuations due to daily temperature variations, however these trends are less severe in the saturated systems. Freezing typically occurs by early- to mid-October and slowly moves downward from the surface over time. The CFT in L1, L2, L4, and L5 typically begins to freeze around January, and the majority of the unit is frozen by April, at which point it begins to thaw. CFT temperatures in these systems are typically between 15–20ºC in summer. Surface

temperatures in the single-cover system show the largest fluctuations and the highest temperatures due to the low albedo of the petroleum coke surface.

*Major Cations*

Calcium concentrations ranged from 11.7 to 534 mg $L^{-1}$, averaging 109 ± 129 mg $L^{-1}$ ($n$=59). Porewater concentrations in the CFT were lower than in the surrounding units, averaging 45.5 ± 56.6 mg $L^{-1}$ ($n$=34). These values are within a similar range to those observed by Heaton (2015). Moving upwards into the petroleum coke units in L4 and L5, Ca increases at a relatively constant rate. In L4, concentrations increase from 36 mg $L^{-1}$ at the surface of the CFT to 278 mg $L^{-1}$ at the surface of the petroleum coke, while in L5 concentrations increase from 22 to 534 mg $L^{-1}$ over this same interval. Concentrations further increase across the reclamation material unit in L4, reaching ~400 mg $L^{-1}$ at surface. In L3 and L6, Ca concentrations increase directly below the CFT interface, and then decrease at the base of the tailings sand unit. Variation in concentrations between fully- and partially-saturated lysimeters is most notable between L1 and L4, where concentrations at equal depths regularly differ by 200 to 300 mg $L^{-1}$. The source of Ca in these systems can largely be attributed to the dissolution of gypsum used during the production of CFT, which Heaton (2015) reported is amended at a rate of 12.3 kg per tonne of dry tailings. Another potential source of Ca is the dissolution of carbonates, which are present in CFT and coke material (Heaton, 2015; Nesbitt, 2016).

Potassium ranged from 7.7 to 95.1 mg $L^{-1}$, averaging 21.7 ± 16.8 mg $L^{-1}$ ($n$=59). Concentrations in the CFT are lower than surrounding units, averaging 15.5 ± 6.2 mg $L^{-1}$ ($n$=34). These values are comparable to those reported by Heaton (2015). Moving upward from the surface of the CFT to the surface of the petroleum coke in L4 and L5, K concentrations increase from 19 to 60 mg $L^{-1}$ and 14 to 84 mg $L^{-1}$, respectively. Potassium concentrations in the reclamation material of L4 decrease, reaching ~20 mg $L^{-1}$ at surface. Concentrations in the tailings sand of L3 and L6 remain constant with depth at ~20 mg $L^{-1}$.

Magnesium concentrations ranged from 5.6 to 460 mg $L^{-1}$, averaging 63 ± 87 mg $L^{-1}$ ($n$=59). Concentrations in the CFT units average 25.8 ± 39.7 mg $L^{-1}$ ($n$=34), which are elevated when compared with those observed by Heaton (2015). In the petroleum coke overlying CFT in L4 and L5, concentrations increase toward surface from 23 to 128 mg $L^{-1}$, and 11 to 462 mg $L^{-1}$, respectively. Concentrations decrease in the reclamation material in L4, but return to ~150 mg $L^{-1}$ at surface. In the tailings sand of L3 and L6, Mg concentrations increase just below the CFT

interface and then decrease with depth. Greatest variability in Mg concentrations between fully- and partially-saturated lysimeters are observed in L1 and L4, where Mg is elevated by 100 to 200 mg $L^{-1}$ in the partially-saturated lysimeter relative to the fully-saturated lysimeter at similar depths.

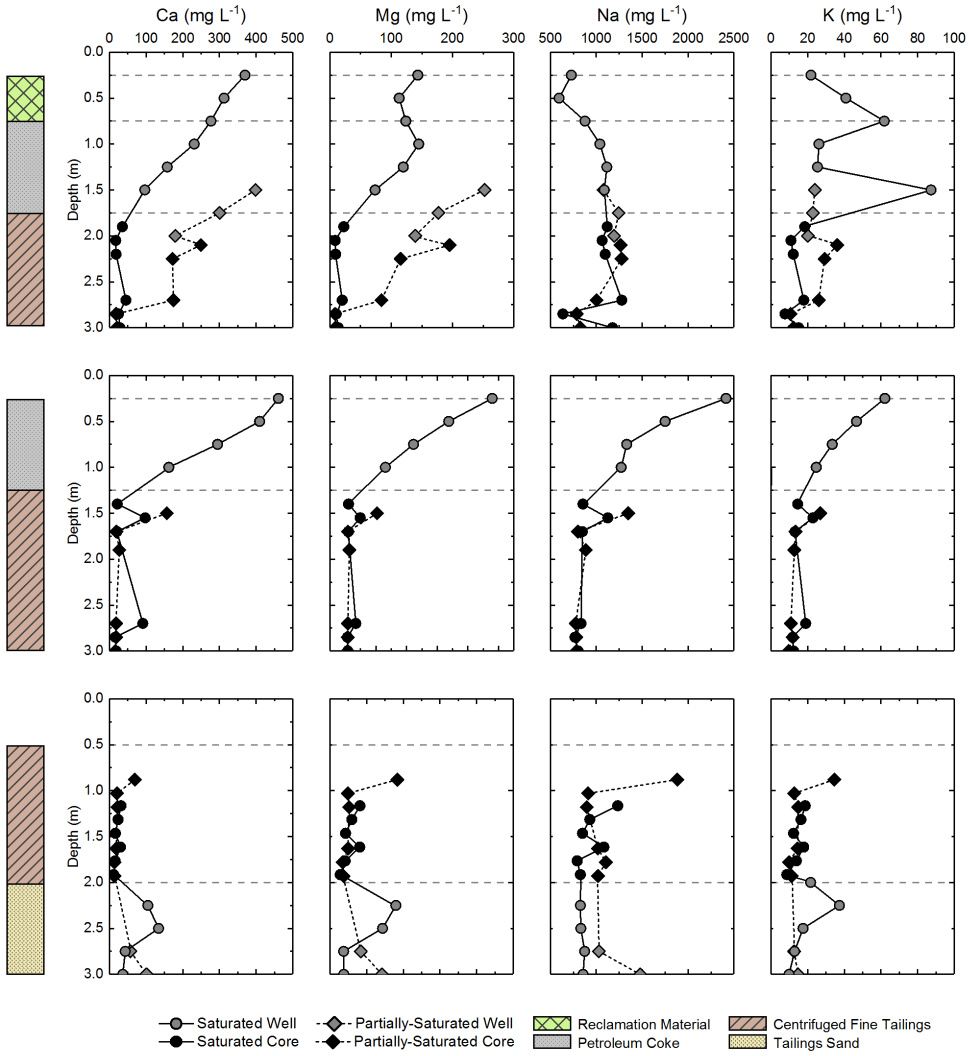


Figure 4-2: Well and core porewater concentrations of Ca, Mg, Na, and K with depth for all lysimeters. The bars along the left-hand side of the graphs designate the material within the three layering schemes.

Sodium concentrations ranged from 530 to 3400 mg $L^{-1}$, averaging 1100 ± 480 mg $L^{-1}$ ($n$=59). CFT porewater averaged 965 ± 183 mg $L^{-1}$ ($n$=34), which is in a similar range to that observed by Heaton (2015). Concentrations in L4 and L5 remain relatively constant with depth. In L4, concentrations decrease from 1120 to 998 mg $L^{-1}$ from the surface of the CFT unit to the surface of the petroleum coke unit, and further decrease from 998 to 791 mg $L^{-1}$ in the reclamation

soil unit above. Sodium concentrations in the tailings sand in L3 and L6 remain close to those in the CFT at ~1000 mg $L^{-1}$. In L5, concentrations rise from 855 mg $L^{-1}$ at the CFT interface to 3381 mg $L^{-1}$ at the surface of the coke. No significant variation in sodium concentrations between fully- and partially-saturated lysimeters were observed in the data. Potential sources of Na in the lysimeter systems include remnant tailings porewater held in the CFT (Heaton, 2015), ion-exchange with Ca in coke and CFT material (Cilia, 2017), and potentially the dissolution of Na salts present in the CFT and coke.

*Anions*

Chloride concentrations ranged from 310 to 2080 mg $L^{-1}$, averaging 726 ± 320 mg $L^{-1}$. CFT porewater averaged 684 ± 181 mg $L^{-1}$. Chloride concentrations in L1 and L4 are highest at the base of the CFT units and then gradually decrease toward surface from around 750 to 310 mg $L^{-1}$ in L4. An opposite trend is observed in L5, where concentrations increase from around 600 to nearly 1200 mg $L^{-1}$ at surface. In the L3 and L6, concentrations in the tailings sand remain fairly constant with depth at around 650 mg $L^{-1}$ and begin to increase upward into the CFT units, reaching around 1500 mg $L^{-1}$ near surface.

Sulfate concentrations ranged from 2.4 to 6800 mg $L^{-1}$, but averaged 1270 ± 572 mg $L^{-1}$. Lysimeter 1 and L4 exhibit notable differences between the fully- and partially-saturated systems. In L4, concentrations of $SO_4^{2-}$ remain relatively constant with depth in the CFT around 250 mg $L^{-1}$ and gradually increase to around 2500 mg $L^{-1}$ in the reclamation material cover. In L1 there is a uniform increase towards surface throughout the CFT, with concentrations generally elevated 1000 to 2000 mg $L^{-1}$ when compared to L4. In L2 and L5, $SO_4^{2-}$ behavior is fairly consistent between the saturated and partially-saturated systems, however comparisons can only be made within the CFT units. Concentrations throughout the CFT of L5 remain around 500 mg $L^{-1}$, and increase dramatically from the base of the petroleum coke unit to a maximum of 6755 mg $L^{-1}$ near surface. In L3 and L6, concentrations remain relatively constant with depth around 400 mg $L^{-1}$ in the CFT unit, increasing to around 1000 mg $L^{-1}$ throughout the tailings sand. Values recorded in this study are lower than those reported by Heaton (2015), who reported mean $SO_4^{2-}$ concentrations of 2300 and 3200 mg $L^{-1}$ in two full-scale CFT deposits. The source of $SO_4^{2-}$ in these systems can largely be attributed to the dissolution of gypsum in the CFT material.

Nitrate ($NO_3^-$) ranged from below the method detection limit to 11.5 mg $L^{-1}$, averaging 1.2 ± 2.5 mg $L^{-1}$. Concentrations are highest in L1, where concentrations increase from below the

method detection limit at the base of the CFT to 11.5 mg $L^{-1}$ at the top of the petroleum coke unit of this system. Nitrate in L4 behaves very differently; concentrations remain low throughout the entire system, reaching a maximum of 2.98 mg $L^{-1}$ in the petroleum coke in this system. In L2 and L5, concentrations are most elevated in the fully-saturated system (L5) and mostly under detection in the sampled portion of the partially-saturated system (L2). The majority of values are under detection in the CFT units in L3 and L6, and a maximum value of 1.43 mg $L^{-1}$ measured in the tailings sand.

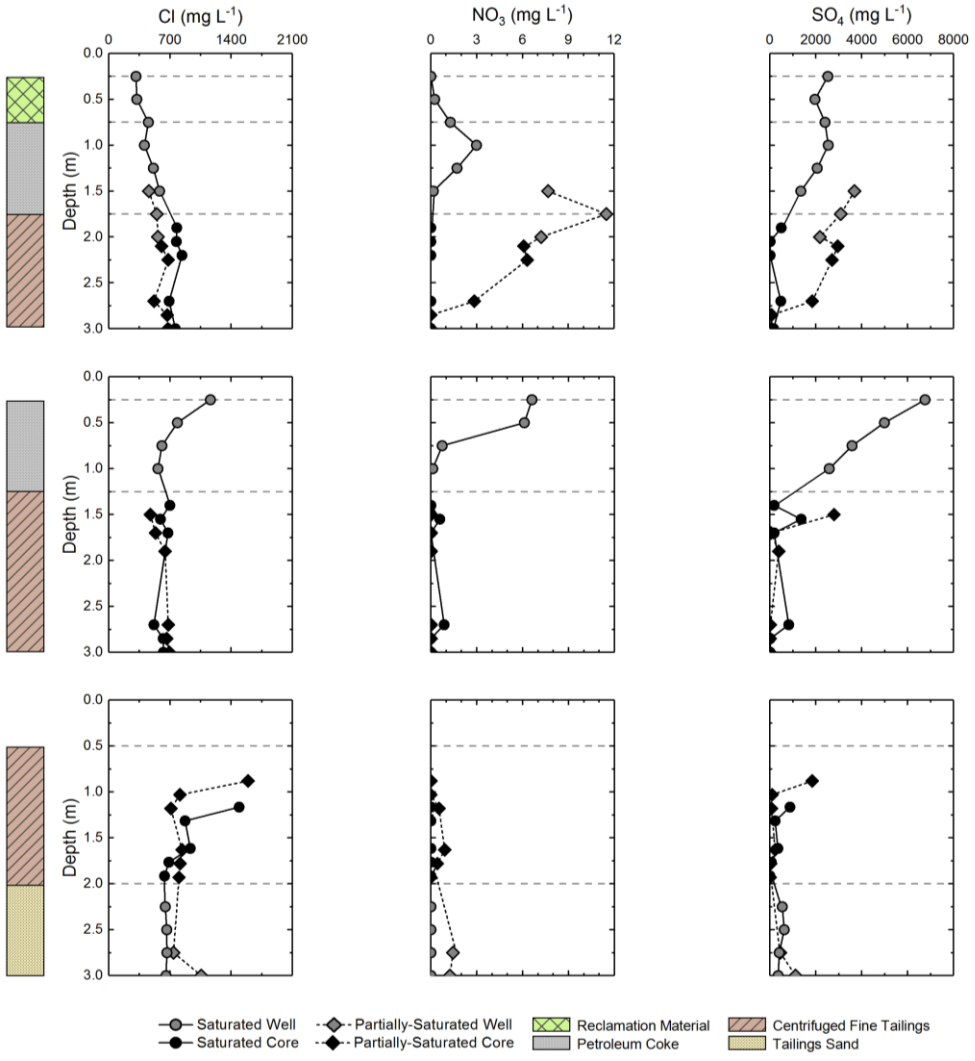


Figure 4-3: Well and core porewater concentrations of Cl, $NO_3^-$, and $SO_4^{2-}$ with depth for all lysimeters. The bars along the left-hand side of the graphs designate the material within the three layering schemes.

*Redox Sensitive Species*

Iron concentrations ranged from below the method detection limit to 3.9 mg $L^{-1}$, averaging 0.29 ± 0.61 mg $L^{-1}$. Porewater Fe concentrations are higher in the CFT layers, where the mean concentration is 0.36 mg $L^{-1}$. Concentrations are highest in the CFT layers in L1 and L4, where Fe increases from 0.17 and 0.27 mg $L^{-1}$ at the base of the CFT to 2.0 and 0.55 mg $L^{-1}$ at just below the petroleum coke interface, for L1 and L4, respectively. Above this interface, concentrations decrease to below detection limits, however a sharp increase is noted in the reclamation material in L4. Similar trends are noted for L2 and L5, where concentrations increase from 0.15 and 0.19 mg $L^{-1}$ at the base of the CFT to 1.2 and 0.3 mg $L^{-1}$ at the top of this layer, for L2 and L5, respectively. Iron concentrations in L3 and L6 porewater are comparable over depth and generally increase slightly toward surface within the CFT layers. All porewater samples collected from tailings sand layers were below detection with respect to Fe.

Manganese concentrations ranged from 0.009 to 2.7 mg $L^{-1}$, averaging 0.35 ± 0.09 mg $L^{-1}$. Contrary to expected redox behavior, Mn increases toward surface in L1, L2, L4 and L5, with the highest concentration measured at the surface of L4. Concentrations in the petroleum coke layer in L5 exhibit an increase in the first meter above the CFT interface, but then decrease slightly above this point toward surface. In L3 and L6, porewater concentrations remain consistent with depth in the CFT, and increase within the tailings sand. In L6 a peak is noted at roughly 2.5 m depth, below which concentrations decrease toward the bottom of the tailings sand layer.

Ammonia as nitrogen concentrations ranged from 0.3 to 34.8 mg $L^{-1}$ and averaged 8.5 ± 6.9 mg $L^{-1}$ ($n$=59) in porewater samples taken from all lysimeters. Ammonia as nitrogen concentrations in the CFT averaged 9.5 ± 5.4 mg $L^{-1}$ ($n$=33), which is in the range of values reported by Heaton (2015). In L4, concentrations increase moving upward in the CFT and then decrease toward the surface of the petroleum coke. There is a small increase in $NH_3$-N concentrations at the coke-reclamation material interface, but concentrations decrease to nearly 0 mg $L^{-1}$ at surface. In L5, concentrations remain constant with depth at ~10 mg $L^{-1}$. Concentrations increase to 33 mg $L^{-1}$ at the CFT-coke interface, and subsequently decrease to ~0 mg $L^{-1}$ at surface. In L3 and L6, $NH_3$-N concentrations in the CFT are relatively constant with depth at ~10 mg $L^{-1}$. Concentrations decrease in the tailings sand below the CFT. The greatest variation between fully- and partially-saturated systems is observed between L1 and L4. There is a much larger increase toward surface in the L1 CFT layer, where $NH_3$-N concentrations peak at

~35 mg $L^{-1}$ and then sharply decrease after the coke-CFT interface. This behaviour at the interface does not occur in L4, where concentrations increase across the interface and then gradually decrease upward in the petroleum coke.

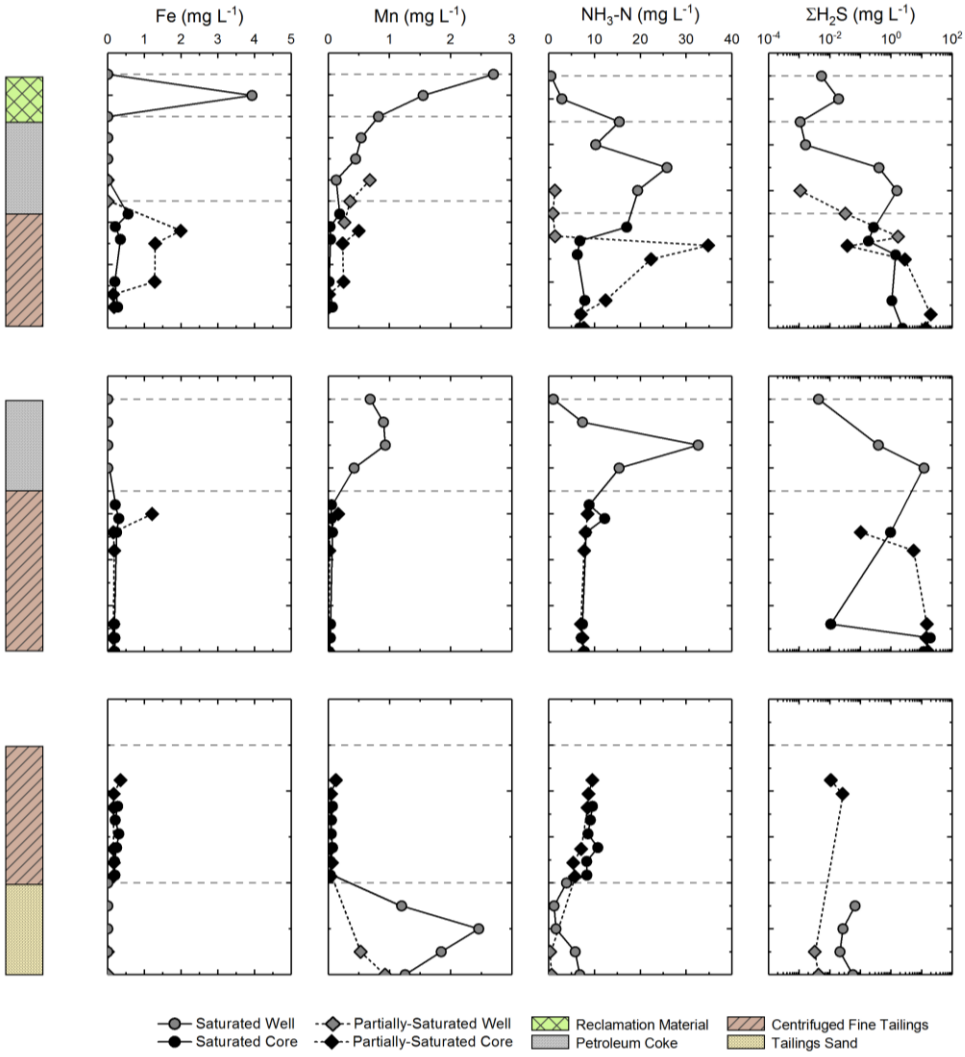


Figure 4-4: Well and core porewater concentrations of Fe, Mn, $NH_3$-N, and $\Sigma H_2S$ with depth for all lysimeters. Note the $\Sigma H_2S$ concentration scale is logarithmic. The bars along the left-hand side of the graphs designate the material within the three layering schemes.

Dissolved sulfide (reported as $\Sigma H_2S$) concentrations ranged from below the method detection limit to 19.7 mg $L^{-1}$, averaging 3.3 ± 6.0 mg $L^{-1}$ ($n$=44). The CFT layers generally contain higher $\Sigma H_2S$ concentrations than the surrounding layers, averaging 6.2 ± 7.4 mg $L^{-1}$. Values measured in this study are highly elevated compared to values from Heaton (2015), who reported an average of 0.028 mg $L^{-1}$ in a number of full scale CFT deposits. In L4, concentrations increase with depth from 0.005 to 0.019 mg $L^{-1}$ across the reclamation material layer, and from

0.019 to 1.54 mg $L^{-1}$ across the petroleum coke layer. Large variation in $\Sigma H_2S$ values are present when comparing the fully- and partially-saturated CFT in L1 and L4. In L4, concentrations in the CFT decrease below the petroleum coke interface and then increase to around 2.34 mg $L^{-1}$ at the bottom of this unit. In L1, concentrations also decrease at the petroleum coke-CFT interface; however, they then increase to 19.7 mg $L^{-1}$ just above the base of this unit. In L2 and L5, there is also a general increase in $\Sigma H_2S$ concentrations with depth. Concentrations in the petroleum coke of L5 rise from 0.004 mg $L^{-1}$ at surface to 11.9 mg $L^{-1}$ at just above the petroleum coke-CFT interface. Concentrations drop over this interface, but continue to increase with depth in the CFT to around 18 mg $L^{-1}$. Sulfide concentrations in L3 and L6 remain low throughout the uncovered system, reaching a maximum of 0.026 mg $L^{-1}$ in the CFT at depth. Values measured in L3 and L6 are comparable to concentrations reported by Heaton (2015), suggesting similar redox conditions occur in the CFT-tailings sand systems.

*Trace Elements*

In total, thirty-eight trace elements were analyzed in the lysimeter porewater samples. Five of these elements (As, Mo, Ni, Se, and V) were selected for further study based on their elevated concentrations, their identification as contaminants that may impact future pore- and surface-water quality, and their presence in porewater in full-scale CFT (Heaton, 2015) and coke (Nesbitt, 2016) deposits.

Arsenic porewater concentrations ranged from below method detection limits to 179.1 µg $L^{-1}$, averaging 58.6 ± 41.7 µg $L^{-1}$. Concentrations are typically higher in the well samples than the core samples. In L4, concentrations increase with depth from near 50 µg $L^{-1}$ at the surface of the reclamation material to around 150 µg $L^{-1}$ just above the petroleum coke–CFT interface. Below the interface concentrations sharply decrease to approximately 25 µg $L^{-1}$ throughout the CFT layer. Concentrations in the wells of L4 are higher than those measured in L1, however this trend reverses in the CFT where concentrations in L1 are elevated by 25 to 50 µg $L^{-1}$ when compared to L4 at similar depths. Similar trends are noted in L2 and L5; with an increase downward from surface, a drop in concentration over the petroleum coke-CFT interface, and elevated concentrations in the CFT of L2 when compared with L5 at similar depths. In L3 and L6, As concentrations increase with depth and exhibit a large increase across the CFT-tailings sand interface. Centrifuged fine tailings concentrations in L3 system are elevated by nearly 100 µg $L^{-1}$

when compared with samples taken at similar depths in L6. Elevated concentrations of As in L3 and L6 suggest that CFT may be the source of As in the lysimeter systems.

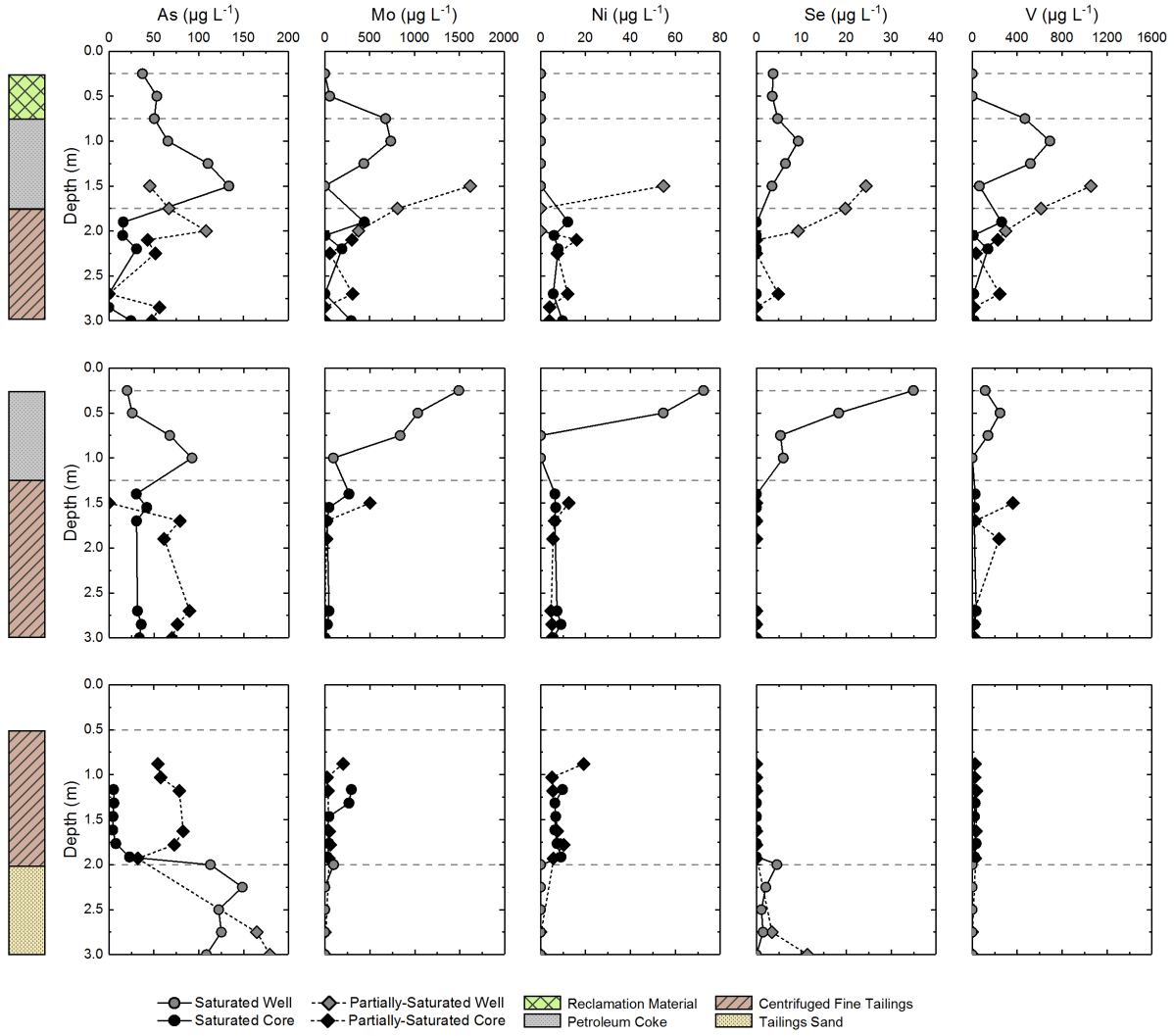


Figure 4-5: Well and core porewater concentrations of As, Mo, Ni, Se, and V with depth for all lysimeters. The bars along the left-hand side of the graphs designate the material within the three layering schemes.

Molybdenum porewater concentrations ranged from below the method detection limit to 1620 µg $L^{-1}$, averaging 217 ± 352 µg $L^{-1}$. Concentrations are generally elevated in the well samples compared to the core samples taken in the CFT. In L4, concentrations are below detection at surface and increase across the reclamation soil and into the petroleum coke layer. Molybdenum concentrations reach a maximum of around 740 µg $L^{-1}$ in the petroleum coke and then decrease toward the CFT layer. Below the petroleum coke-CFT interface concentrations increase slightly, remaining stable throughout the CFT at around 180 µg $L^{-1}$. In L1 concentrations are highest at the

top of the water table in the petroleum coke (1620 µg $L^{-1}$) and decrease across the petroleum coke-CFT interface. Molybdenum concentrations throughout the CFT of L1 are comparable to those measured in the L4. In L5 concentrations are highest at surface (1490 µg $L^{-1}$) and decrease rapidly with depth in the coke layer. Below the petroleum coke-CFT interface Mo concentrations average 80 µg $L^{-1}$ in both L2 and L5 and remain stable with depth. In L3 and L6 concentrations average 94 µg $L^{-1}$ in the CFT and 46 µg $L^{-1}$ in the tailings sand. Concentrations in the systems decrease slightly across the CFT-tailings sand interface, and remain constant with depth. Elevated Mo concentrations in coke layers and relatively low concentrations in L3 and L6 suggest coke is likely the principal material source of Mo in the lysimeter systems.

Table 4-1: Summary statistics for trace element porewater concentrations for all lysimeters (*n*=56). Only trace elements with a mean above 1 µg $L^{-1}$ are shown. Minimum values are excluded as all elements had at least one measurement below method detection limits. Median values that were below method detection limits are displayed as BMDL. All values are in µg $L^{-1}$.

| Element | Mean | Standard Deviation | Median | Maximum | 90% Confidence Interval |
|---|---|---|---|---|---|
| Al | 16 | 47 | BMDL | 210 | 42 |
| As | 58 | 42 | 48 | 180 | 120 |
| B | 3,300 | 1,200 | 3,280 | 5,300 | 4,600 |
| Ba | 170 | 140 | 150 | 420 | 340 |
| Co | 45 | 77 | 26 | 260 | 250 |
| Fe | 290 | 620 | 160 | 3,900 | 550 |
| Li | 270 | 100 | 230 | 650 | 400 |
| Mn | 380 | 590 | 930 | 2,700 | 930 |
| Mo | 220 | 360 | 48 | 1,600 | 740 |
| Ni | 8.0 | 14 | 5.6 | 73 | 13 |
| Pb | 1.4 | 1.9 | BMDL | 6.2 | 4.3 |
| Rb | 28 | 17 | 22 | 120 | 46 |
| Sb | 1.6 | 1.9 | 1.2 | 7.4 | 4.6 |
| Se | 4.6 | 9.1 | BMDL | 52 | 14 |
| Sr | 2.0 | 2.1 | 0.95 | 10 | 4.2 |
| U | 3.6 | 4.3 | 2.9 | 18 | 11 |
| V | 110 | 210 | 22 | 1,100 | 360 |
| W | 3.2 | 6.9 | 2.1 | 43 | 5.1 |
| Zn | 4.8 | 8.5 | BMDL | 36 | 17 |
| Zr | 9.2 | 8.4 | 12 | 27 | 19 |

Nickel porewater concentrations ranged from below the method detection limit to 73 µg $L^{-1}$, averaging 7.8 ± 13 µg $L^{-1}$ across all lysimeters. Average Ni concentrations are similar in both the well and core porewater samples. In L1 and L4, Ni remains below detection in all samples above the CFT, with the exception of a sample in the partially-saturated system that measured 54.8 µg $L^{-1}$ just above the coke-CFT interface. Below this interface concentrations of Ni are somewhat elevated but remain relatively constant with depth, averaging 8.5 µg $L^{-1}$ throughout. Concentrations are most highly elevated at the surface of L5, where Ni rapidly increases above the petroleum coke-CFT interface toward surface, reaching a maximum of 72.6 µg $L^{-1}$. Below the petroleum coke-CFT interface in L5, Ni concentrations remain consistent with depth at an average value of 6.7 µg $L^{-1}$. In L3 and L6, concentrations in the CFT again remain stable with depth, averaging 8.3 µg $L^{-1}$. Below the CFT-tailings sand interface Ni concentrations drop to below detection in all samples.

Selenium porewater concentrations ranged from below the method detection limit to 52.5 µg $L^{-1}$, averaging 4.53 ± 8.96 µg $L^{-1}$ across all lysimeters. Porewater concentrations are elevated in petroleum coke layers, and typically below the detection limit in CFT layers. In L4, Se is present at the surface of the reclamation material (3.7 µg $L^{-1}$) and increases downward into the petroleum coke where it begins a decrease at approximately one meter depth. Selenium is below detection in all CFT porewater samples in this system. In L1 concentrations are elevated above the coke-CFT interface at around 30 µg $L^{-1}$ and decrease across the interface. Selenium decreases to below detection limits in the CFT porewater with a small increase at approximately 2.75 m depth. In L5, a sharp increase above the petroleum coke-CFT interface is observed, with concentrations reaching a maximum of 52.5 µg $L^{-1}$ at surface. Selenium was below detection limits in all CFT porewater samples from these systems. In L3 and L6, Se is below detection in all CFT porewater samples. Concentrations increase into the tailings sand of this system, averaging 7.1 µg $L^{-1}$ throughout.

Vanadium porewater concentrations ranged from below the method detection limit to 1060 µg $L^{-1}$, averaging 111 ± 203 µg $L^{-1}$ across all lysimeters. Average concentrations are around three-fold higher in the petroleum coke porewater samples compared to those collected from the CFT cores. In L4 V concentrations are below detection at the surface of the reclamation material and increase downward into the petroleum coke. Concentrations reach a maximum of 691 µg $L^{-1}$ at around 1.0 m depth and then begin to decrease toward the coke-CFT interface in this system. In

L1, concentrations are highest just above the coke-CFT interface and decrease into the CFT. In both L1 and L4, V concentrations remain relatively stable with depth in the CFT, averaging 97.2 µg $L^{-1}$ throughout. In L5, concentrations are elevated at surface (116 µg $L^{-1}$) but a rapid decrease with depth is not observed as with Mo, Ni, and Se. Concentrations in L5 CFT remain fairly stable with depth, averaging 68.3 µg $L^{-1}$. In L3 and L6, V is below detection limits in all well samples collected from both the saturated and partially-saturated systems. Vanadium is, however, present in the CFT core samples, and remains constant with depth at around 25 µg $L^{-1}$. Elevated V concentrations in coke layers and relatively low concentrations in L3 and L6 porewater suggest that coke is likely the principal source of V in the lysimeter systems.

*Stable Isotopes of Water*

Oxygen-18 ($\delta^{18}O$) values ranged from -13.98 to -11.30‰, and averaged -12.71‰ across all lysimeters. Deuterium ($\delta^{2}H$) values ranged from -122.50 to -108.60‰, averaging -115.43‰ across all lysimeters. All isotopic values plotted below the local meteoric water line (LMWL; Baer et al., 2016), indicating that the waters are enriched in both isotopes compared to local meteoric waters. Porewater values tended to plot along the local evaporative line (LEL; Gibson et al., 2015), indicating that the porewater has undergone evaporation.

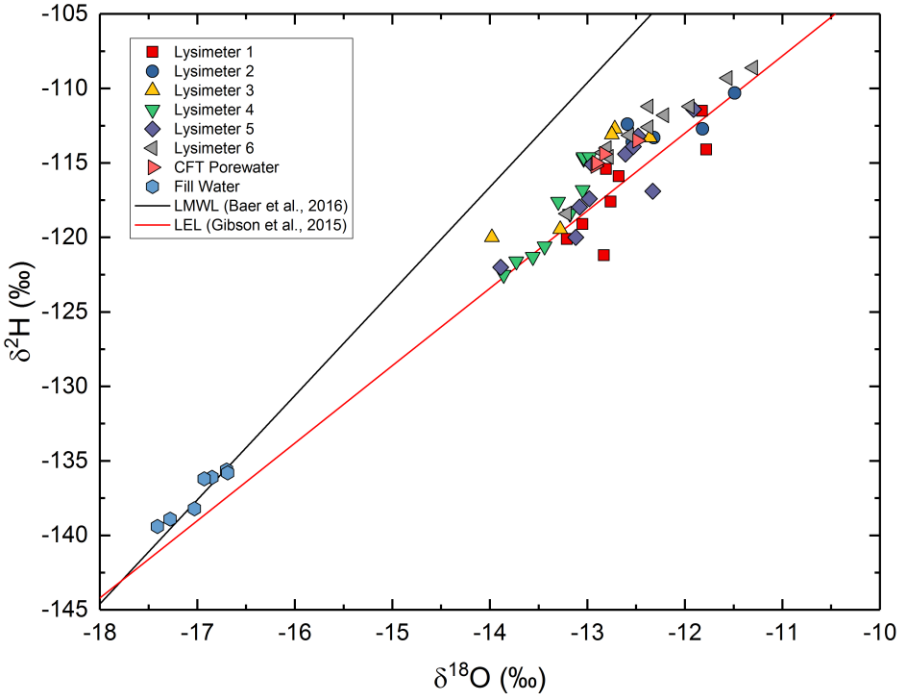


Figure 4-6: Isotopic plot of lysimeter porewater samples, initial CFT porewater samples, and lysimeter fill water. "LMWL" is the local meteoric water line as described by Baer et al. (2016). "LEL" is the local evaporation line as described by Gibson et al. (2015).

### *4.1.2 Mineralogy*

XRD patterns were generally consistent between all CFT samples, including those from the partially-saturated lysimeters ($n$=8), saturated lysimeters ($n$=9), and fresh CFT ($n$=2). All samples exhibited peaks for illite [$K_{0.6}(H_3O)_{0.4}Al_{1.3}Mg_{0.3}Fe^{2+}_{0.1}Si_{3.5}O_{10}(OH)_2 \cdot (H_2O)$], kaolinite [$Al_2Si_2O_5(OH)_4$], chlorite [$(Mg,Fe,Li)_6AlSi_3O_{10}(OH)_8$], and quartz [$SiO_2$]. Several samples also contained montmorillonite [$Na_{0.2}Ca_{0.1}Al_2Si_4O_{10}(OH)_2(H_2O)_{10}$], calcite [$CaCO_3$], and dolomite [$CaMg(CO_3)_2$]. The results of this study are similar to those by Heaton (2015), who found that quartz, kaolinite, illite, and chlorite dominate the CFT mineral assemblage. These results are consistent with the mineralogic composition of petrologic end members in oil sands ore reported by Osacky et al. (2013).

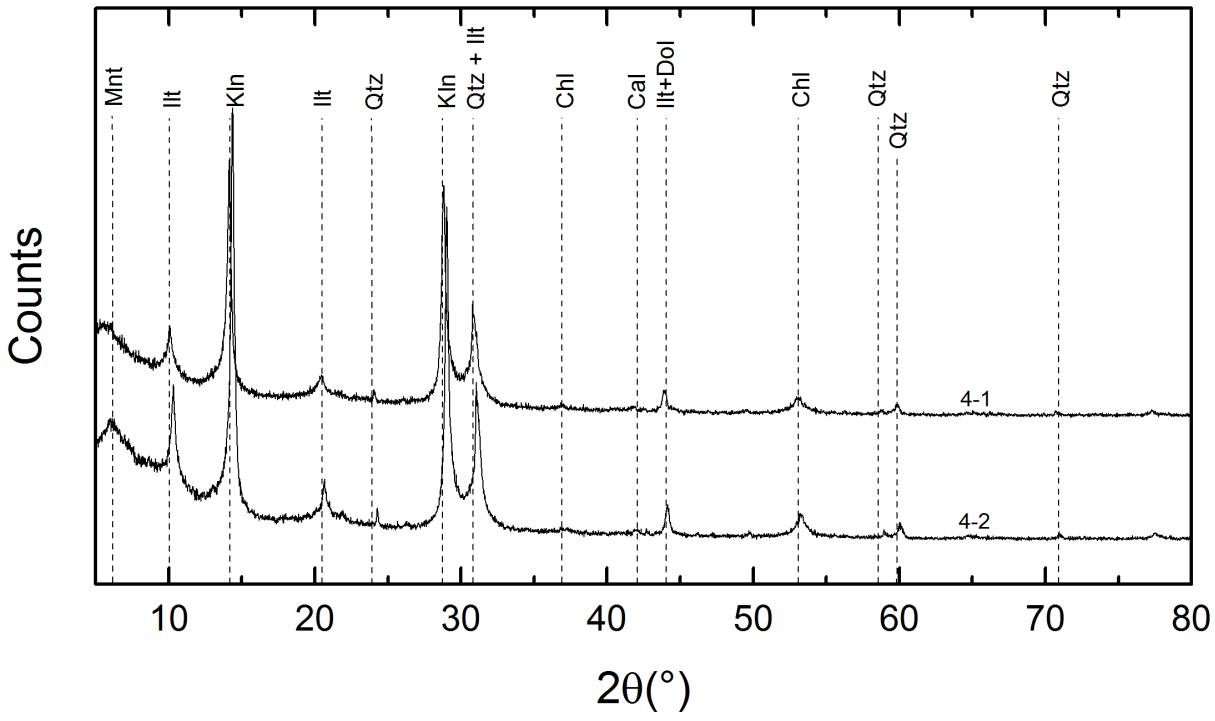


Figure 4-7: X-ray diffraction spectra for initial CFT oriented samples prepared by ethylene glycol solvation.

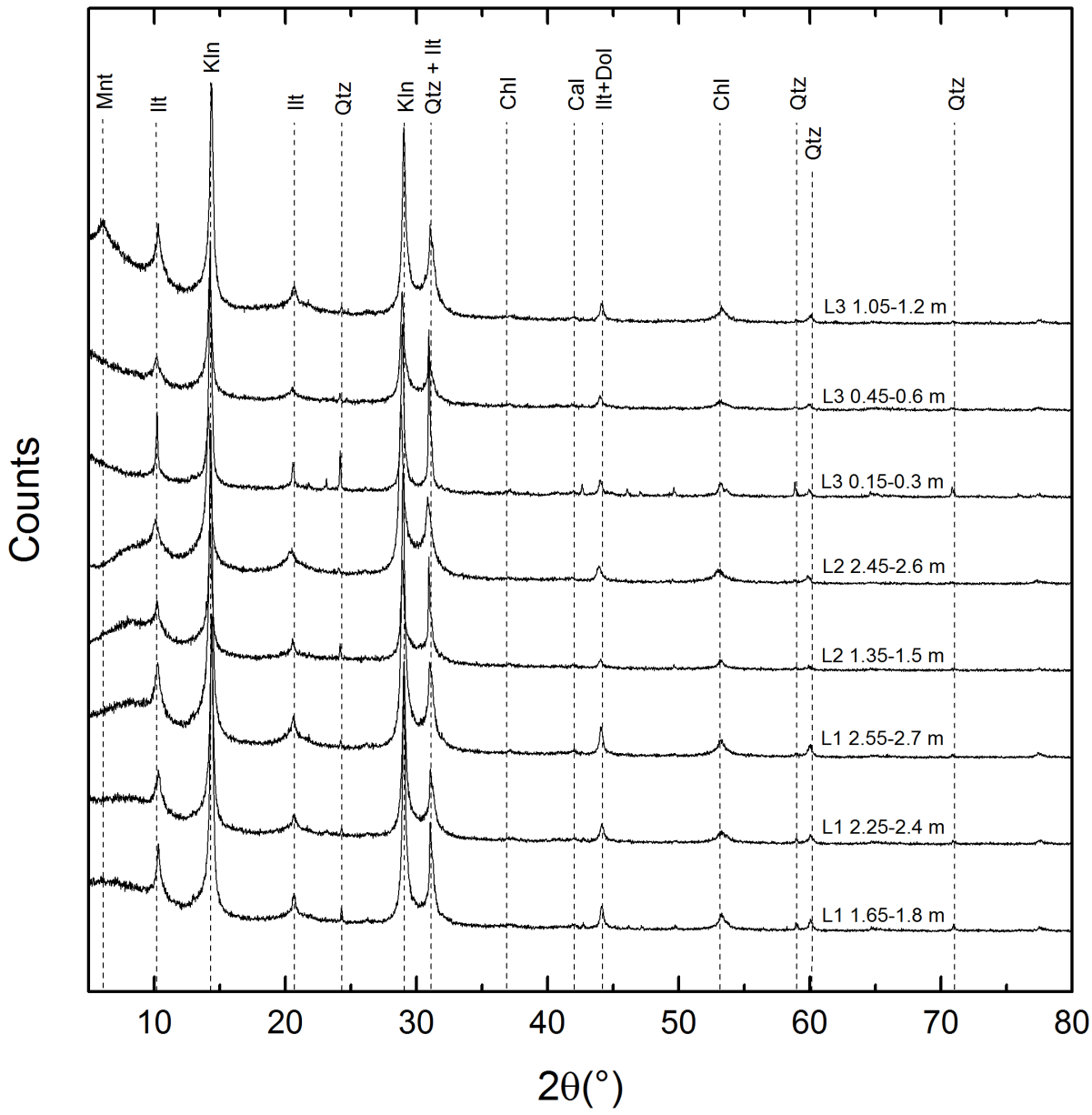


Figure 4-8: X-ray diffraction spectra for CFT oriented samples collected from the unsaturated lysimeters. Oriented samples were prepared by ethylene glycol solvation.

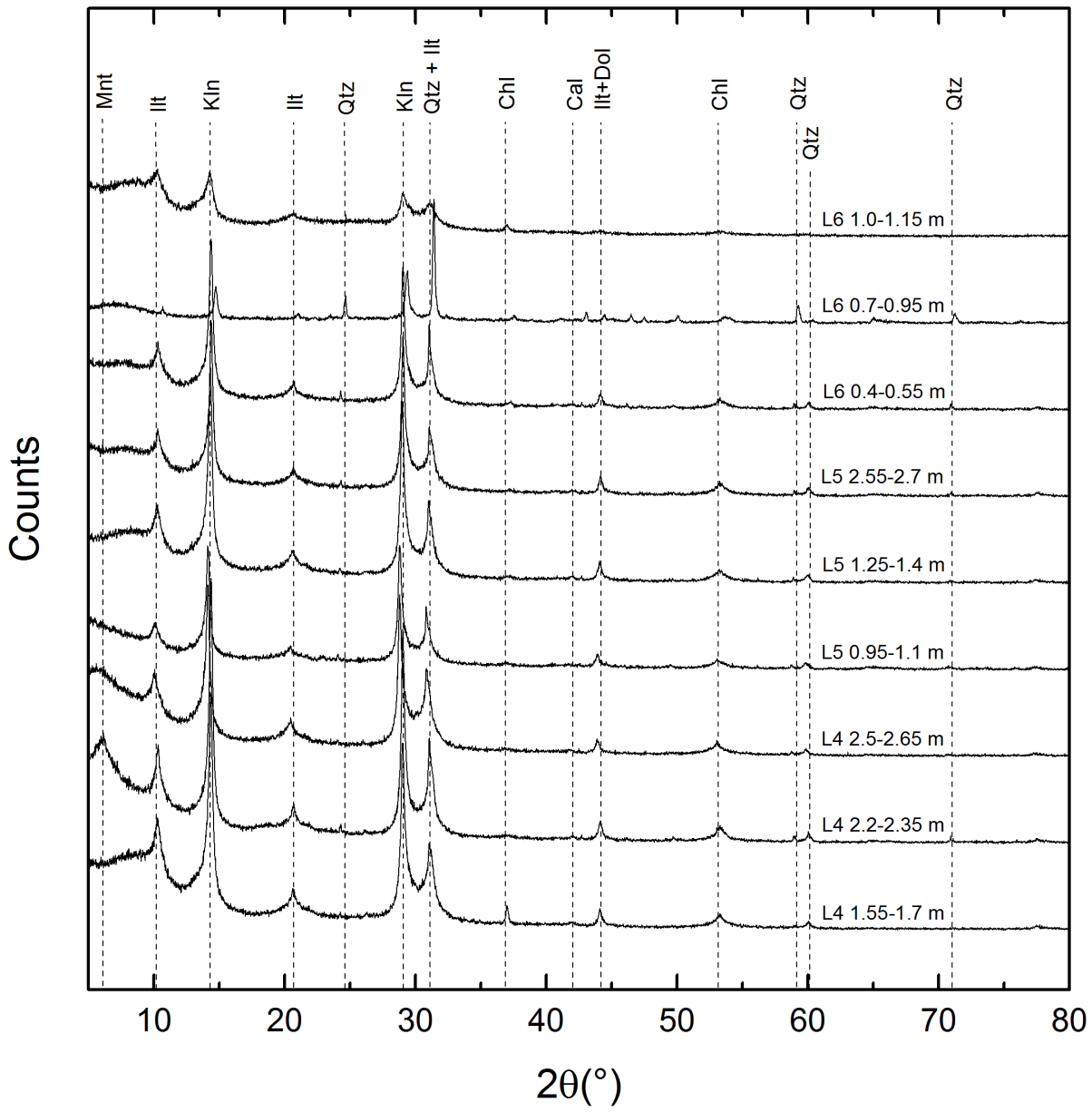


Figure 4-9: X-ray diffraction spectra for the CFT oriented samples collected from the saturated lysimeters. Oriented samples were prepared by ethylene glycol solvation.

## 4.2 Sequential Extractions

Overall total leachability was calculated by taking the sum of leachable concentrations from each extraction step for a single sample. Overall mean values were then calculated for all samples for Mo, V and Ni (Table 4-2). Arsenic and Se were also analyzed at each extraction step during this study, however concentrations for these elements were below detectable concentrations in all samples–suggesting they are not leachable from petroleum coke. Statistical analyses were only performed on samples from sites AM, CX, and DM ($n$ = 110), as samples for the oxidizable

fraction from site AB were lost due to lab error and not analyzed. Statistical analyses were performed in OriginPro 2017 (Version 9.40) using the descriptive statistics function. Large standard deviations can be attributed to the wide range of sample depths, ages, and grain sizes used in this study.

Table 4-2: Overall average leachability values for Mo, Ni, and V in petroleum coke at each extraction step. All values are presented in mg $kg^{-1}$.

| Element | Extraction Step | | | | |
|---|---|---|---|---|---|
| | **F1 Water Soluble** | **F2 Exchangeable** | **F3 Fe & Mn Oxides** | **F4 Acid Soluble** | **F5 Organics** |
| Molybdenum | 0.16 ± 0.067 | 0.44 ± 1.0 | 0.11 ± 0.23 | 0.040 ± 0.017 | 0.15 ± 0.24 |
| Nickel | 0.27 ± 0.20 | 3.1 ± 0.71 | 0.22 ± 0.46 | 0.47 ± 0.097 | 0.20 ± 0.48 |
| Vanadium | 3.8 ± 2.4 | 5.5 ± 2.3 | 1.3 ± 0.66 | 0.93 ± 0.23 | 1.02 ± 0.30 |

Vanadium total potential leachability ranged from 3.63 to 25.2 mg $kg^{-1}$, averaging 12.0 ± 5.72 mg $kg^{-1}$. The majority of V is strongly bound to exchangeable surfaces (~43%), however a large portion is also associated with weak binding sites and is readily liberated in the water soluble fraction (~33%).

Nickel total potential leachability ranged from below the method detection limit to 12.8 mg $kg^{-1}$, averaging 3.56 ± 2.48 mg $kg^{-1}$. The majority of nickel is associated with the exchangeable fraction (~72%) and acid soluble minerals (~11%).

Molybdenum total potential leachability ranged from 0.04 to 7.20 mg $kg^{-1}$, averaging 1.14 ± 1.75 mg $kg^{-1}$. The majority of molybdenum is strongly bound to exchangeable surfaces (~50%), with equal amounts weakly bound to exchangeable surfaces (~17%) and associated with organic matter (~17%).

Comparing leachability at each grain size fraction (Figure 4-10) further shows the association of Mo, Ni and V with water soluble and exchangeable surfaces. Additionally, an apparent relationship between grain size and overall leachability is present, where the smallest grain size fraction ($f_1 \leq 149$ μm) generally exhibits higher leachability compared to larger grain size fractions.

## 4.3 Petroleum Coke Surface Area

Surface area of non-sieved petroleum coke ranged from 1.04 to 9.28 $m^2\ g^{-1}$, averaging 5.59 $m^2\ g^{-1}$. Surface area was related to grain size distribution for whole rock samples (Figure 4-11), where coarser samples had lower surface area and finer samples had larger surface area.

Average surface area for sieved samples (Table 4-3) show the decrease in surface area with increasing coke grain size.

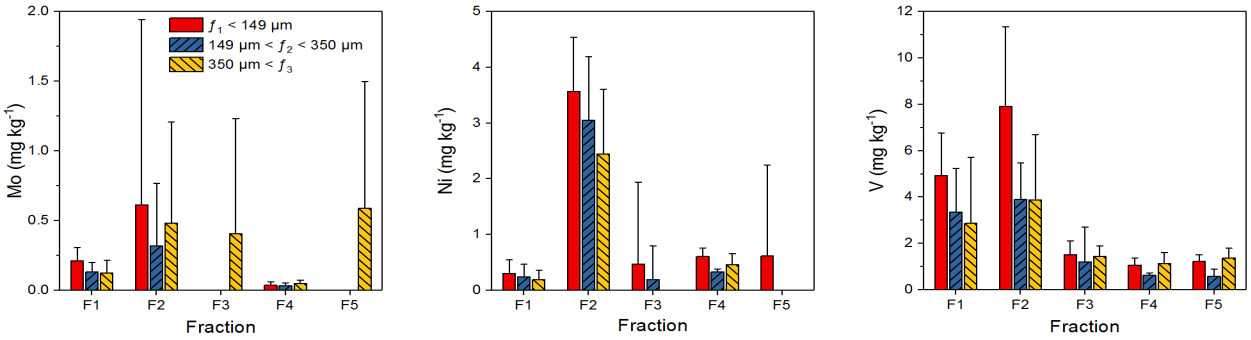


Figure 4-10: Mean results from the sequential extraction of Syncrude fluid coke as a function of grain size. The vertical axes display the trace element of interest in mg $kg^{-1}$, and the horizontal axes separate the different sequential extraction fractions. F1 is the water-soluble fraction, F2 is the exchangeable fraction, F3 is the reducible fraction, F4 is the acid-soluble fraction, and F5 is the oxidizable fraction.

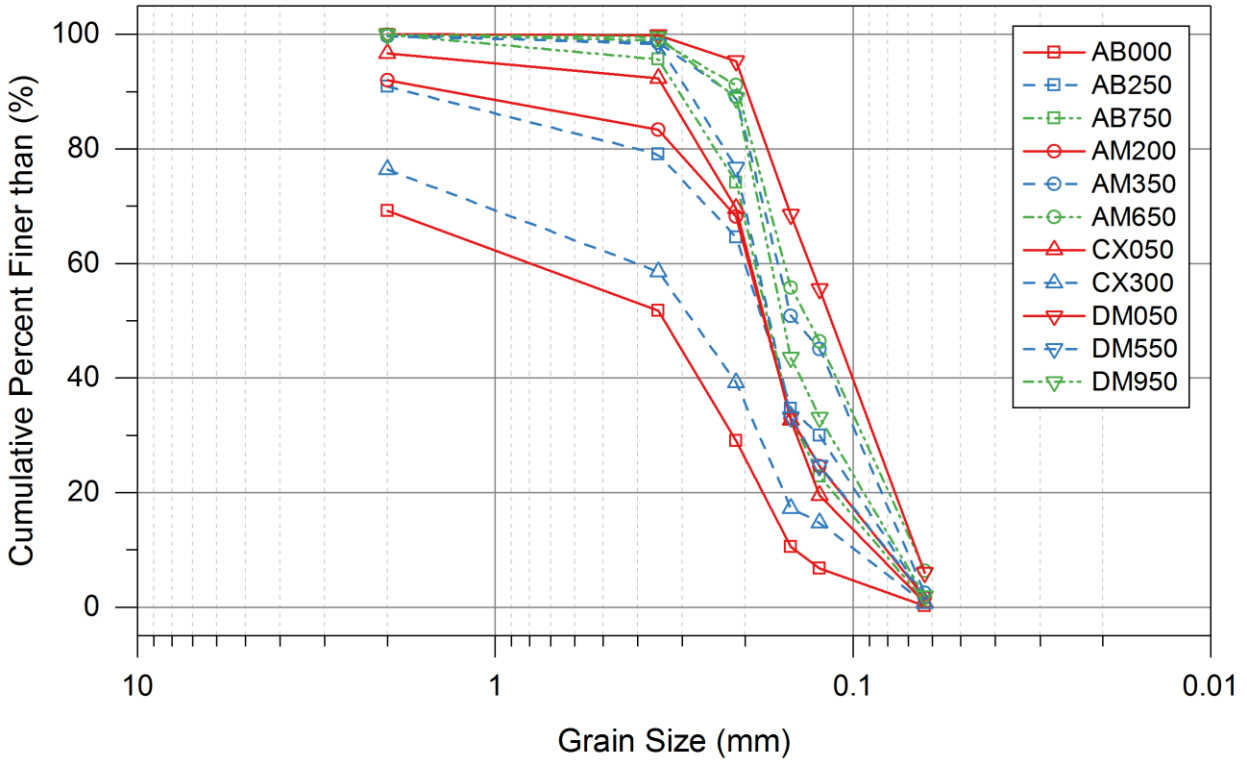


Figure 4-11: Grain size distribution curves for samples used in the sequential extraction experiments. Samples AB000, AB250, AB750, AM350, CX050 and DM550 were used for whole rock surface area analysis.

Table 4-3: Mean surface area results for each of the grain size fractions used in the coke extraction study. Surface areas for the sieved coke were measured in triplicate for each grain size fraction. Whole rock is the average of six samples of un-sieved coke.

| **Grain Size Fraction ($m^2$ $g^{-1}$)** | | | |
|---|---|---|---|
| **$f_1$ < 149 µm** | **149 µm < $f_2$ < 350 µm** | **350 µm < $f_3$** | **Whole Rock** |
| 6.268 | 3.036 | 2.191 | 5.59 |

# CHAPTER 5: DISCUSSION

## 5.1 Lysimeter Experiments

### *5.1.1 Water Movement*

To evaluate Hypothesis 1, 2 and 3, there must be an upward movement of porewater from the CFT layers through the petroleum coke layers, or downward through the tailings sand layer. This porewater movement will affect the system in two ways: (1) the upward or downward flux of CFT porewater will transport trace elements, exchangeable cations, and inorganic anions into adjacent units; and (2) the influx of these ions will drive the release and influence the transport of trace elements from petroleum coke and associated mineral surfaces.

During CFT production, MFT is dredged from the mudline of tailings ponds, amended with gypsum and polyacrylamide, and decanter centrifuged at several times the force of gravity. While significant dewatering of the tailings occurs during this process, remnant porewater held in the CFT pores preserves the composition of the original OSPW influenced MFT porewater. Oil sands process-affected water typically contains distinct water isotope signatures due to evaporation during the extraction process, and elevated Cl, B, and Li from the bitumen ore that becomes enriched during continual water recycling. Therefore, by observing changes in $\delta^{18}O$, $\delta^{2}H$, Cl, B, and Li we can evaluate the movement of CFT porewater in the lysimeter systems.

Water used in the bitumen extraction circuit becomes enriched in the heavy isotopes of water ($\delta^{18}O$ and $\delta^{2}H$) due to intense evaporation during steam generation (Baer et al., 2014). Tailings pond waters derived from the water used during extraction are further enriched in these isotopes due to the continual recycling of OSPW in the extraction circuit. As a result, OSPW has a unique isotopic signature that can be used to trace water moving from associated tailings. Stable isotopes of several Mildred Lake site waters were catalogued by Baer et al. (2016). In that study, OSPW averaged -13.1 and -115.0 ‰ for $\delta^{18}O$ and $\delta^{2}H$, respectively. This same study also characterized MFT porewater, and found isotopic averages of -12.5 and -115.8 ‰ for $\delta^{18}O$ and $\delta^{2}H$, respectively. Porewater collected from CFT in the lysimeter study averaged -12.8 and -114.9 ‰ for $\delta^{18}O$ and $\delta^{2}H$, respectively. Comparing these values to those measured in the

lysimeters, it becomes clear that there is a definite influence of CFT porewater in each system. The overall average for all porewaters in the lysimeter study were -12.7 and -115.4 ‰ for $\delta^{18}O$ and $\delta^{2}H$, respectively; exhibiting a relatively good fit with average isotopic compositions of OSPW, MFT and CFT porewaters.

Further evidence of CFT porewater influence is observed when comparing the values measured in the lysimeters to those of the fill water used to saturate the lysimeters, and the isotopic composition of Mildred Lake meteoric waters (Figure 4-6). Fill water isotopic compositions averaged -17.0 and -137.2 ‰ for $\delta^{18}O$ and $\delta^{2}H$, respectively. Mildred Lake precipitation averaged -17.5 and -141.6 ‰ for $\delta^{18}O$ and $\delta^{2}H$, respectively. Clearly, these values are depleted relative to CFT porewater and other process-affected water on site.

Moving to depth trends of $\delta^{18}O$ (Figure 5-1) some differences between each respective layering scheme become clear. In L4, porewaters become slightly more depleted toward surface but remain relatively constant throughout, indicating lower evaporation rates in this system (Baer et al., 2016). Lysimeter 5 displays an opposite trend as porewaters become increasingly more enriched in $\delta^{18}O$ toward surface. This trend of increase is evidence for high evaporation rates from the uncovered petroleum coke surface. Lack of detailed $\delta^{18}O$ profiles in L3 and L6 prohibit robust conclusions for water movement; however, measurements in the tailings sand are similar to those in the CFT, indicating CFT is main source of porewater in this layer.

Assuming Cl acts as a conservative tracer in the lysimeter systems, conclusions can be made based on the trends observed in porewater concentrations over depth (Figure 5-1). In L1 and L4, Cl porewater concentrations decrease slightly toward surface, but remain highly elevated above precipitation and fill water concentrations. Elevated Cl concentrations at surface are evidence for the large influence CFT porewater has on these systems, and a relatively uniform concentration gradient suggests low evaporation. In L5, Cl concentrations remain uniform with depth in the CFT and increase toward surface in the petroleum coke. As in L1 and L4, high Cl concentrations indicate a large influence of CFT porewater in this system, while increasing concentrations toward surface provide further evidence for a high level of evaporation, consistent with isotope data. In L3 and L6, Cl depth profiles in the tailings sand remain homogenous over depth at concentrations nearly identical to the porewater in the CFT directly above this unit– providing evidence to suggest that porewaters in the tailings sand are almost entirely derived from CFT.

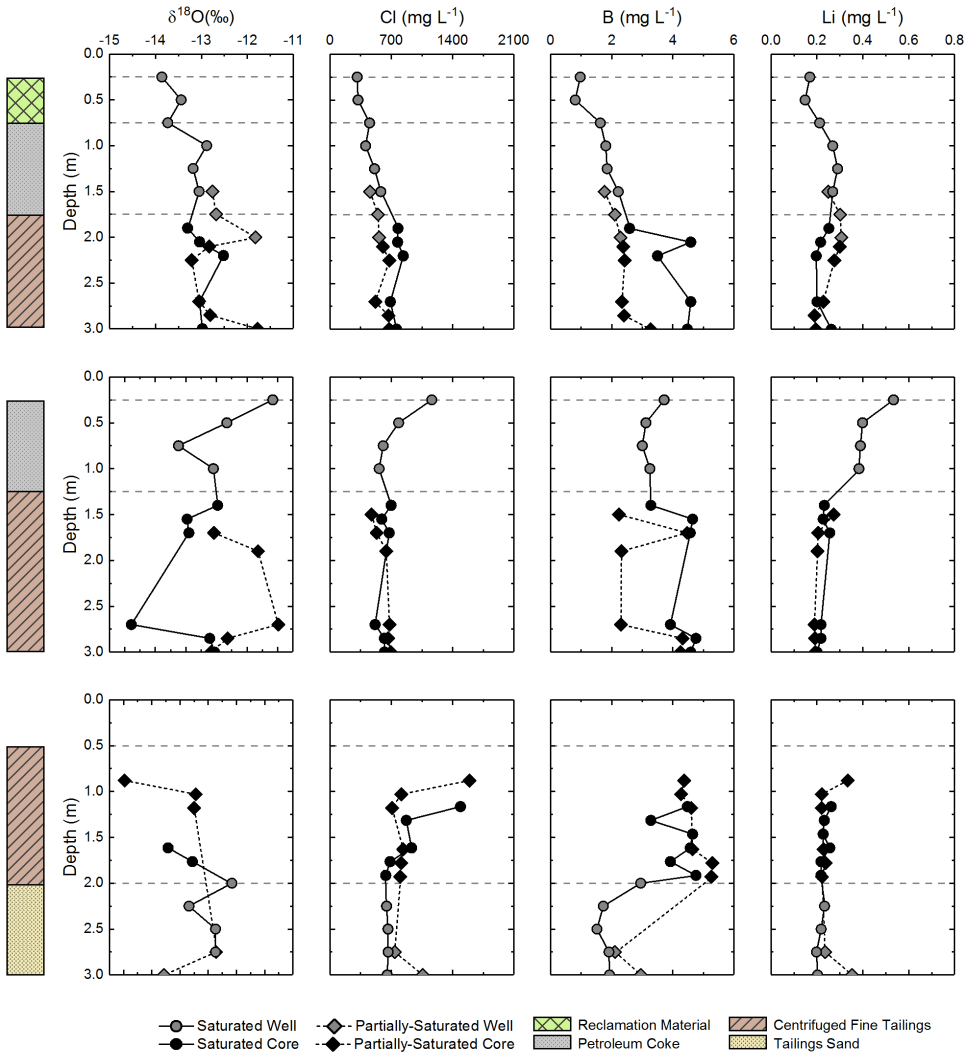


Figure 5-1: Porewater $\delta^{18}O$ signatures, and Cl, B, and Li concentrations over depth for all lysimeters. The bars along the left-hand side of the graphs designate the material within the three layering schemes.

Similar to Cl, elevated B and Li are indicative of OSPW influenced CFT porewater. While not completely conservative in nature, elevated concentrations of these elements provide more evidence for the interaction of CFT porewater with overlying units. Depth trends for B and Li (Figure 5-1) show similar concentrations to CFT porewater throughout all systems. In L1 and L4, there is a slight decrease moving toward surface, and this decrease is more pronounced in the fully-saturated system due to dilution by the fill water. In L5, concentrations of both elements tend to increase toward surface, again indicative of the strong evaporative gradient in this system. It is important to note that, in the fill water, B was below the method detection limit and Li was

measured at 0.013 mg $L^{-1}$. Therefore, inputs of these elements from the fill water was negligible and the majority of B and Li is sourced from the CFT porewater.

Further evidence for CFT porewater release in each system is the noted compaction, which is attributed to CFT dewatering and consolidation (Cilia, 2017; Table 5-1). Measurements taken throughout the study period indicate that within a year of placement, settlement occurred at an average of 25% of the CFT height, with a higher rate of consolidation occurring in those lysimeters containing thicker CFT units. The consolidation–or physical dewatering–of CFT releases porewater proportional to the total volume of compaction occurring. Due to the lack of bottom drain in the covered layering schemes (L1, L2, L4, and L5), dewatering would drive an advective flux toward surface as pore spaces are compacted and porewater is displaced. In the saturated covered systems (L4 and L5), dewatering results in mixing between the CFT porewater and fill water and the eventual transport of dissolved ions to surface. Conversely, dewatering in the partially-saturated systems (L1 and L2) may be held in the overlying petroleum coke pore space, reducing transport of dissolved ions to surface (Hypothesis 2) due to the low capillary fringe occurring in this relatively coarse material. In the uncovered systems (L3 and L6), CFT porewater would migrate downward until filling all the available tailings sand pore space. Some upward migration of porewater is likely to occur simultaneously during dewatering of the CFT layers in L3 and L6.

Porewater isotopic signatures and chemistry, and the observation of physical dewatering provide evidence to support the hypothesis that interaction between CFT porewater and adjacent layers is occurring. The fully-saturated covered systems are interacting with CFT porewater throughout their entire depth, while the partially-saturated covered systems accommodate the influx of CFT porewater and prevent movement to surface.

Table 5-1: Material surface measurements for each lysimeter over the study period. All values are in cm below the top lip of each lysimeter.

| **Lysimeter ID** | **Material Surface Position (cm)** | | | |
|---|---|---|---|---|
| | **October 2015** | **July 2016** | **November 2016** | **October 2017** |
| US-L1 | 8.5 | 39.5 | 41 | N/A |
| US-L2 | 12.7 | 58.5 | 59.2 | N/A |
| US-L3 | 8.8 | 60 | 65.5 | N/A |
| US-L4 | 6.2 | 40 | 45.2 | 54.5 |
| US-L5 | 7.6 | 44.8 | 53.5 | 68.5 |
| US-L6 | 14.8 | 63.5 | 69 | 80 |

### *5.1.2 Geochemical Setting*

The geochemical setting of each lysimeter system also has broad implications for the release, mobility, and transport of trace elements. To generalize, the lysimeter systems are sub-alkaline (pH ~7.7), exhibit decreasing redox potential with depth, have high electrical conductivity (~5 mS $cm^{-1}$), and high alkalinity (~800 mg $L^{-1}$ as $CaCO_3$). This generalization provides a base expectation for the behavior of different trace elements in the systems; however, to understand the wide variations in trace element concentrations observed with depth a more detailed discussion of these parameters within each system is required.

The pH in all lysimeters is relatively constant with depth in the CFT and tends to decrease moving away from this unit. The lowest pH observed in the petroleum coke unit is 7.2 in L5, and 7.3 in both L1 and L4; remaining at or above the pH point of zero charge ($pH_{pzc}$) for petroleum coke (6.5 ± 0.3; Pourrezaei et al., 2014) in both systems. In L4 a sharp decrease (and the lowest pH encountered in these systems) is observed within the reclamation material, where pH dips below neutral, reaching 6.8. One explanation for this drop in pH is the oxidation of organic matter producing increased carbon dioxide ($CO_2$) in this layer, which increases the $H^+$ concentration following the formation and subsequent dissociation of carbonic acid ($H_2CO_3$). An increase in pH at the surface of both covered systems is observed, where conditions are influenced by precipitation and the use of the fill water, as well as $CO_2$ degassing during atmospheric equilibration.

Redox potential generally decreases with depth; however, a more detailed analysis of the redox data reveals more complex trends throughout layers and across layer interfaces. In L1 and L4, for example, redox potential increases from the surface to the base of the reclamation material. This trend is followed by a relatively steady decrease toward the coke-CFT interface. At this point a comparison between the fully- and partially-saturated systems can be made, and a distinct difference becomes clear: redox conditions are generally less oxic in the fully-saturated system. Relatively decreased redox conditions in the fully-saturated system can be attributed to the role of oxygen, where the high water table reduces the downward flushing of oxygenated meteoric water, decreases the downward diffusion of atmospheric oxygen, and allows organic matter present in the reclamation material to consume dissolved oxygen during oxidation. Although lack of porewater data prohibits these comparisons in L2 and L5, similar processes are likely occurring (minus oxidation of organic matter) driving more reduced conditions just above the coke-CFT

interface in L5. While useful for observing qualitative trends over depth, measured redox potentials are often inconsistent with values calculated using the Nernst equation (Appelo & Postma, 2005; Markelova, 2017). Therefore, further evidence of redox conditions is necessary to support conclusions drawn from the trends observed in the $E_h$ data.

Analyzing $NO_3^-$ and $\Sigma H_2S$ concentrations can assist interpretation of redox conditions based on $E_h$ measurements. For example, an increase in $NO_3^-$ concentrations above the coke-CFT interface in L1 supports the conclusion that this system is more oxic than L4, where $NO_3^-$ concentrations are only slightly above zero or below detection limits. Sulfide concentrations are indicative of $SO_4^{2-}$ reduction near the base of the CFT in L1, L2, L4 and L5, where $\Sigma H_2S$ concentrations consistently rise, and $SO_4^{2-}$ concentrations fall as S(VI) is reduced to S(-II). Iron and Mn profiles can also be indicative of redox conditions. Porewater Fe is typically elevated in the CFT layers where elevated $\Sigma H_2S$ concentrations and mildly alkaline pH occur. Since Fe(III) (hydr)oxides exhibit limited solubility at pH > 5, these elevated Fe concentrations can principally be attributed to Fe(II). In contrast, dissolved Fe concentrations are typically below detection limits in coke and sand layers. One explanation for low Fe concentrations above and below CFT layers is oxidation of Fe(II) to Fe(III), which would promote precipitation of Fe(III) (hydr)oxides including ferrihydrite and goethite. This observation is further supported by the large spike in Fe observed in the reclamation material of L4, where Fe(III) may act as an electron acceptor during oxidation of organic matter (Appelo & Postma, 2005), leading to an increase in dissolved Fe(II). Manganese porewater profiles in L4 indicate increasing dissolved Mn toward surface. Typically, trends opposite to this are seen for Mn in oxic groundwaters, as Mn(II) remains mobile and the oxidized Mn(IV) precipitates from solution as oxides (Alloway, 2013). Porewater $E_h$ values measured in L4 are below the ~+500 to +600 mV conditions where oxidation of Mn(II) to Mn(IV) takes place (Appelo & Postma, 2005; Markelova, 2017), and the presence of $NH_3$ thoughout the system suggests the redox potential is at or below the $NO_3^-/NH_4^+$ transition (~+190 mV at pH 7; Markelova, 2017). This observation indicates that Mn may be present as Mn(II) throughout L4, and may be influenced by the decreasing pH and increased competition with Ca and Mg for sorption sites toward surface (Alloway, 2013). Oxic conditions at the surface of L1 (high $E_h$ and $NO_3^-$; low $NH_3$-N and $\Sigma H_2S$) suggest that Mn(IV) may have promoted precipitation of Mn(IV)-oxides, resulting in the lower concentrations relative to L4. In summary, two main conclusions can be drawn with respect to the redox conditions present in each potential closure system: (1)

partially-saturated systems are more oxidized over depth; and (2) conditions are reducing within, and at the base of, the CFT in the covered systems.

Electrical conductivity in L1 and L4 exhibits a consistent profile over depth–averaging $5.1 \pm 0.9$ mS $cm^{-1}$–and only increasing slightly from top to bottom. Conductivity is roughly 1.5 mS $cm^{-1}$ lower in L4 above the coke-CFT interface, simply due to higher dilution derived from the fill water creating lower concentrations of dissolved ions. Lysimeter 1 exhibits uniform conductivity in the CFT over depth, followed by a large increase toward surface caused by evaporative concentration. High conductivities in overlying cover layers suggest that CFT porewater is pervasive in these systems, and that dilution by precipitation and fill water is somewhat limited. However, the saturation of petroleum coke may also influence conductivity through ion-exchange reactions at coke and associated mineral surfaces; therefore, a comparison of conductivity in full-scale petroleum coke and CFT deposits can suggest which of these materials is the main contributor of conductance. Full-scale petroleum coke deposits studied by Nesbitt (2016) and full-scale CFT deposits studied by Heaton (2015) exhibit mean conductivity values of $1970 \pm 1350$ µS $cm^{-1}$ and $6100 \pm 2750$ µS $cm^{-1}$, respectively; indicating that CFT porewater is likely the largest control on conductivity in the lysimeter systems. In summary, all systems appear to be influenced by CFT porewater, and therefore these porewaters will be the largest control on conductivity in closure systems.

Alkalinity increases with depth in both covered systems, reaching relative maxima near the base of the CFT units. In the uncovered systems, alkalinity increases with depth in the CFT and appears to reach stable conditions with depth in the tailings sand. Simple speciation modelling indicates that dissolved carbonate speciation is dominated by bicarbonate ($HCO_3^-$) in all samples, with elevated $H_2CO_3$+$CO_2$ ($H_2CO_3^*$; $pK_a = 6.4$) present in the reclamation material due to the decrease in pH caused by the oxidation of organic matter.

After closer observation of each parameter, it becomes clear that each system is more complex than the initial summary suggests: oxidation of organic matter occurring in L4 is affecting pH, oxidation-reduction potential, and carbonate speciation; and evaporative concentrating at the surface of L5 is affecting electrical conductivity and therefore concentrations of all dissolved ions. These differences between the covered systems (and their respective fully- and partially-saturated duplicates) will affect trace element release, mobility, and transport–influencing the overall success of each closure system.

### *5.1.3 Trace Element Release through Sorption-Desorption Reactions*

The presence of major ions–specifically readily exchangeable cations and inorganic anions–will drive sorption-desorption and ion-exchange reactions with petroleum coke, and may influence the release and mobility of trace elements in the lysimeter systems. The subject of ion-exchange within the lysimeter systems has been studied in detail by Cilia (2017). Using data collected in the lysimeter field study and laboratory-scale column experiments, Cilia (2017) found that the cation exchange capacity (CEC) of petroleum coke (0.41 meq per 100 g) was much lower than that of CFT (11 meq per 100 g), suggesting that coke has a low capacity for ion exchange reactions. While some trace element release may be associated with ion-exchange, the main source of release is typically associated with trace element desorption from variably charged mineral and organic material surfaces (Appelo & Postma, 2005). Therefore, it is likely that trace element release is mostly influenced by pH dependent sorption-desorption reactions at coke and associated mineral surfaces within the lysimeter systems.

Evidence of trace element release from coke was found through the sequential extractions performed in this study (Section 4.2). Immediately apparent from the sequential extraction results (Figure 4-10) is that the exchangeable phase (and the water-soluble phase, in the case of V) dominates the extractable phases for each trace element. Furthermore, there is an apparent relationship between coke grain size and water-soluble and exchangeable fractions. This relationship is particularly apparent in the water-soluble fractions for Ni and V, and in the exchangeable fraction for Ni. While the relationship is not clearly present for Mo and the exchangeable fraction in V, the smallest grain size fraction ($f_1$ < 149 µm diameter) consistently produced the highest concentrations for the water soluble and exchangeable fractions. This trend is likely due to the increased surface area per unit mass in the smaller grain size fractions (Table 4-3), and suggests that surface complexes involving these trace elements occur readily with the coke grain surface. Increased concentrations in the larger grain size fraction indicate that minerals associated with coke (eg. Fe-(hydr)oxides) may also host appreciable concentrations of trace elements bound by surface-complexation.

Conditions created in the sequential extraction experiments are similar to those in the lysimeters following the release of CFT porewater into overlying coke units. Initially, the coke interacts with the fill-water and infiltrating precipitation, which drives the release of trace elements associated with water-soluble minerals and weakly-bound surface complexes. Over time, the

dewatering of CFT brings $Ca^{2+}$, $Na^{+}$, $Cl^{-}$, $SO_4^{2-}$, and $HCO_3^{-}$ ions into solution at highly concentrated values (concentrations within the lysimeters shown in Figure 5-2), which promote exchange with more strongly-bound surface complexes. While the extraction study provides evidence for exchange with high concentrations of $Ca^{2+}$ and $Na^{2+}$, it does not provide direct evidence for interaction with inorganic anions, as the extractant solutions did not contain appreciable concentrations of those anions associated with CFT porewater (Table 3-1). The interaction of petroleum coke with varying concentrations of $Cl^{-}$, $HCO_3^{-}$, and $SO_4^{2-}$ was studied by Puttaswamy and Liber (2010), who found that $SO_4^{2-}$ increased the release of cationic metals (eg. Ni), while $HCO_3^{-}$ both increased the release of oxyanionic forming metals (eg. Mo and V) and

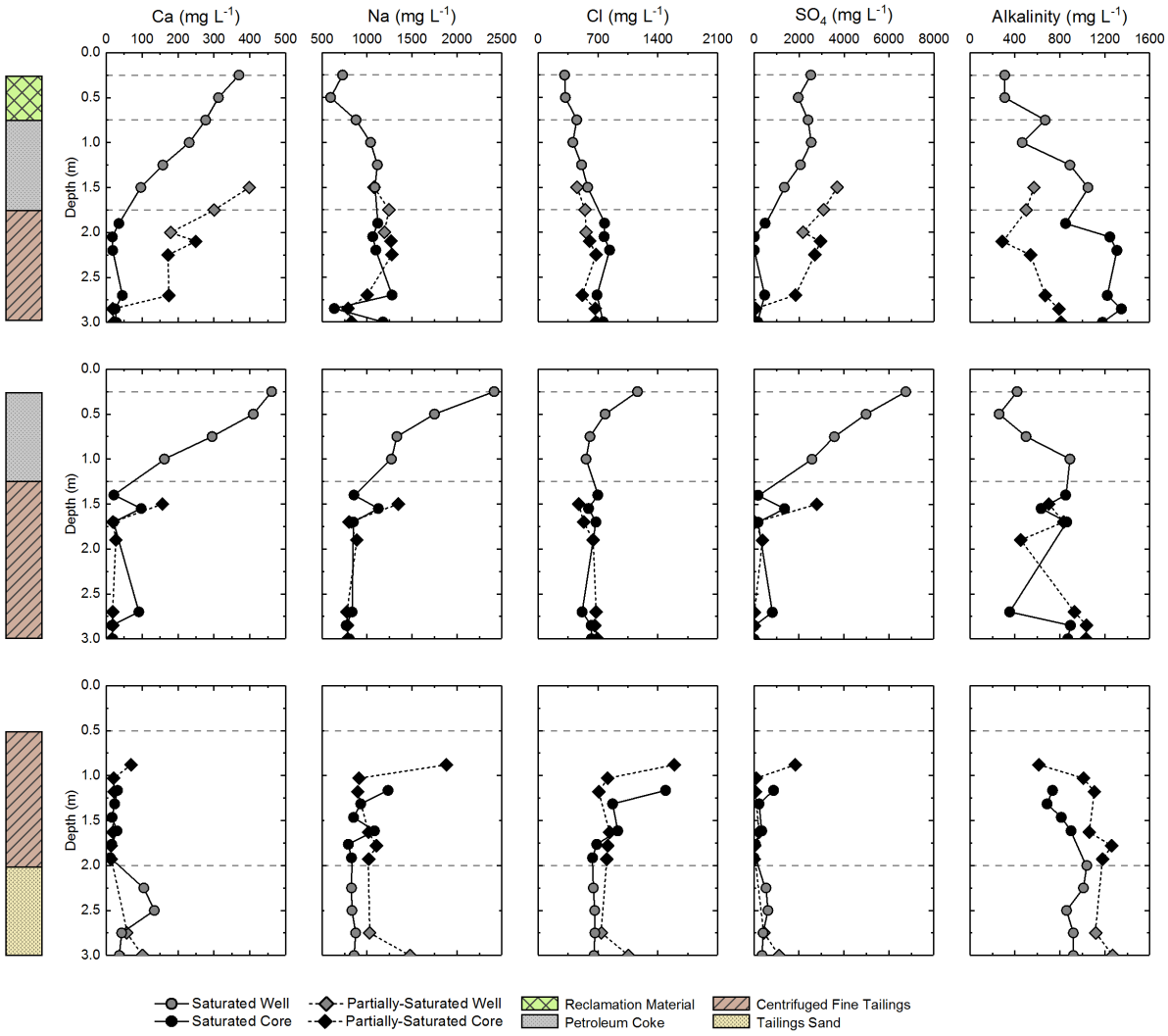


Figure 5-2: Porewater concentrations for Ca, Na, Cl, $SO_4$ and total alkalinity within the lysimeter systems. Alkalinity is displayed as mg $L^{-1}$ as $CaCO_3$. The bars on the left-hand side of the graph designate the different units of the three layering schemes.

reduced Ni mobility. An important caveat is that the concentrations of inorganic anions used in the Puttaswamy and Liber (2010) study are in some cases an order of magnitude less than those observed in the lysimeter porewater. Therefore, a reasonable conclusion can be made that inorganic ions, especially at the highly concentrated values observed in the lysimeter systems, may promote the release of trace elements within the lysimeter systems.

Based on these findings, it stands to reason that a partially-saturated system will release less sorbed trace element mass when compared with a fully-saturated system containing the same amount of petroleum coke. A fully-saturated system will facilitate transport of elevated concentrations of exchangeable ions in CFT porewater throughout the entire height of a coke column and release both the water-soluble and exchangeable fractions. Conversely, a partially-saturated system will only react with a small fraction of the coke column, and while the water-soluble component will still be released from the material due to infiltrating precipitation, the exchangeable fraction will remain bound to the surface of the unsaturated petroleum coke.

### *5.1.4 Trace Element Mobility*

Following evaluation of water movement, geochemical setting, and the degree of ion exchange (and ion ingress), it is now possible to assess trace element behavior in each lysimeter system. Overall mobility for most trace elements will largely depend on pH and redox conditions; however, certain ions and the characteristics of each material also influence speciation and sorption dynamics. Arsenic, Mo, Ni, Se, and V were chosen for further analysis due to their elevated concentrations in full-scale CFT and petroleum coke deposits (Heaton, 2015; Nesbitt, 2016). The main questions with respect to these trace elements are: (1) what is the main source of each element? And (2) what are the major controls on mobility in the systems?

*Arsenic*

Arsenic porewater concentrations in the lysimeters are typically highest directly above (covered systems) or below (uncovered systems) the CFT unit. Concentrations tend to increase with depth throughout all systems. Thus far, petroleum coke has been deemed the main source of trace elements within oil sands mining landscapes; however, As is present at highest concentrations below the CFT in the uncovered system where no petroleum coke is present. Therefore, it is hypothesized that CFT is a principal source of As in all systems.

Initial evidence for this hypothesis came by the logical observation that CFT is the only material present in all systems, and that all systems contain elevated As concentrations. Further

evidence was found during the sequential extraction of petroleum coke, where As is below detection in all fractions (Section 4.2); and by porewater sampled in full-scale CFT deposits by Heaton (2015), where As was present at concentrations similar to those observed in the lysimeter CFT. From this information, the conclusion is drawn that CFT is the main material producing elevated As concentrations in the lysimeter systems. This raises the question: if CFT is the material source, what are the mechanisms by which As is released from this material?

In most natural systems, the main control on As solubility is sorption to Fe-(oxy)(hydr)oxides (Fordham and Norrish, 1979; Manceau et al., 2007; Alloway, 2013). Osacky et al. (2013) showed that lepidocrocite [γ-FeO(OH)] is concentrated in the fine particle fraction (<2 μm) of oil sands ore, and Kaminsky et al. (2009) suggested Fe-oxides play an important role in bitumen-clay interactions in the froth tailings stream (1–2% of clay mineral composition). Furthermore, Heaton (2015) described the reduction of crystalline and amorphous Fe-(hydr)oxides as an important biogeochemical process occurring in FFT and CFT. In the CFT porewater of the lysimeter systems, the presence of dissolved Fe indicates the presence of an Fe source in the low redox environment of the CFT layers. Therefore, one potential mechanism promoting the release of As from CFT is the reductive dissolution of Fe-(hydr)oxide minerals containing As bound in surface complexes. Thermodynamic evidence for this conclusion within the lysimeter systems is provided when considering the presence of sulfate reduction at the base of the CFT units; this reaction is less thermodynamically favourable than reduction of amorphous Fe(III)-(hydr)oxides and indicates that the latter reaction is likely occurring in the systems. Sulfate reduction also influences reduction of crystalline Fe-oxide minerals (Kocar et al., 2010; Jia et al., 2017), whereby the production of $HS^-$ causes reductive dissolution by the following reaction:

$$2FeOOH_{(s)} + 3HS^-_{(aq)} \rightarrow 2FeS_{(s)} + S^0_{(aq)} + H_2O_{(l)} + 3OH^-_{(aq)} \quad (5.1)$$

If this reaction were prevalent in the systems, there should be an increase in the concentration of zero-valent sulfur ($S^0_{(aq)}$) within the CFT. When comparing molar concentrations of dissolved total S, $SO_4^{2-}$ and $\Sigma H_2S$, it becomes clear that there is some discrepancy in the major forms of S in the system, particularly with increasing depth in the dual- and single-cover systems (Figure 5-3). This discrepancy may be due to an increase in the presence of $S^0_{(aq)}$ produced during the reduction of Fe-(hydr)oxide minerals, as described in Eq. 5.1. Therefore, due to favourable redox conditions and the role of sulfur, it is likely that reduction of amorphous and crystalline Fe-(hydr)oxides are

occurring within the lysimeter systems; providing a mechanism for the release of As present on the mineral surfaces.

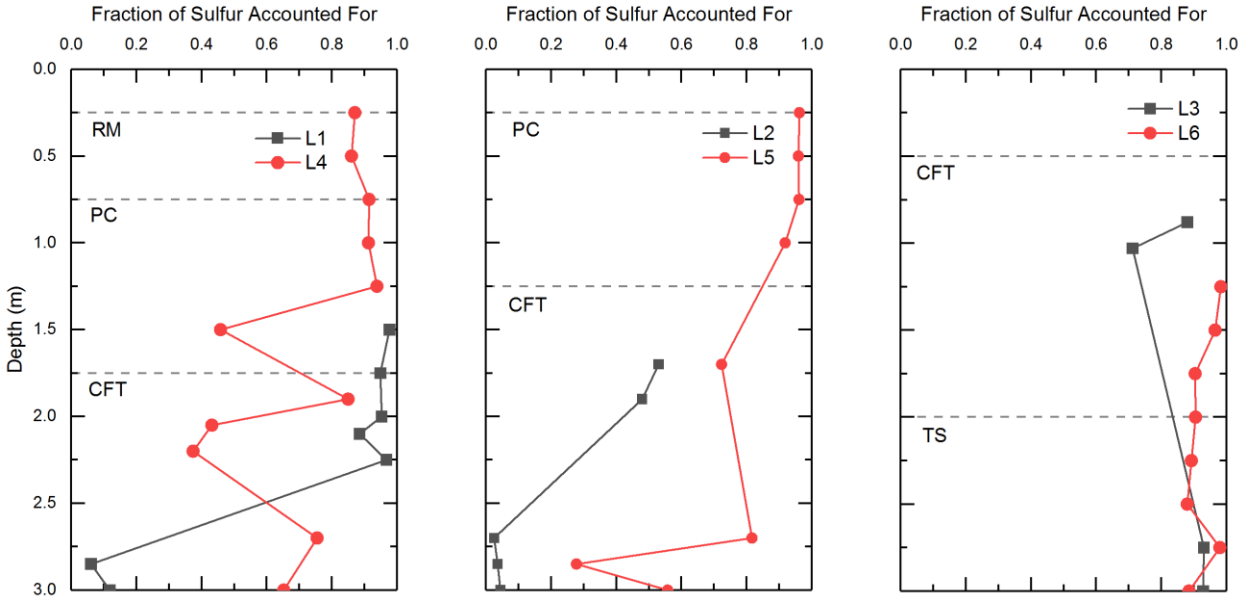


Figure 5-3: Fraction of total dissolved S accounted for in porewater samples. The fraction was calculated by adding molar concentrations of $SO_4^{2-}$ and $\Sigma H_2S$ and dividing by the molar concentration of total S in each sample.

Another potential source of As is the oxidation of pyrite ($FeS_2$), which is present in the oil sands ore at 0.1 to 0.5 % (w/w; Osacky et al., 2013), and in the tailings stream in trace quantities (Kaminsky et al., 2009). Pyrite commonly contains As and Se impurities, where these elements are bound in the mineral structure and may be released by breakdown of the mineral during oxidation (Diehl et al., 2012; Hendry et al., 2015; Essilfie-Dughan et al., 2017). While oxidation of pyrite would not occur within the low redox environment of the CFT, this process could proceed during dredging and centrifugation of the FFT and MFT–producing a soluble pool of these elements prior to placement within the lysimeter systems.

Major controls on As mobility in the lysimeter systems include pH and redox conditions, the presence of Fe-(hydr)oxides (Fordham and Norish, 1979; Manceau et al., 2007; Alloway, 2013), and the high concentrations of sulfur species (Couture and Van Cappellen, 2011; Jia et al., 2017). Under aerobic conditions, the stable form of As is arsenate [As(V)] and forms the $HAsO_4^{2-}$ and $H_2AsO_4^-$ oxyanions in the pH range 6.5–8.5. These negatively charged species exhibit comparable sorption behavior to phosphate, and are strongly sorbed to soil and mineral surfaces (Goldberg et al., 2005; Alloway, 2013). Anaerobic conditions result in the reduction of As to

arsenite [As(III)], forming a neutral ion ($H_3AsO_3^0$) in the pH range observed in the lysimeters. Due to the neutral charge on the dominant As(III) species, reduced As tends to be more mobile and exhibits weaker sorption to soil and mineral surfaces (Müller et al., 2010). Equilibrium modelling performed by Couture and Van Cappellen (2011) suggests that $S^0_{(aq)}$ may act as an electron acceptor in sulfidic environments, stabilizing As(V) in reducing conditions by the oxidation of As(III) and formation of thioarsenates. Major As speciation under the conditions suggested by Couture and Van Cappellen (2011) in the pH range observed in the lysimeters would be $AsS_4^{3-}$, a negatively charged As(V) thioanion; and $H_3AsO_3^0$, the neutral As(III) species described earlier.

Following the reduction of Fe-(hydr)oxides and As release to the lysimeter systems, reducing conditions in the covered systems likely promote the stability of As(III); increasing As mobility and improving transport during the dewatering of CFT. After movement to surface, As(III) would be gradually oxidized to As(V) as conditions shift to sub-oxic and aerobic. In the covered lysimeter systems, As concentrations remain relatively constant in the CFT and then exhibit an increase across the CFT-coke interface. This may reflect the change from the high surface area CFT to the relatively low surface area in the coke; coupled with the fact that As(III) may still be present in appreciable quantities and thus highly mobile. Equilibrium modelling indicates that ferrihydrite [$Fe^{3+}_2O_3 \cdot 0.5(H_2O)$], goethite [α-FeO(OH)], and lepidocrocite [γ-FeO(OH)] are above saturation at the surface of the CFT in these systems, suggesting that they may be forming in the less reducing areas of these layers, providing binding sites for As(V) thioarsenate species as they move toward the CFT-coke interface. A gradual decrease toward surface in both L4 and L5 reflects the oxidation of As(III) to As(V) and the subsequent sorption to available coke (and associated mineral) surfaces. Conditions are generally less reducing in the uncovered systems relative to the covered systems, suggesting less reduction of Fe-(hydr)oxides. Evidence for this conclusion is present in the sulfur accounting (Figure 5-3), where $\Sigma H_2S$ and $SO_4^{2-}$ make up the majority of total sulfur, indicating a lower potential presence of $S^0_{(aq)}$ produced during Eq. 5.1. Nonetheless, $\Sigma H_2S$ is still present in porewater samples (albeit at relatively low concentrations) indicating that reduction of Fe-(hydr)oxides could still occur and release As to the system. An increase in As concentrations below the CFT may be attributed to the potentially low surface area of the tailings sand (quartz) as well as the stability of As(III) under anoxic conditions.

*Molybdenum*

Porewater Mo concentrations in the lysimeter systems tend to increase toward surface and are highest in the petroleum coke units. Low concentrations were measured in the uncovered system, indicating that CFT and tailings sand are not a large source of Mo. Due to high concentrations observed within the petroleum coke of both the dual- and single-cover systems, it is hypothesized that this material is the main source of Mo within the lysimeter systems.

Nesbitt (2017) measured concentrations averaging ~800 µg $L^{-1}$ and in a similar range to those observed in this study in several full-scale fluid coke deposits. The sequential extractions performed in this study (Section 4.2) revealed that water soluble and exchangeable fractions made up the bulk of extractable Mo at 19% (0.16 mg $kg^{-1}$) and 48% (0.41 mg $kg^{-1}$), respectively. The sequential extraction results imply that Mo is associated with weak to strong binding sites on the coke and associated mineral surfaces, and as a result would be readily liberated during interaction with a high ionic strength fluid. Furthermore, Puttaswamy and Liber (2012) have shown that petroleum coke in contact with fluids containing increasing doses of inorganic anions increase the release of Mo (and other trace elements) from petroleum coke. Therefore, following consolidation and concomitant dewatering, the upward movement of CFT porewater would provide exchangeable cations and inorganic ions and drive the release of Mo from coke.

Following release from petroleum coke, Mo mobility would be largely influenced by pH and redox conditions, as well as the availability of mineral surface binding sites (Fe/Al-(hydr)oxides and organic matter). Molybdenum is typically present as the Mo(VI) oxyanion molybdate ($MoO_4^{2-}$) under aerobic conditions, and as a result is most mobile under alkaline conditions or pH values near or above the $pH_{pzc}$ of available mineral surfaces. Under reducing conditions in the presence of available sulfide, $MoO_4^{2-}$ may become sulfidized to form thiomolybdates ($MoS_4^{2-}$ and intermediates; Erickson & Helz, 2000; Vorlicek et al., 2004; Dahl et al., 2013), which are generally more reactive and are more likely to be removed from solution by binding with Fe sulfide phases and organic matter (Smedley and Kinniburgh, 2017). Molybdenum has a high affinity to bind with organic matter and Fe/Al-(hydr)oxides, however a sharp decrease in sorption to these materials occurs at pH greater than ~8 (Wichard et al., 2009; Smedley and Kinniburgh, 2017). Mobility may also be influenced by the precipitation of Mo-bearing minerals (e.g., Ca-molybdate, Ni-molybdate, Mo-sulfides), however, the kinetics of these reactions are generally slow unless microbially mediated (Vorlicek, 2004; Smedley and Kinniburgh, 2017).

Following release from petroleum coke in the lysimeter systems, Mo would be relatively mobile as conditions are alkaline from the influence of CFT porewater. Molybdenum concentrations within the coke layers, however, decrease toward the CFT layers, even though pH conditions are becoming more alkaline. One simple explanation for this is that during the upward movement of CFT porewater, porewater with lower Mo concentrations are mixed with coke porewater, leading to an overall decrease in dissolved Mo. When comparing porewater Cl and Li concentrations over depth (Section 5.1.1), however, no dilution trend is noted directly above the CFT and coke interface. This behavior suggests that redox conditions may be exhibiting a strong control on Mo mobility. At the base of the coke units, the increased concentrations of $\Sigma H_2S$ could promote formation of thiomolybdates, causing Mo to be less mobile due to higher reactivity (Smedley and Kinniburgh, 2017). Another potential cause of decreased Mo mobility in the lower coke may be the formation of Mo-bearing minerals and solid solutions under reducing conditions. For example, equilibrium modelling indicated that molybdenite ($MoS_{2(s)}$) was above saturation in the lower coke and CFT layers of the covered systems and therefore could be forming and removing Mo from solution. A problem arises with this explanation as precipitation of $MoS_2$ is not kinetically favourable in low temperature systems; however, the precipitation of a cuboidal Mo-Fe-S solid solution mineral has been shown to occur relatively quickly in the presence of $S^0_{(aq)}$ (Vorlicek et al., 2004, Dahl et al., 2013). As discussed earlier, $S^0_{(aq)}$ may be present in the system from the reductive dissolution of Fe-(hydr)oxides by $\Sigma H_2S$ (Eq. 5.1), and would act as an electron donor during the reduction of Mo(VI) to Mo(IV).

Moving toward surface Mo tends to increase in the coke, especially in L5. In L1, a similar increase is noted within the coke toward the surface of the water table. The increase toward surface is likely caused by increasingly aerobic conditions causing Mo to remain largely as the mobile $MoO_4^{2-}$ oxyanion in solution and the relatively low surface area of the coke. The large increase of Mo in L5 may also be due to evaporative concentration discussed in Chapter 5.1.1. Moving to L4, a marked decrease in Mo concentrations occur within the reclamation material. This is likely due to the strong affinity Mo has for binding to organic matter (Xu et al., 2013; Smedley and Kinniburgh, 2017), coupled with the decrease in pH occurring within the reclamation material. The result of this interaction is that Mo is below the method detection limits in the porewater at the surface of L4, indicating that the reclamation soil cover is effective with respect to attenuation of Mo.

*Nickel*

Nickel release from fluid petroleum coke has been the subject of many studies (Puttaswamy and Liber, 2012; Zubot et al., 2012; Nesbitt, 2016; Nesbitt et al., 2017) as coke is typically seen as the main source of this element within the oil sands and therefore the mechanisms controlling its release and mobility from this material are relatively well understood. In the lysimeter systems, however, Ni is consistently present in the CFT units, including the uncovered systems where no petroleum coke is present. Therefore, it is hypothesized that both CFT and petroleum coke are contributing to total Ni concentrations within the lysimeter systems.

Evidence for this hypothesis can be found in the full-scale deposits of fluid petroleum coke and CFT studied by Nesbitt (2016) and Heaton (2015), respectively. In the full-scale petroleum coke deposits, porewater Ni concentrations ranged from 2.3 to 120 µg $L^{-1}$, averaging 16 ± 20 µg $L^{-1}$ ($n$=65). Conversely, CFT porewater Ni concentrations ranged from 4.2 to 110 µg $L^{-1}$, averaging 26 ± 18 µg $L^{-1}$ ($n$=65). Interestingly, mean Ni concentrations are actually higher in the full-scale CFT deposits than the coke deposits, indicating that both materials are able to contribute Ni to solution (Heaton, 2015; Nesbitt, 2016).

As for the mechanism of release from these materials, the sequential extraction experiment performed in this study (Section 4.2) indicated that Ni is highly associated with the exchangeable (70%; 2.6 mg $kg^{-1}$) and acid-soluble (13%; 0.47 mg $kg^{-1}$) phases in fluid petroleum coke. Additionally, Nesbitt (2016) also showed a negative correlation between pH and Ni concentrations in full-scale coke deposits. This suggests that Ni release is largely influenced by pH dependent desorption reactions at the fluid coke and associated mineral surfaces, or mineral dissolution reactions (eg. Ni-hydroxide dissolution at low pH). Trace element release from CFT is not well studied, however Ni has a relatively high affinity to bind to Fe-(hydr)oxide surfaces (Fischer et al., 2007; Gomez et al., 2013; Eldridge et al., 2015) and may be released during the reductive dissolution of these minerals (eg. Eq. 5.1).

Unlike As and Mo, Ni does not exhibit particularly complex redox speciation, as the dominant ion under a wide range of environmental conditions is $Ni^{2+}$. Equilibrium modelling indicates that porewater Ni speciation is dominated by $Ni^{2+}$ (~50%), $NiHCO_3^+$ (~20%), $NiCO_3^0$ (~20%), and $NiSO_4^0$ (~10%). Nickel mobility is more largely controlled by pH conditions, and the availability of organic and inorganic ligands. In the lysimeter systems, pH tends to remain above the $pH_{pzc}$ for petroleum coke and therefore surface sites would have a net-negative charge. This

would cause Ni to have a higher affinity for sorption, and reduce desorption from the coke surfaces and may explain why most concentrations are below method detection limits within coke. Most notable in L1 and L5, a drop in pH toward the water table surface causes increased Ni mobility and produces the highest porewater concentrations recorded in this study. Highly elevated concentrations at the surface of L5 are also indicative of the high evaporation rate occurring at the surface of this system. Nickel concentrations were below method detection limits in the reclamation soil of L1, indicating that this unit may be attenuating Ni due to the elements high affinity for organic matter (Alloway, 2013).

Following release into CFT porewater, high pH concentrations and the availability of inorganic ligands may influence the mobility of Ni. The relatively uniform concentrations with depth suggest that precipitation of Ni-minerals may be exhibiting a solubility control on Ni. Nickel sulfide (NiS) precipitation has been shown to proceed at room temperature with $H_2S/HS^-$ concentration as the limiting factor (Karbanee et al., 2008), and therefore this reaction could be occurring in the CFT units with high levels of $\Sigma H_2S$. Porewater is supersaturated with respect to $NiS_{(s)}$, and therefore this mineral could be precipitating and exhibiting a control in Ni solubility. Nickel-hydroxides are typically seen as the main mineral control on Ni solubility at alkaline pH, however modelling suggests these minerals are below saturation in all porewater samples. Nickel may also be more mobile due to the loss of binding sites in the CFT following the reductive dissolution of Fe-(hydr)oxides, and the fact that pH conditions may be nearing or below the $pH_{pzc}$ of remaining Fe-(hydr)oxides–causing these minerals to have less affinity for binding positively charged Ni(II) cations.

*Selenium*

Porewater Se concentrations in the lysimeter systems are typically highest toward the surface of the petroleum coke units. Initially, high concentrations within the petroleum coke suggested that this material was the main source of Se within the lysimeter systems; however, following the sequential extraction study (Section 4.2) it became clear that petroleum coke does not contain appreciable amounts of this element as leachable Se in all extractions were below detectable concentrations. Therefore, like As, it is hypothesized that CFT is the main source of Se within the lysimeter systems.

Initial evidence for this hypothesis came by the same logical observation made for As, where CFT is the only material present in all systems, and that all systems contain elevated Se

concentrations. This assumption, however, was weaker for Se as porewater concentrations are almost always below detection in the cored CFT, and that concentrations are relatively low in the system with only CFT. Following the sequential extraction study–as described above–it became clear that CFT had to be the source, as no Se appears to be released from coke. Further evidence came when comparing the lysimeter results to the full-scale CFT deposits studied by Heaton (2015), where Se concentrations averaged 8.8 ± 15 µg $L^{-1}$ and reached a maximum of 124 µg $L^{-1}$. These values are much higher than those measured in full-scale petroleum coke deposits, where Se concentrations averaged just 0.89 ± 1.2 µg $L^{-1}$ and only reached a maximum of 6.3 µg $L^{-1}$ (Nesbitt, 2016). Therefore, it is concluded that CFT is the likely source of Se within the lysimeter systems. As for the mineral source within the CFT, it is possible that a similar mechanism of release is occurring as with As. Selenium has a high affinity for sorption to Fe-(hydr)oxides (Manceau & Charlet, 1994; Peak & Sparks, 2002) and therefore may be released initially during the thermodynamic reduction of Fe(III) and later during further reductive dissolution by $HS^-$ (Eq. 5.1). As discussed above for As, oxidation of pyrite prior to placement of CFT in the lysimeters could also be a source of Se within the lysimeter systems, where the reduced Se(-II) commonly replaces S(-II) in the mineral structure of pyrite (Hendry et al., 2015).

Selenium mobility is largely controlled by pH and redox conditions (Masscheleyn et al., 1990), and the presence of Fe-(hydr)oxides (Manceau & Charlet, 1994; Peak & Sparks, 2002) and organic matter (Gustafsson & Johnsson, 1994). Under fully oxic conditions, Se is present as the Se(VI) selenate ion ($SeO_4^{2-}$), while the Se(IV) ions selenite ($SeO_3^{2-}$) and biselenite ($HSeO_3^-$) dominate become prevalent as redox potential decreases. Selenium(VI) commonly forms weakly-bound complexes with mineral surfaces (Peak & Sparks, 2002; Winkel et al., 2012) and competition with $SO_4^{2-}$ and other inorganic anions increases its mobility (Massecheleyn et al., 1990). Conversely, Se(IV) forms strongly-bound surface complexes (Winkel et al., 2012) and the presence of inorganic anions has little effect on sorption (Alloway, 2013). Sorption of Se(IV), and to a lesser extent Se(VI), generally decreases with increasing pH (Manceau & Charlet, 1994; Peak & Sparks, 2002), dependent on the $pH_{pzc}$ of the available mineral surfaces. Under sub-oxic and anoxic conditions Se(VI) and Se(IV) can be reduced to elemental selenium [Se(0)] and selenide [Se(-II)]. Elemental Se is thermodynamically stable across a wide range of pH and redox conditions, and is generally not soluble following precipitation from solution (Winkel et al., 2012). Selenide also exhibits low mobility, as only very small concentrations are needed to reach

supersaturation and drive precipitation of a Fe-Se(-II) solid solution (Masscheleyn et al., 1990). Therefore, Se mobility is highest in aerobic, alkaline, and high ionic strength porewater, and decreases with decreasing redox potential and pH.

In the lysimeter systems, Se should be most mobile at the surface, and less mobile with increasing depth as Se(VI) is reduced to Se(IV), and then to Se(0) and Se(-II). Selenium behaves as expected in L5 and shows a strong increase toward the surface of the petroleum coke. This large increase is likely due to the presence of Se(VI) as conditions become more oxidizing; the low number of binding sites in petroleum coke; strong competition for surface sites caused by the large increase in inorganic anions due to evaporation; and evaporative concentrating of Se itself. A similar explanation can be made for L1, where Se concentrations exhibit a large increase across the CFT-coke interface. In L4 however, the presence of the reclamation material appears to be influencing Se mobility. Concentrations increase toward surface in the petroleum coke, and then exhibit a slight drop followed by uniform concentrations within the reclamation material. Within the petroleum coke in L4, increasing concentrations of $NO_3^-$ indicate the increased presence of Se(VI); as the oxidation of Se(IV) to Se(VI) occurs at similar thermodynamic conditions as the oxidation $NH_3/NH_4^+$ to $NO_3^-$ (Appelo and Postma, 2005; Borch et al., 2010). A drop in $NO_3^-$ concentrations, coupled with the decrease in $E_h$ and pH in the reclamation material suggest increased presence of Se(IV), which would have a strong interaction with the organic matter and increased binding sites present in this unit. The presence of $NO_3^-$ can also influence mobility by retarding reduction of Se (Weres et al., 1990) and may be influencing Se behavior in L1, where the highest $NO_3^-$ concentrations in all systems are observed above the CFT-coke interface. Below the CFT in L3 and L6, presence of selenium increases due to the decrease in binding sites in the tailings sand. Higher concentrations are noted in L3 due to more aerobic conditions produced by the lack of water cover.

Selenium concentrations are almost always below detection limits within the CFT, likely influenced by the increased presence of Se(0) and Se(-II), and the increased binding sites present in the material. As conditions become more reducing within the CFT, Se solubility would be decreased by both the increased presence of clay and Fe-(hydr)oxide surfaces; and by the precipitation of $Se_{(s)}$ following reduction of Se(IV) to Se(0). Further reduction to Se(-II) could be occurring deeper within the CFT, and precipitation of $FeSe_{(s)}$ could be acting as a solubility control (Masscheleyn et al., 1990). Precipitation of Se(VI) and Se(IV) are generally not

thermodynamically stable under natural conditions (Masscheleyn et al., 1990) and therefore are not expected to be influencing mobility in the upper portion of the lysimeter systems.

*Vanadium*

Porewater V concentrations were highest in the petroleum coke units of L1, L4 and L5, and the lowest concentrations were observed throughout the CFT and tailings sand units in L3 and L6. Based on these observations, it is hypothesized that petroleum coke is the main source of V within the lysimeter systems.

Numerous studies have been conducted on V leaching from full-scale petroleum coke deposits (Zubot et al., 2012; Puttaswamy & Liber, 2012; Nesbitt, 2016; Nesbitt & Lindsay, 2017), providing a high level of confidence in this hypothesis. Zubot et al. (2012) showed that the V concentration in OSPW significantly increased with increasing petroleum coke addition. Nesbitt & Lindsay (2017) found that V was largely associated with porphyrin complexes within the petroleum coke, and Nesbitt (2016) found that V was significantly leached during water-soluble and exchangeable extractions. Sequential extractions performed in this study (Section 4.2) indicated that 33% (3.8 mg $kg^{-1}$) and 40% (4.6 mg $kg^{-1}$) of leachable V was released during the water soluble and exchangeable extractions, respectively. This indicates that V is associated with water-soluble minerals, and weakly- and strongly-adsorbed surface complexes, and would be readily leached during flushing by precipitation and interaction with high ionic strength fluids (like CFT porewater). Based on in-depth research on V leaching from petroleum coke and the sequential extraction experiments performed in this study, it is concluded that petroleum coke is the main source of V within the lysimeter systems.

Vanadium mobility is strongly controlled by pH and redox conditions (Wehrli & Stumm, 1989), as well as sorption-desorption and precipitation-dissolution reactions (Peacock & Sherman, 2003; Wright et al., 2014; Telfayan et al., 2015). The aqueous chemistry of V is dominated by soluble V(IV) and V(V) species (Wehrli & Stumm, 1989). Under aerobic and alkaline conditions, V(V) is the dominant oxidation state, and is most commonly present as the vanadate ions $H_2VO_4^-$ and $HVO_4^{2-}$. Decreasing pH and redox conditions increase the stability of V(IV), typically present as the vanadyl ion ($VO^{2+}$). Vanadium(IV) has a higher affinity for sorption to mineral surfaces and complexation with organic ligands (Wehrli & Stumm, 1989), and its presence as the oxycation $VO^{2+}$ suggests that it would be most readily sorbed at alkaline pH (dependent on the $pH_{pzc}$ of available mineral surfaces). Conversely, V(V) has a lower affinity for sorption to mineral surfaces

(Wehrli & Stumm, 1989), and its presence as an oxyanion suggests that sorption would be least favourable at alkaline pH. Many studies suggest that sorption-desorption reactions are the main solubility control on V in groundwater (Wright et al., 2014; Telfeyan et al., 2015; Nesbitt, 2016; Nesbitt & Lindsay, 2017) and, as discussed above, sorption of V is favoured at alkaline pH and suboxic redox conditions. Mineral precipitation may also present a solubility control on V in suboxic and anoxic groundwater, where V(III) and V(IV) can substitute for Fe in the structure of Fe-oxides and clay minerals (Wisawapipat & Kretzschmar, 2017). In summary, V is most mobile under alkaline oxic conditions, and is least mobile under alkaline suboxic to anoxic conditions.

Release of V within the lysimeter systems is likely influenced by two main interactions: (1) infiltration of precipitation through petroleum coke units releases V through oxidative weathering of the coke, and dissolution of water-soluble minerals and weakly-sorbed surface complexes; and, (2) following self-weight consolidation and dewatering of CFT, the upward flux of high ionic strength porewater liberates strongly-sorbed surface complexes through ion exchange. Evidence for this is observed in the high V concentrations in L1, where flushing by precipitation would be most prevalent due to partial-saturation, and interaction with CFT porewater is not diluted by saturation. In L4, the controls of pH and $E_h$ can be seen where V exhibits the highest concentrations at alkaline pH and elevated $E_h$. Following a drop in $E_h$ moving downward, V(V) is likely transitioning to V(IV) and the increasing pH with depth provides favourable conditions for sorption of this oxycation. Conditions are below detection at the surface of the reclamation material in L4, which may be due to the increased availability of binding sites, a drop in pH, and the abiotic reduction of V(V) to V(IV) due to reaction with humic acids in the highly-organic material (Wisawapipat & Kretzschmar, 2017). In contrast to other trace elements, V concentrations are low at the surface of L5 and do not appear to be influenced by evaporative concentration. This behavior is the opposite of the expected conditions, as V should be mostly present as V(V) and quite mobile at the surface of this system. Equilibrium modelling does not indicate that any V minerals are near or above saturation in the system, and therefore it is not expected that mineral precipitation is providing a solubility control. One explanation may be the relatively low pH (<7.5) providing more favourable conditions for the sorption of V(V) to petroleum coke and associated mineral surfaces, however similar behavior would then be expected for other oxyanion forming trace elements, like Se. As expected, V is lowest in the CFT units, and remains only slightly above or below the method detection limits throughout L3 and L6. In the

lysimeters containing coke, this is likely due to reducing conditions driving V speciation toward V(IV) and V(III) complexes resulting in increased potential for mineral precipitation and sorption to abundant clay and Fe-(hydr)oxide minerals; or, simply that the advective flux moves porewater upward and very little V mixes with CFT below coke layers.

### 5.1.5 Conceptual Lysimeter Models

An understanding of the geochemical controls occurring within the lysimeters allows simple conceptual models to be constructed for each system. These models can serve as a reference when designing closure systems as they show simplified porewater concentration profiles and geochemical settings.

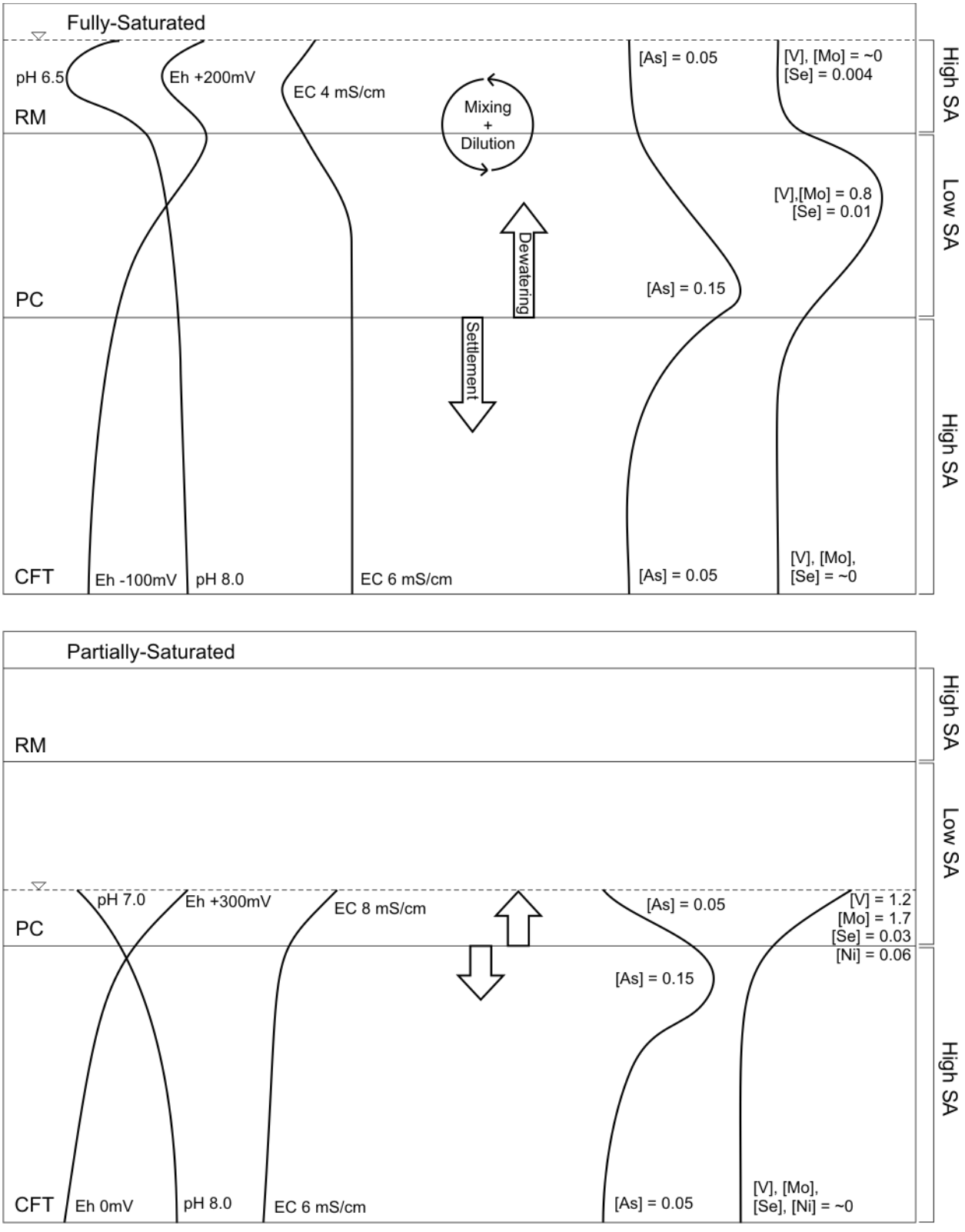


Figure 5-4: Conceptual model for both the fully- and partially-saturated dual-cover closure systems (L1 and L4). Concentrations are in mg $L^{-1}$. RM = reclamation material; PC = petroleum coke; CFT = centrifuged fine tailings.

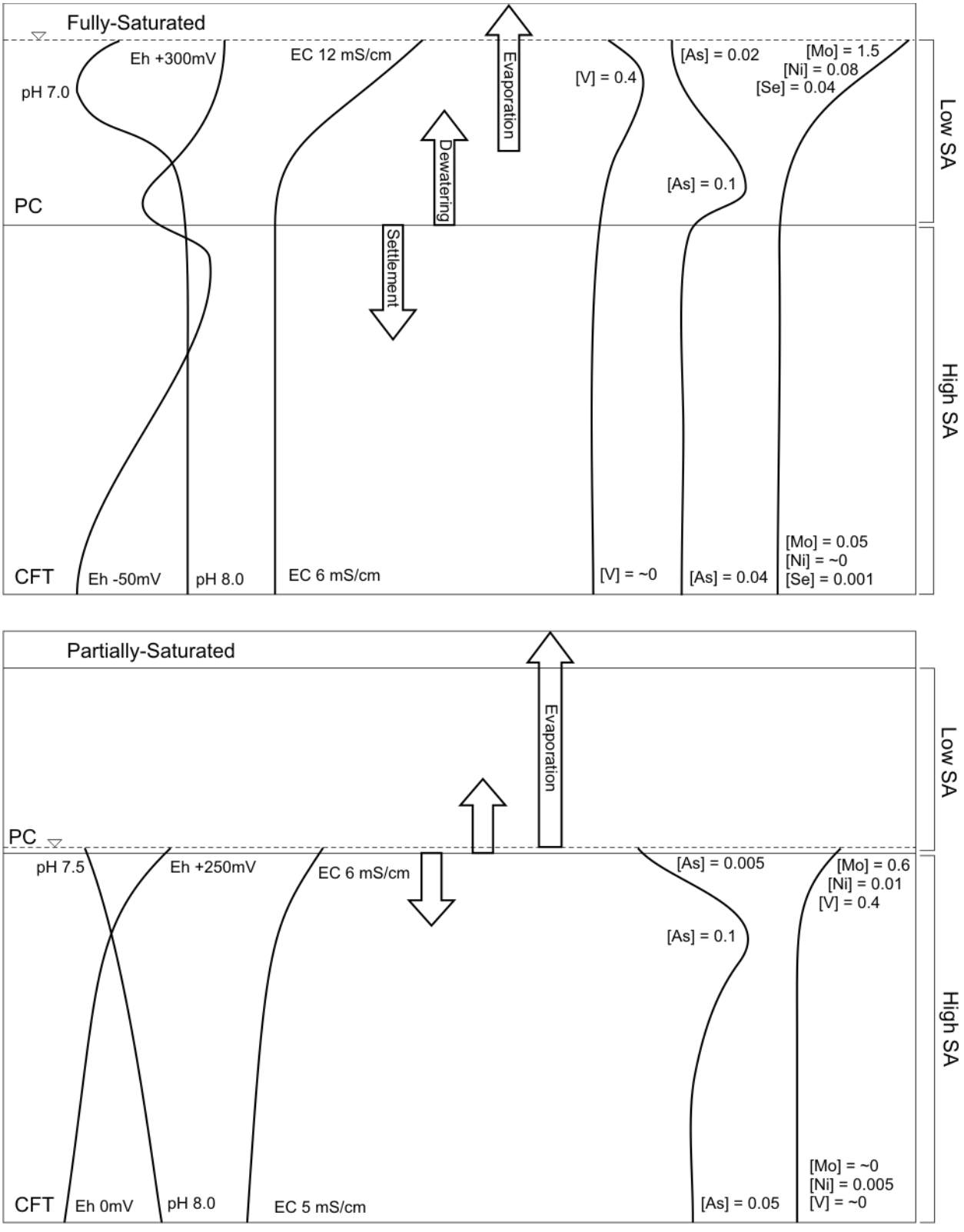


Figure 5-5: Conceptual model for both the fully- and partially-saturated single-cover closure systems (L2 and L5). Concentrations are in mg $L^{-1}$. PC = petroleum coke; CFT = centrifuged fine tailings.

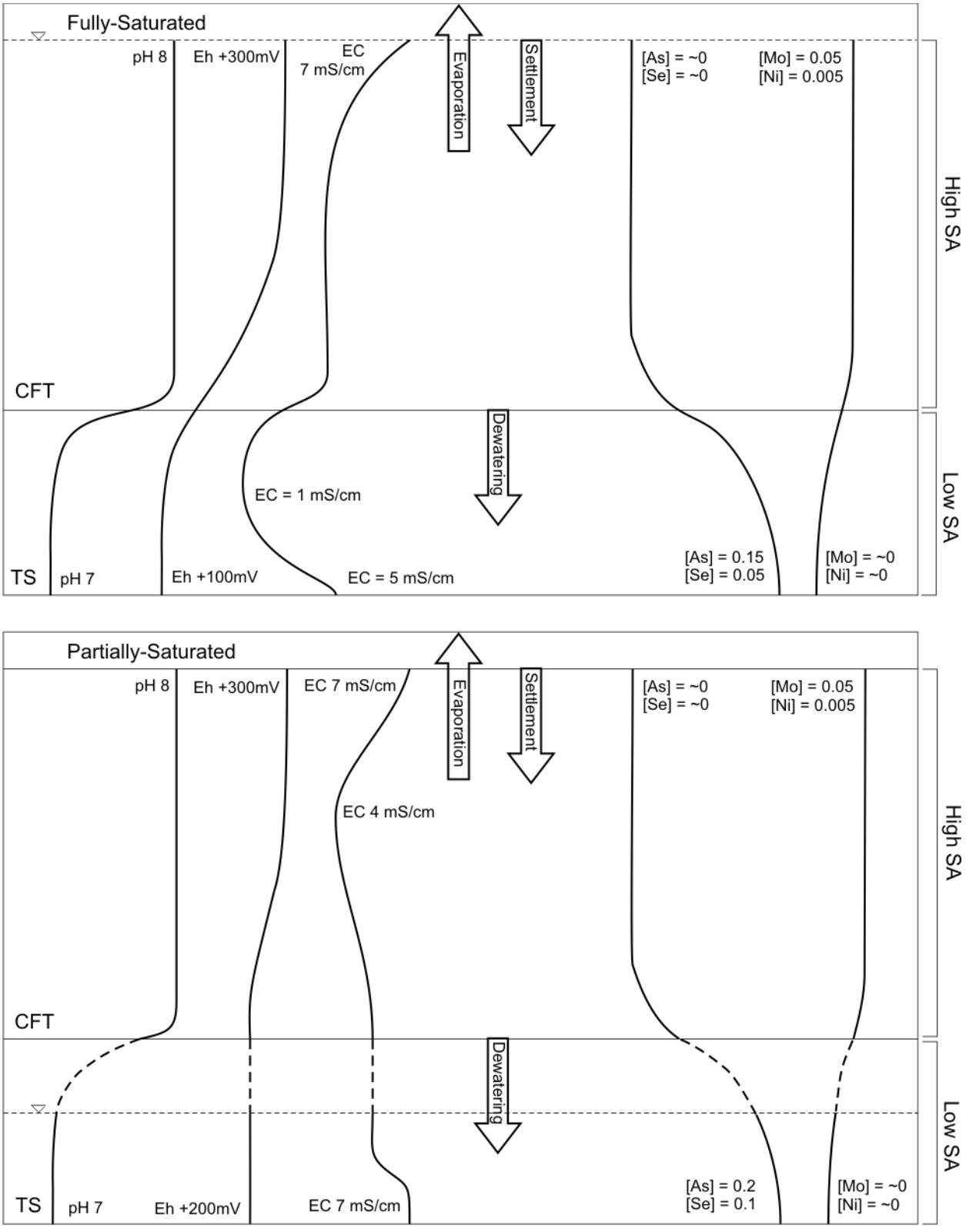


Figure 5-6: Conceptual model for both the fully- and partially-saturated uncovered closure systems (L3 and L6). Concentrations are in mg $L^{-1}$. CFT = centrifuged fine tailings; TS = tailings sand.

# CHAPTER 6: CONCLUSIONS AND RECCOMENDATIONS

## 6.1 Conclusion

The main hypotheses presented at the beginning of this thesis were (1) that petroleum coke and CFT will act as a source of trace elements within mine closure systems; (2) that petroleum coke layers within these systems will act as a capillary break between successive cover layers, reducing the movement of trace elements to surface; and, (3) that soil covers will promote attenuation of trace elements in closure systems, reducing porewater concentrations at surface. To evaluate these hypotheses, a series of six lysimeter systems were set up on an oil sands mine site and filled with varying assemblages of petroleum coke, CFT, reclamation material, and tailings sand. Three layering schemes were used to represent systems where CFT was overlain by a coke and reclamation material cover (L1 and L4); where CFT was overlain by a single coke cover (L2 and L5); and where CFT was left uncovered overlying a tailings sand underdrain (L3 and L6). Each layering scheme had a partially-saturated and fully-saturated duplicate to observe the effects of saturation on trace element mobility.

This study has identified that As ($60 \pm 15$ µg $L^{-1}$), Mo ($220 \pm 350$ µg $L^{-1}$), Ni ($7.8 \pm 13$ µg $L^{-1}$), Se ($4.5 \pm 9.0$ µg $L^{-1}$), and V ($110 \pm 200$ µg $L^{-1}$) are contaminants of potential concern within these closure systems. Furthermore, this research concluded that CFT is likely the main source of As and Se, and that petroleum coke is the main source of Mo, Ni, and V within these systems. The findings of this investigation complement those of earlier studies by Heaton (2015) and Nesbitt (2016), who found similar results in the porewater of full-scale CFT and petroleum coke deposits, respectively. Previously unknown, however, was the effect of storing these materials together under fully- or partially-saturated conditions, and the effectiveness of a reclamation cover on closure landscapes containing these materials. This study concluded that porewater released during compaction and dewatering of CFT influenced the release of trace elements from coke layers through the influx of highly concentrated inorganic ions and exchangeable cations. It also suggested that a major mechanism that may be releasing trace elements from CFT was the reductive dissolution of Fe-(hydr)oxides, however this claim should

be investigated further before concrete conclusions are formed. Higher concentrations of some trace elements at and below the water table in the partially-saturated systems suggest that lack of saturation may lead to increased oxidative weathering and flushing by precipitation of coke layers. However, lack of hydraulic connection to surface cover layers would prevent transport of trace elements to surface vegetation, dependent on reclamation soil and coke layer cover thickness and vegetation root depth. Results from the fully-saturated systems suggest that a cover layer is effective in both reducing evaporative concentrating, and reducing contaminant concentrations through complexation with organic material and surface complexation with available mineral surfaces.

Several practical applications may be drawn from this study regarding best-practice for closure system design with respect to trace element mobility. For partially-saturated systems (dry landscapes), it appears that a coke layer overlying CFT can volumetrically accommodate the release of CFT porewater. While fresh water infiltration increases the weathering of petroleum coke, the lack of hydraulic connection to surface layers could allow vegetation to persist unaffected by these elevated concentrations. Another positive of partially-saturated systems is that it may reduce the degree of reduction occurring within the CFT units, thereby reducing the release of trace elements. A drawback to partially-saturated systems is that the majority of the trace elements of potential concern are most mobile under oxic conditions, and therefore long-term attenuation may be compromised. For fully-saturated systems (wet landscapes) it appears that a reclamation material cover layer is effective at reducing the concentrations of several trace elements at surface. The more reduced conditions may lower oxidative trace element release from coke, however the hydraulic connection of the system allows transport of CFT porewater that also influences leaching from coke. Another drawback of this method may be the increasingly reductive conditions imposed on CFT layers, which appears to increase the release of As, Ni, and Se. Based on the available results, for these specific layering schemes it appears that a partially-saturated system is most effective at reducing trace element release and transport to surface. However, long-term attenuation may be increased in the fully-saturated system due to interaction with a reclamation material layer. This research extends the knowledge of the geochemical behavior of trace elements within oil sands mine closure landscapes, and provides industry with information to aid in end-of-life planning for mine closure.

## 6.2 Recommendations and Future Work

Based on the results of this study, several recommendations can be made regarding future work:

- Continued sampling of the lysimeter experiments will provide valuable knowledge of the long-term mobility, transport, and attenuation of trace elements within potential closure systems.
- Continued monitoring of the data logger systems and material heights will provide valuable data to understand the freeze-thaw cycling effects on the compaction rates of CFT and release of CFT porewater.
- Future lysimeter sampling should include microbial analyses to better understand the biotic controls on redox conditions and trace element mobility present in these systems.
- Future lysimeter sampling should also include analyses for organic acids (humic and fulvic), as these likely influence trace element mobility within the reclamation material cover.
- Thermodynamic modelling or specialized sampling should be conducted to provide further evidence for the presence of zero-valent sulfur or other sulfur trace element species, as this may be a strong influence on redox conditions and trace element mobility within the CFT units.
- Sequential extractions should be performed on CFT to better understand the sediment phase association of trace elements within the material.
- Scanning electron microprobe or synchrotron beamline work on CFT would provide a better understanding of the sources of trace element release from this material.
- Full-scale reclamation landscapes should consider CFT porewater volumes and compaction rates when calculating the thickness of petroleum coke and reclamation soil cover layers.

## REFERENCES


Abolfazlzadehdoshanbehbazari, M., Birks, S. J., Moncur, M. C., & Ulrich, A. C. (2013). Fate and Transport of Oil Sand Process-Affected Water into the Underlying Clay Till: A Field Study. *Journal of Contaminant Hydrology*, *151*, 83–92. https://doi.org/10.1016/j.jconhyd.2013.05.002

Alberta Energy Regulator. (2015). *Alberta's Energy Reserves 2014 and Supply/Demand Outlook 2015–2024* (No. ST98-2015) (p. 299). Government of Alberta. Retrieved from www.aer.ca

Allen, E. W. (2008). Process Water Treatment in Canada's Oil Sands Industry: I. Target Pollutants and Treatment Objectives. *Journal of Environmental Engineering and Science*, *7*, 123–138. https://doi.org/10.1139/S07-038

Alloway, B. J. (Ed.). (2013). *Heavy Metals in Soils: Trace Metals and Metalloids in Soils and Their Bioavailability* (Vol. 22). Dordrecht: Springer Netherlands. Retrieved from http://link.springer.com/10.1007/978-94-007-4470-7

Anderson, J. C., Wiseman, S. B., Wang, N., Moustafa, A., Perez-Estrada, L., Gamal El-Din, M., Giesy, J. P. (2012). Effectiveness of Ozonation Treatment in Eliminating Toxicity of Oil Sands Process-Affected Water to *Chironomus dilutus*. *Environmental Science & Technology*, *46*(1), 486–493. https://doi.org/10.1021/es202415g

Appelo, C. A. J., & Postma, D. (2005). *Geochemistry, Groundwater and Pollution (2nd edition).* Leiden, The Netherlands: A.A. Balkema.

Baer, T. (2014). *An evaluation of the use of natural stable isotopes of water to track water movement through oil sands mine closure landforms*. University of Saskatchewan, Saskatoon, SK.

Baer, T., Barbour, S. L., & Gibson, J. J. (2016). The stable isotopes of site wide waters at an oil sands mine in northern Alberta, Canada. *Journal of Hydrology*, *541*, 1155–1164. https://doi.org/10.1016/j.jhydrol.2016.08.017

Borch, T., Kretzschmar, R., Kappler, A., Cappellen, P. V., Ginder-Vogel, M., Voegelin, A., & Campbell, K. (2010). Biogeochemical Redox Processes and their Impact on Contaminant Dynamics. *Environmental Science & Technology*, 44(1), 15–23. https://doi.org/10.1021/es9026248

Carrigy, M. A. (1959). Geology of the McMurray Formation Part III General Geology of the McMurray Area. Retrieved from http://ags.aer.ca/document/MEM/MEM_01.pdf

Chalaturnyk, R. J., Don Scott, J., & Özüm, B. (2002). Management of Oil Sands Tailings. *Petroleum Science and Technology*, *20*(9–10), 1025–1046. https://doi.org/10.1081/LFT-120003695

Chen, M., Walshe, G., Chi Fru, E., Ciborowski, J. J. H., & Weisener, C. G. (2013). Microcosm Assessment of the Biogeochemical Development of Sulfur and Oxygen in Oil Sands Fluid Fine Tailings. *Applied Geochemistry*, *37*, 1–11. https://doi.org/10.1016/j.apgeochem.2013.06.007

Cilia, C. (2017). *Characterizing the Physical and Chemical Mass Transport of Dissolved Salts in Layered Oil Sands Waste Undergoing Reclamation*. University of Saskatchewan. Saskatoon, SK.

Couture, R.-M., & Van Cappellen, P. (2011). Reassessing the role of sulfur geochemistry on arsenic speciation in reducing environments. *Journal of Hazardous Materials*, *189*(3), 647–652. https://doi.org/10.1016/j.jhazmat.2011.02.029

Dahl, T. W., Chappaz, A., Fitts, J. P., & Lyons, T. W. (2013). Molybdenum reduction in a sulfidic lake: Evidence from X-ray absorption fine-structure spectroscopy and implications for the Mo paleoproxy. *Geochimica et Cosmochimica Acta*, *103*, 213–231. https://doi.org/10.1016/j.gca.2012.10.058

Devito, K., Mendoza, C., & Qualizza, C. (2012). *Conceptualizing Water Movement in the Boreal Plains: Implications for Watershed Reconstruction* (Synthesis) (p. 164). Canadian Oil Sands Network for Research and Development, Environmental and Reclamation Research Group.

Diehl, S. F., Goldhaber, M. B., Koenig, A. E., Lowers, H. A., & Ruppert, L. F. (2012). Distribution of arsenic, selenium, and other trace elements in high pyrite Appalachian coals: Evidence for multiple episodes of pyrite formation. *International Journal of Coal Geology*, 94, 238–249. https://doi.org/10.1016/j.coal.2012.01.015

Eldridge, D. S., Crawford, R. J., & Harding, I. H. (2015). The role of metal ion-ligand interactions during divalent metal ion adsorption. Journal of Colloid and Interface Science, 454, 20–26. https://doi.org/10.1016/j.jcis.2015.04.056

Environment Canada. (2017). Historical Climate Data. Retrieved July 1, 2017, from http://climate.weather.gc.ca

Erickson, B. E., & Helz, G. R. (2000). Molybdenum (VI) speciation in sulfidic waters: stability and lability of thiomolybdates. *Geochimica et Cosmochimica Acta*, *64*(7), 1149–1158.

Essilfie-Dughan, J., Hendry, M. J., Dynes, J. J., Hu, Y., Biswas, A., Lee Barbour, S., & Day, S. (2017). Geochemical and mineralogical characterization of sulfur and iron in coal waste

rock, Elk Valley, British Columbia, Canada. *Science of The Total Environment, 586*, 753–769. https://doi.org/10.1016/j.scitotenv.2017.02.053

Fischer, L., Brümmer, G. W., & Barrow, N. J. (2007). Observations and modelling of the reactions of 10 metals with goethite: adsorption and diffusion processes. *European Journal of Soil Science*, *58*(6), 1304–1315. https://doi.org/10.1111/j.1365-2389.2007.00924.x

Fordham, A. W., & Norrish, K. (1979). Arsenate-73 uptake by components of several acidic soils and its implications for phosphate retention. *Soil Research*, *17*(2), 307–316.

Gamal El-Din, M., Fu, H., Wang, N., Chelme-Ayala, P., Pérez-Estrada, L., Drzewicz, P., … Smith, D. W. (2011). Naphthenic acids speciation and removal during petroleum-coke adsorption and ozonation of oil sands process-affected water. *Science of The Total Environment*, *409*(23), 5119–5125. https://doi.org/10.1016/j.scitotenv.2011.08.033

Gibson, J. J., Birks, S. J., Yi, Y., & Vitt, D. H. (2015). Runoff to boreal lakes linked to land cover, watershed morphology and permafrost thaw: a 9-year isotope mass balance assessment: Boreal Lakes Isotope Mass Balance Assessment. *Hydrological Processes*, *29*(18), 3848–3861. https://doi.org/10.1002/hyp.10502

Goldberg, S., Lesch, S. M., Suarez, D. L., & Basta, N. T. (2005). Predicting Arsenate Adsorption by Soils using Soil Chemical Parameters in the Constant Capacitance Model. *Soil Science Society of America Journal*, *69*(5), 1389. https://doi.org/10.2136/sssaj2004.0393

Gomez, M. A., Jim Hendry, M., Hossain, A., Das, S., & Elouatik, S. (2013). Abiotic reduction of 2-line ferrihydrite: effects on adsorbed arsenate, molybdate, and nickel. *RSC Advances*, *3*(48), 25812. https://doi.org/10.1039/c3ra44769c

Government of Alberta. (2015). *Environment and Sustainable Resource Development Annual Report 2014-2015* (p. 187). Edmonton, Alberta: Government of Alberta. Retrieved from http://aep.alberta.ca/about-us/corporate-documents/documents/ESRD-AnnualReport-2014-2015.pdf

Government of Alberta (2017). Oil Sands Mine Reclamation and Disturbance Tracking by Year. Oil Sands Information Portal. http://osip.alberta.ca/library/Dataset/Details/27, accessed: May 1, 2018.

Gray, M. R. (2015). *Upgrading Oilsands Bitumen and Heavy Oil*. Pica Pica Press.

Gustafsson, J. P., & Johnsson, L. (1994). The association between selenium and humic substances in forested ecosystems—laboratory evidence. *Applied Organometallic Chemistry*, *8*(2), 141–147.

Heaton, K. K. (2015, September). *Biogeochemical Investigation of Centrifuged Fine Tailings Deposits at an Oil Sands Mine in Northern Alberta, Canada*. University of Saskatchewan, Saskatoon, SK.

Hein, F., Cotterill, D. K., Weiss, J., & Berhane, H. (2007). *Subsurface Geology and Facies Characterization of the Athabasca Wabiskaw-McMurray Succession: Firebag-Sunrise Area, Northeastern Alberta* (No. NTS 74D/74E) (p. 73). Edmonton, Alberta: Alberta Geological Survey. Retrieved from http://ags.aer.ca/document/ESR/ESR_2006_08.PDF

Hendry, M. J., Biswas, A., Essilfie-Dughan, J., Chen, N., Day, S. J., & Barbour, S. L. (2015). Reservoirs of Selenium in Coal Waste Rock: Elk Valley, British Columbia, Canada. *Environmental Science & Technology*, *49*(13), 8228–8236. https://doi.org/10.1021/acs.est.5b01246

Holden, A. A., Donahue, R. B., & Ulrich, A. C. (2011). Geochemical interactions between process-affected water from oil sands tailings ponds and North Alberta surficial sediments. *Journal of Contaminant Hydrology*, *119*(1–4), 55–68. https://doi.org/10.1016/j.jconhyd.2010.09.008

Jia, Y., Guo, H., Xi, B., Jiang, Y., Zhang, Z., Yuan, R., … Xue, X. (2017). Sources of groundwater salinity and potential impact on arsenic mobility in the western Hetao Basin, Inner Mongolia. *Science of The Total Environment*, *601–602*, 691–702. https://doi.org/10.1016/j.scitotenv.2017.05.196

Kaminsky, H. A. W., Etsell, T. H., Ivey, D. G., & Omotoso, O. (2009). Distribution of clay minerals in the process streams produced by the extraction of bitumen from Athabasca oil sands. *The Canadian Journal of Chemical Engineering*, *87*(1), 85–93. https://doi.org/10.1002/cjce.20133

Karbanee, N., van Hille, R. P., & Lewis, A. E. (2008). Controlled Nickel Sulfide Precipitation Using Gaseous Hydrogen Sulfide. *Industrial & Engineering Chemistry Research*, *47*(5), 1596–1602. https://doi.org/10.1021/ie0711224

Kasperski, K. L., & Mikula, R. J. (2011). Waste Streams of Mined Oil Sands: Characteristics and Remediation. *Elements*, *7*(6), 387–392.

Kessler, S., & Hendry, M. J. (2006). *Geochemistry and Leaching of Coke from Syncrude and Suncor Sites*. University of Saskatchewan.

Kocar, B. D., Borch, T., & Fendorf, S. (2010). Arsenic repartitioning during biogenic sulfidization and transformation of ferrihydrite. *Geochimica et Cosmochimica Acta*, *74*(3), 980–994. https://doi.org/10.1016/j.gca.2009.10.023

Lis, G., Wassenaar, L. I., & Hendry, M. J. (2008). High-Precision Laser Spectroscopy D/H and 18 O/ 16 O Measurements of Microliter Natural Water Samples. *Analytical Chemistry*, *80*(1), 287–293. https://doi.org/10.1021/ac701716q

Liu, J., Xu, Z., & Masliyah, J. (2005). Processability of Oil Sand Ores in Alberta. *Energy & Fuels*, *19*(5), 2056–2063. https://doi.org/10.1021/ef050091r

Luna Wolter, G. L., & Naeth, M. A. (2014). Dry Mature Fine Tailings as Oil Sands Reclamation Substrates for Three Native Grasses. *Journal of Environment Quality*, *43*(4), 1510–1516. https://doi.org/10.2134/jeq2013.10.0415

Manceau, A., & Charlet, L. (1994). The Mechanism of Selenate Adsorption on Goethite and Hydrous Ferric Oxide. *Journal of Colloid and Interface Science*, *168*, 87–93.

Manceau, A., Lanson, M., & Geoffroy, N. (2007). Natural speciation of Ni, Zn, Ba, and As in ferromanganese coatings on quartz using X-ray fluorescence, absorption, and diffraction. *Geochimica et Cosmochimica Acta*, *71*(1), 95–128. https://doi.org/10.1016/j.gca.2006.08.036

Markelova, E. (2017). *Redox potential and mobility of contaminant oxyanions (As, Sb, Cr) in argillaceous rock during oxic and anoxic cycles*. University of Waterloo, Waterloo, ON, Canada.

Masliyah, J., Zhou, Z., Xu, Z., Czarnecki, J., & Hamza, H. (2004). Understanding Water-Based Bitumen Extraction from Athabasca Oil Sands. *The Canadian Journal of Chemical Engineering*, *82*, 628–654.

Masscheleyn, P. H., Delaune, R. D., & Patrick Jr, W. H. (1990). Transformations of selenium as affected by sediment oxidation-reduction potential and pH. *Environmental Science & Technology*, *24*(1), 91–96.

McPherson, R. A., & Cathol, C. P. (1997). Surficial Geology of Potential Mining Areas in the Athabasca Oil Sands Region. Retrieved from http://ags.aer.ca/document/OFR/OFR_1977_04.pdf

Mikula, R. J., Munoz, V. A., & Omotoso, O. (2009). Centrifugation Options for Production of Dry Stackable Tailings in Surface-Mined Oil Sands Tailings Management. *Journal of Canadian Petroleum Technology*, *48*(09), 19–23.

Müller, K., Ciminelli, V. S. T., Dantas, M. S. S., & Willscher, S. (2010). A comparative study of As(III) and As(V) in aqueous solutions and adsorbed on iron oxy-hydroxides by Raman spectroscopy. *Water Research*, *44*(19), 5660–5672. https://doi.org/10.1016/j.watres.2010.05.053

Nakata, C., Qualizza, C., MacKinnon, M., & Renault, S. (2011). Growth and Physiological Responses of Triticum aestivum and Deschampsia caespitosa Exposed to Petroleum Coke. *Water, Air, & Soil Pollution*, *216*(1–4), 59–72. https://doi.org/10.1007/s11270-010-0514-x

Nesbitt, J. A. (2016). *Geochemical investigation of fluid petroleum coke deposits at an oil sands mine in northern Alberta, Canada*. University of Saskatchewan. Retrieved from https://ecommons.usask.ca/handle/10388/7303

Nesbitt, J. A., & Lindsay, M. B. J. (2017). Vanadium Geochemistry of Oil Sands Fluid Petroleum Coke. *Environmental Science & Technology*, *51*(5), 3102–3109. https://doi.org/10.1021/acs.est.6b05682

Nesbitt, J. A., Lindsay, M. B. J., & Chen, N. (2017). Geochemical characteristics of oil sands fluid petroleum coke. *Applied Geochemistry*, *76*, 148–158. https://doi.org/10.1016/j.apgeochem.2016.11.023

Osacky, M., Geramian, M., Dyar, M. D., Sklute, E. C., Valter, M., Ivey, D. G., … Etsell, T. H. (2013). Characterisation of Petrologic End Members of Oil Sands from the Athabasca Region, Alberta, Canada. *The Canadian Journal of Chemical Engineering*, *91*(8), 1402–1415. https://doi.org/10.1002/cjce.21860

Parkhurst, D. L., & Appelo, C. A. J. (2013). *Description of Input and Examples for PHREEQC Version 3 - A Computer Program for Speciation, Batch-Reaction, One-Dimensional Transport, and Inverse Geochemical Calculations*. US Department of the Interior; US Geological Survey.

Peacock, C. L., & Sherman, D. M. (2004). Vanadium(V) adsorption onto goethite (α-FeOOH) at pH 1.5 to 12: a surface complexation model based on ab initio molecular geometries and EXAFS spectroscopy. *Geochimica et Cosmochimica Acta*, *68*(8), 1723–1733. https://doi.org/10.1016/j.gca.2003.10.018

Peak, D., & Sparks, D. L. (2002). Mechanisms of Selenate Adsorption on Iron Oxides and Hydroxides. *Environmental Science & Technology*, *36*(7), 1460–1466. https://doi.org/10.1021/es0156643

Peel, M. C., Finlayson, B. L., & McMahon, T. A. (2007). Updated world map of the Köppen-Geiger climate classification. *Hydrology and Earth System Sciences*, *11*, 1633–1644.

Proskin, S., Sego, D., & Alostaz, M. (2012). Oil Sands MFT Properties and Freeze-Thaw Effects. *Journal of Cold Regions Engineering*, *26*(2), 29–54.

Puttaswamy, N., & Liber, K. (2012). Influence of inorganic anions on metals release from oil sands coke and on toxicity of nickel and vanadium to Ceriodaphnia dubia. *Chemosphere*, *86*(5), 521–529. https://doi.org/10.1016/j.chemosphere.2011.10.018

Puttaswamy, N., Turcotte, D., & Liber, K. (2010). Variation in toxicity response of Ceriodaphnia dubia to Athabasca oil sands coke leachates. *Chemosphere*, *80*(5), 489–497. https://doi.org/10.1016/j.chemosphere.2010.04.071

Rima, U. S., & Azam, S. (2015). Centrifuge Dewatering of Polymer-Amended Oil Sand Tailings. *Environmental Geotechnics*, *2*(3), 175–180. https://doi.org/10.1680/envgeo.13.00083

Rogers, V. V., Wickstrom, M., Liber, K., & MacKinnon, M. D. (2002). Acute and Subchronic Mammalian Toxicity of Naphthenic Acids from Oil Sands Tailings. *Toxicological Sciences*, *66*, 347–355.

Siddique, T., Kuznetsov, P., Kuznetsova, A., Arkell, N., Young, R., Li, C., Guigard, S., Underwood, E., Foght, J. M. (2014). Microbially-Accelerated Consolidation of Oil Sands Tailings. Pathway I: Changes in Porewater Chemistry. *Frontiers in Microbiology*, *5*. https://doi.org/10.3389/fmicb.2014.00106

Simhayov, R. B., Price, J. S., Smeaton, C. M., Parsons, C., Rezanezhad, F., & Van Cappellen, P. (2017). Solute pools in Nikanotee Fen watershed in the Athabasca oil sands region. *Environmental Pollution*, 225(Supplement C), 150–162. https://doi.org/10.1016/j.envpol.2017.03.038

Small, C. C. (2011, Spring). *Activation of Delayed and Fluid Petroleum Coke for the Adsorption and Removal of Naphthenic Acids from Oil Sands Tailings Pond Water*. University of Alberta, Edmonton, Alberta.

Smedley, P. L., & Kinniburgh, D. G. (2017). Molybdenum in natural waters: A review of occurrence, distributions and controls. *Applied Geochemistry*, *84*, 387–432. https://doi.org/10.1016/j.apgeochem.2017.05.008

Sobkowicz, J., McKenna, G., & Dawson, R. (2012). *Oil Sands Tailings Technology Deployment Roadmap*. Retrieved from http://www.cosia.ca/uploads/documents/id10/Tailings%20Roadmap%20Volume%202%20June%202012.pdf

Suncor Energy Inc. (2015). *2014 Report on Sustainability*. Retrieved from http://suncor360.nonfiction.ca/2014/ros-en/files/extfiles/downloadURL.PDF

Syncrude Canada Limited. (2015). *Syncrude 2014 Sustainability Report*. Retrieved from http://syncrudesustainability.com/2014/pdfs/Syncrude-CSR2014.pdf

Telfeyan, K., Johannesson, K. H., Mohajerin, T. J., & Palmore, C. D. (2015). Vanadium geochemistry along groundwater flow paths in contrasting aquifers of the United States: Carrizo Sand (Texas) and Oasis Valley (Nevada) aquifers. *Chemical Geology*, *410*, 63–78. https://doi.org/10.1016/j.chemgeo.2015.05.024

USEPA. (1998). MINTEQA2/PRODEFA2, A Geochemical Assessment Model for Environmental Systems: User Manual Supplement for Version 4.0.

Vorlicek, T. P., Kahn, M. D., Kasuya, Y., & Helz, G. R. (2004). Capture of molybdenum in pyrite-forming sediments: role of ligand-induced reduction by polysulfides. *Geochimica et Cosmochimica Acta*, *68*(3), 547–556.

Wang, C., Harbottle, D., Liu, Q., & Xu, Z. (2014). Current state of fine mineral tailings treatment: A critical review on theory and practice. *Minerals Engineering*, *58*, 113–131. https://doi.org/10.1016/j.mineng.2014.01.018

Wehrli, B., & Stumm, W. (1989). Vanadyl in natural waters: Adsorption and hydrolysis promote oxygenation. *Geochimica et Cosmochimica Acta*, *53*, 69–77.

Weres, O., Bowman, H. R., Goldstein, A., Smith, E. C., Tsao, L., & Harnden, W. (1990). The effect of nitrate and organic matter upon mobility of selenium in groundwater and in a water treatment process. *Water, Air, and Soil Pollution*, *49*(3–4), 251–272.

Wichard, T., Mishra, B., Myneni, S. C. B., Bellenger, J.-P., & Kraepiel, A. M. L. (2009). Storage and bioavailability of molybdenum in soils increased by organic matter complexation. *Nature Geoscience*, *2*(9), 625–629. https://doi.org/10.1038/ngeo589

Winkel, L. H. E., Johnson, C. A., Lenz, M., Grundl, T., Leupin, O. X., Amini, M., & Charlet, L. (2012). Environmental Selenium Research: From Microscopic Processes to Global Understanding. *Environmental Science & Technology*, *46*(2), 571–579. https://doi.org/10.1021/es203434d

Wisawapipat, W., & Kretzschmar, R. (2017). Solid Phase Speciation and Solubility of Vanadium in Highly Weathered Soils. *Environmental Science & Technology*, *51*(15), 8254–8262. https://doi.org/10.1021/acs.est.7b01005

Wright, M. T., Stollenwerk, K. G., & Belitz, K. (2014). Assessing the solubility controls on vanadium in groundwater, northeastern San Joaquin Valley, CA. *Applied Geochemistry*, *48*, 41–52. https://doi.org/10.1016/j.apgeochem.2014.06.025

Xu, N., Braida, W., Christodoulatos, C., & Chen, J. (2013). A Review of Molybdenum Adsorption in Soils/Bed Sediments: Speciation, Mechanism, and Model Applications. *Soil and Sediment Contamination: An International Journal*, *22*(8), 912–929. https://doi.org/10.1080/15320383.2013.770438

Zubot, W., MacKinnon, M. D., Chelme-Ayala, P., Smith, D. W., & Gamal El-Din, M. (2012). Petroleum Coke Adsorption as a Water Management Option for Oil Sands Process-Affected Water. *Science of The Total Environment*, *427–428*, 364–372. https://doi.org/10.1016/j.scitotenv.2012.04.024

# APPENDIX A  DATA LOGGER PLOTS

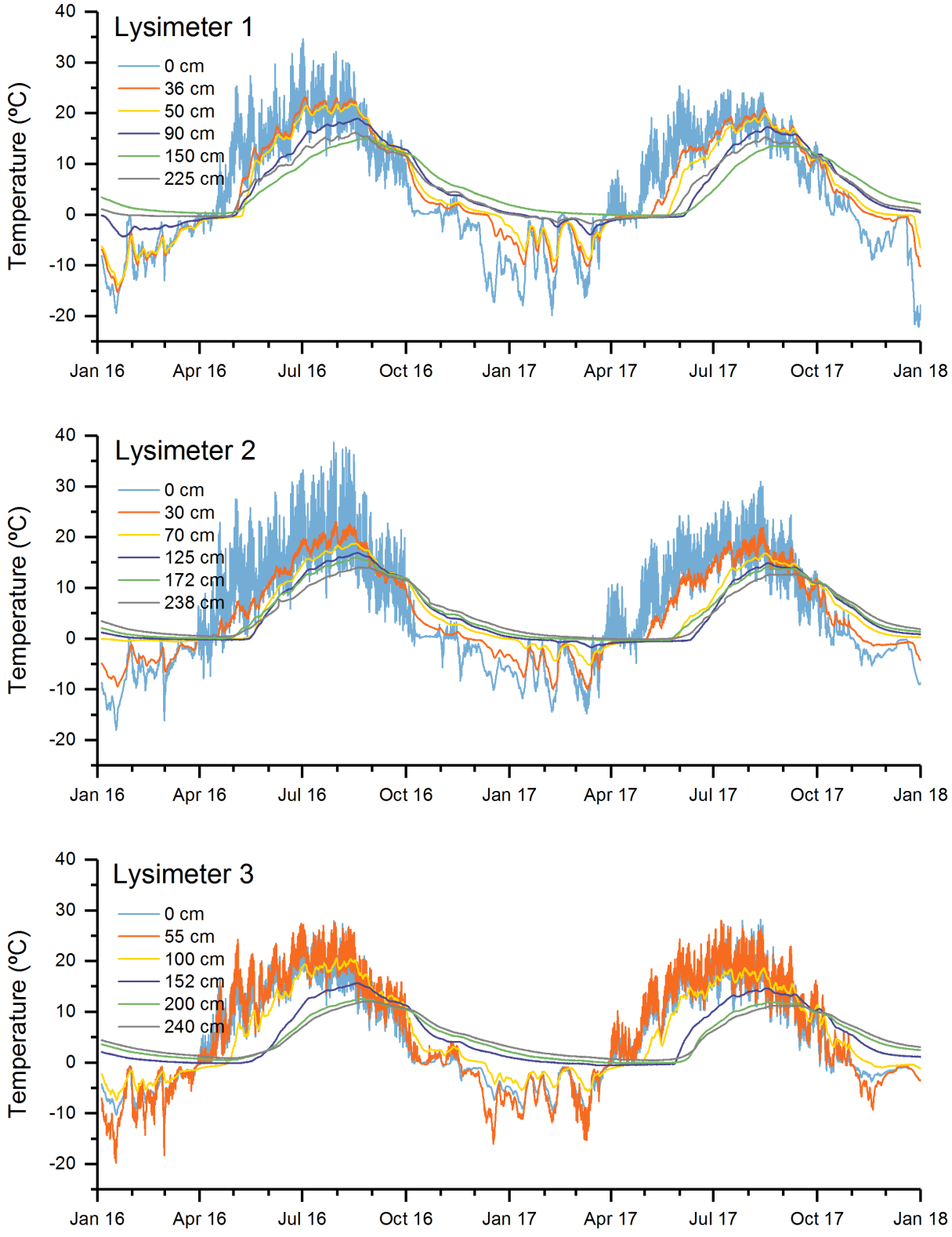


Figure B-1: Temperature measurements in the partially-saturated lysimeters plotted from January 2016 to January 2018.

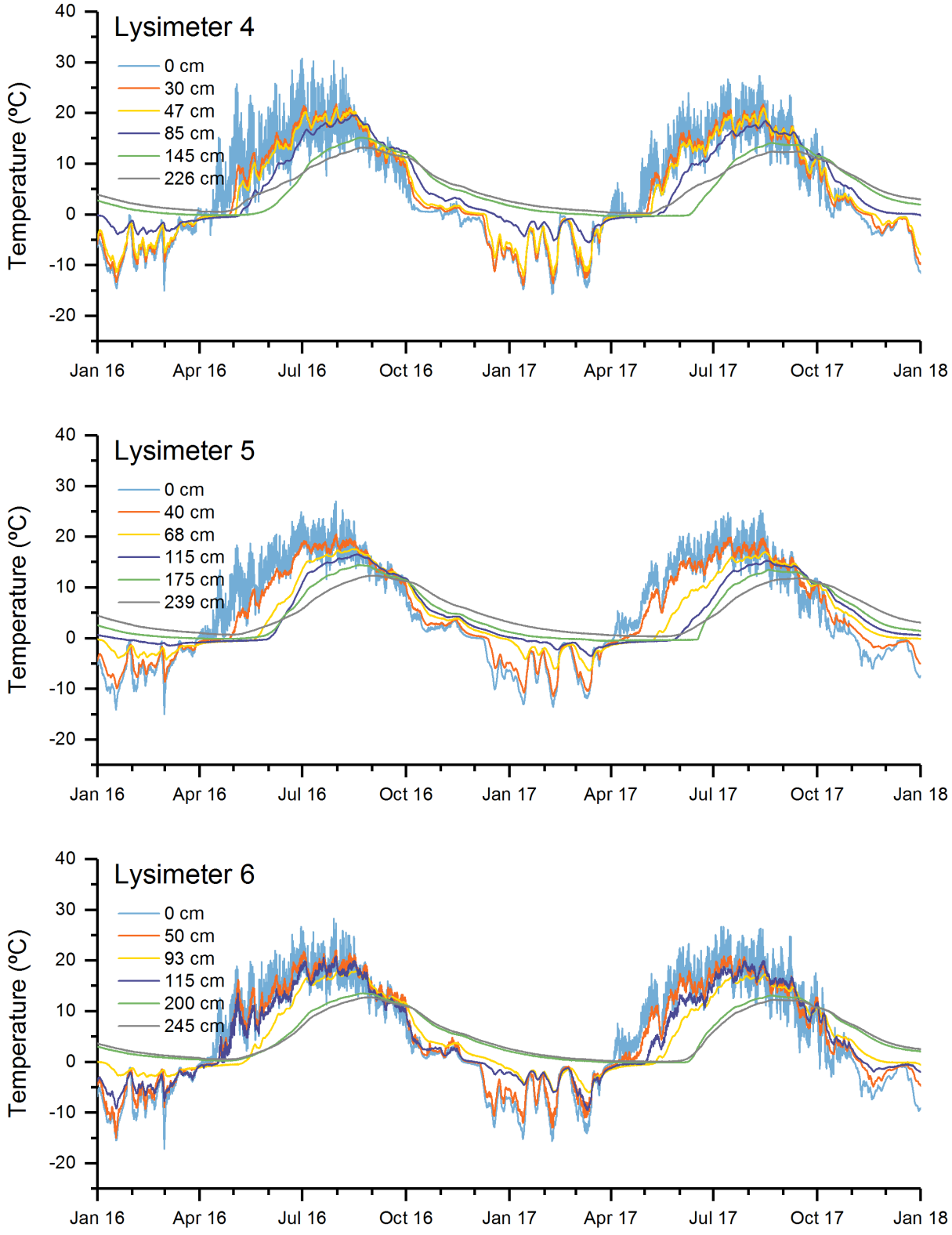


Figure B-2: Temperature measurements in the fully-saturated lysimeters plotted from January 2016 to January 2018.

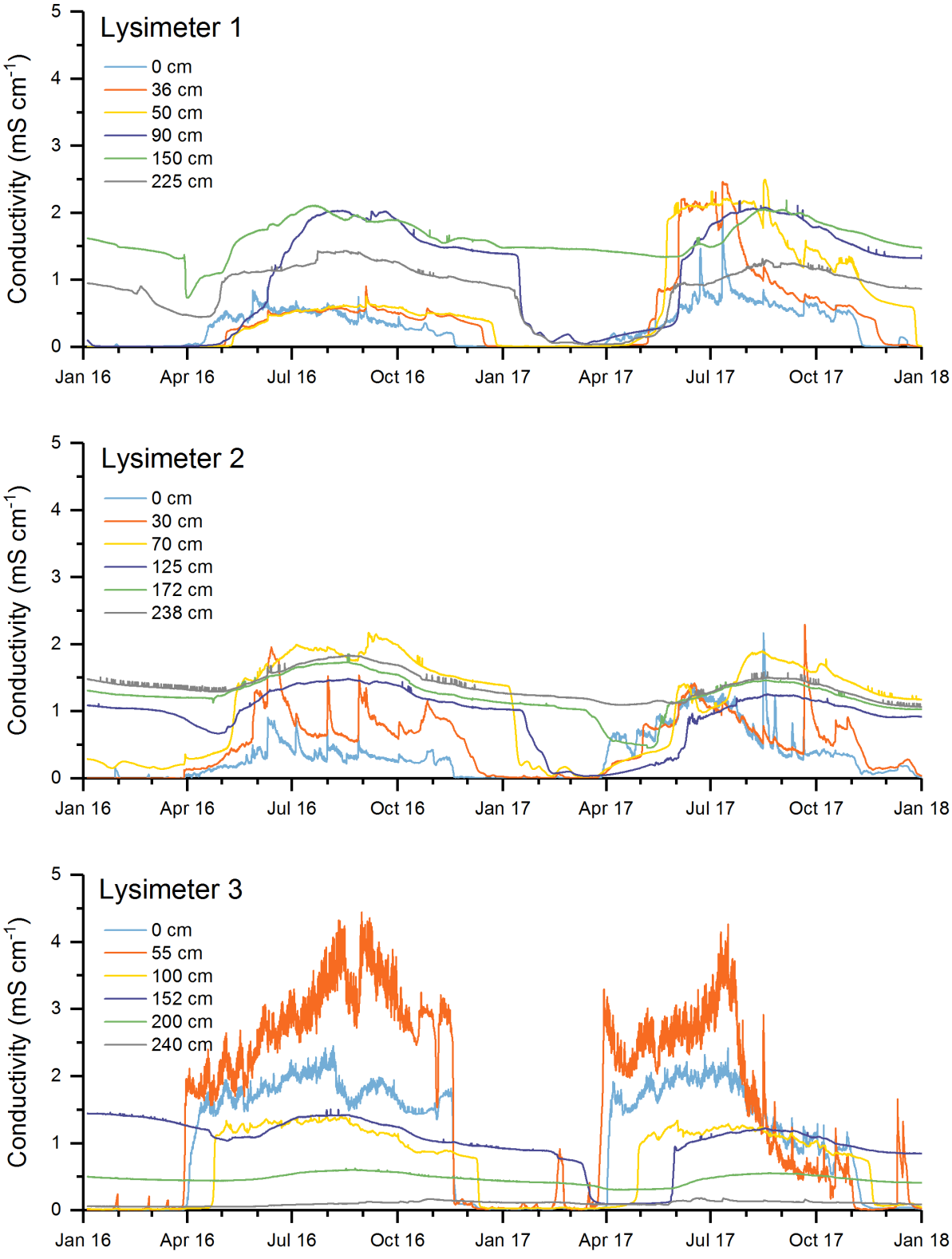


Figure B-3: Bulk EC measurements in the partially-saturated lysimeters plotted from January 2016 to January 2018.

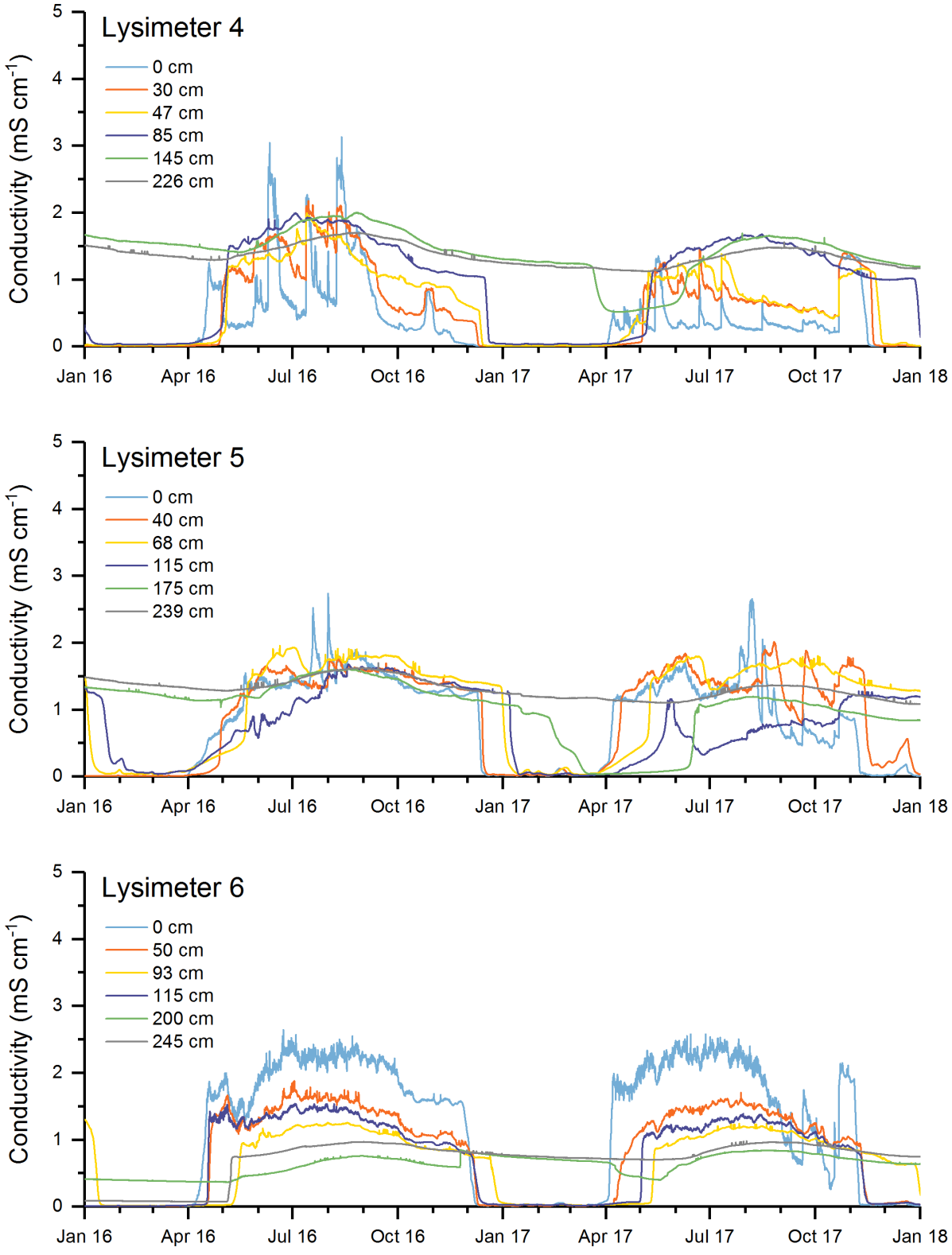


Figure B-4: Bulk EC measurements in the fully-saturated lysimeters plotted from January 2016 to January 2018.

## APPENDIX B LYSIMETER DATA

Table B-1: Sample ID and associated lysimeter ID, well/core identification, sampling depth, and sampling date.

| Lysimeter ID | Well/Core? | Sample ID | Depth | | Date | |
|---|---|---|---|---|---|---|
| | | | [1](m) | [2](m) | Sampling | Centrifuging |
| 1 | Well | US-L1-P175 | | 1.50 | Aug 16 | |
| 1 | Well | US-L1-P200 | | 1.75 | Aug 16 | |
| 1 | Well | US-L1-P225 | | 2.00 | Aug 16 | |
| 1 | Core | L1 1.65-1.8 m | 1.65-1.8 | 2.10 | Nov 16 | Jan 17 |
| 1 | Core | L1 1.8-1.95 m | 1.8-1.95 | 2.25 | Nov 16 | Jan 17 |
| 1 | Core | L1 2.25-2.4 m | 2.25-2.4 | 2.70 | Nov 16 | Jan 17 |
| 1 | Core | L1 2.4-2.55 m | 2.4-2.55 | 2.85 | Nov 16 | Jan 17 |
| 1 | Core | L1 2.55-2.7 m | 2.55-2.7 | 3.00 | Nov 16 | Jan 17 |
| 2 | Core | L2 0.95-1.15 m | 0.95-1.15 | 1.50 | Nov 16 | Jan 17 |
| 2 | Core | L2 1.15-1.35 m | 1.15-1.35 | 1.70 | Nov 16 | Jan 17 |
| 2 | Core | L2 1.35-1.5 m | 1.35-1.5 | 1.90 | Nov 16 | Jan 17 |
| 2 | Core | L2 2.15-2.3 m | 2.15-2.3 | 2.70 | Nov 16 | Jan 17 |
| 2 | Core | L2 2.3-2.45 m | 2.3-2.45 | 2.85 | Nov 16 | Jan 17 |
| 2 | Core | L2 2.45-2.6 m | 2.45-2.6 | 3.00 | Nov 16 | Jan 17 |
| 3 | Core | L3 0.15-0.3 m | 0.15-0.3 | 0.88 | Nov 16 | Jan 17 |
| 3 | Core | L3 0.3-0.45 m | 0.3-0.45 | 1.03 | Nov 16 | Jan 17 |
| 3 | Core | L3 0.45-0.6 m | 0.45-0.6 | 1.18 | Nov 16 | Jan 17 |
| 3 | Core | L3 0.9-1.05 m | 0.9-1.05 | 1.63 | Nov 16 | Jan 17 |
| 3 | Core | L3 1.05-1.2 m | 1.05-1.2 | 1.78 | Nov 16 | Jan 17 |
| 3 | Core | L3 1.2-1.35 m | 1.2-1.35 | 1.93 | Nov 16 | Jan 17 |
| 3 | Well | US-L3-P300 | | 2.75 | Aug 16 | |
| 3 | Well | US-L3-P300C | | 3 | Aug 16 | |
| 4 | Well | US-L4-P050 | | 0.25 | Aug 16 | |
| 4 | Well | US-L4-P075 | | 0.5 | Aug 16 | |
| 4 | Well | US-L4-P100 | | 0.75 | Aug 16 | |
| 4 | Well | US-L4-P125 | | 1 | Aug 16 | |
| 4 | Well | US-L4-P150 | | 1.25 | Aug 16 | |
| 4 | Well | US-L4-P175 | | 1.5 | Aug 16 | |
| 4 | Core | L4 1.4-1.55 m | 1.4-1.55 | 1.9 | Nov 16 | Jan 17 |
| 4 | Core | L4 1.55-1.7 m | 1.55-1.7 | 2.05 | Nov 16 | Jan 17 |
| 4 | Core | L4 1.7-1.85 m | 1.7-1.85 | 2.2 | Nov 16 | Jan 17 |
| 4 | Core | L4 2.2-2.35 m | 2.2-2.35 | 2.7 | Nov 16 | Jan 17 |
| 4 | Core | L4 2.35-2.5 m | 2.35-2.5 | 2.85 | Nov 16 | Jan 17 |
| 4 | Core | L4 2.5-2.65 m | 2.5-2.65 | 3 | Nov 16 | Jan 17 |
| 5 | Well | US-L5-P050 | | 0.25 | Aug 16 | |
| 5 | Well | US-L5-P075 | | 0.5 | Aug 16 | |
| 5 | Well | US-L5-P100 | | 0.75 | Aug 16 | |
| 5 | Well | US-L5-P125 | | 1 | Aug 16 | |

| Lysimeter ID | Well/Core? | Sample ID | Depth | | Date | |
|---|---|---|---|---|---|---|
| | | | [1](m) | [2](m) | Sampling | Centrifuging |
| 5 | Core | L5 0.95-1.1 m | 0.95-1.1 | 1.4 | Nov 16 | Jan 17 |
| 5 | Core | L5 1.1-1.25 m | 1.1-1.25 | 1.55 | Nov 16 | Jan 17 |
| 5 | Core | L5 1.25-1.4 m | 1.25-1.4 | 1.7 | Nov 16 | Jan 17 |
| 5 | Core | L5 2.25-2.4 m | 2.25-2.4 | 2.7 | Nov 16 | Jan 17 |
| 5 | Core | L5 2.4-2.55 m | 2.4-2.55 | 2.85 | Nov 16 | Jan 17 |
| 5 | Core | L5 2.55-2.7 m | 2.55-2.7 | 3 | Nov 16 | Jan 17 |
| 6 | Well | US-L6-P150 | | 1.25 | Aug 16 | |
| 6 | Well | US-L6-P175 | | 1.5 | Aug 16 | |
| 6 | Well | US-L6-P200 | | 1.75 | Aug 16 | |
| 6 | Well | US-L6-P225 | | 2 | Aug 16 | |
| 6 | Well | US-L6-P250 | | 2.25 | Aug 16 | |
| 6 | Well | US-L6-P275 | | 2.5 | Aug 16 | |
| 6 | Well | US-L6-P300 | | 2.75 | Aug 16 | |
| 6 | Well | US-L6-P300C | | 3 | Aug 16 | |
| 6 | Core | L6 0.4-0.55 m | 0.4-0.55 | 1.165 | Nov 16 | Jan 17 |
| 6 | Core | L6 0.55-0.7 m | 0.55-0.7 | 1.315 | Nov 16 | Jan 17 |
| 6 | Core | L6 0.7-0.85 m | 0.7-0.85 | 1.465 | Nov 16 | Jan 17 |
| 6 | Core | L6 0.85-1.0 m | 0.85-1.0 | 1.615 | Nov 16 | Jan 17 |
| 6 | Core | L6 1.0-1.15 m | 1.0-1.15 | 1.765 | Nov 16 | Jan 17 |
| 6 | Core | L6 1.15-1.3 m | 1.15-1.3 | 1.915 | Nov 16 | Jan 17 |

**NOTES:**

[1]Coring depth interval.

[2]Depth of well, or depth recalculated from top of lysimeter to centre of coring interval.

Table B-2: Field measurements performed on each sample.

| Sample ID | pH | $E_h$ (mV) | EC (mS $cm^{-1}$) | [1]Alkalinity (mg $L^{-1}$) | $S^{2-}$ (µg $L^{-1}$) | $NH_3$-N (mg $L^{-1}$) |
|---|---|---|---|---|---|---|
| US-L1-P175 | 7.30 | 276 | 7.07 | 570 | 1 | 1.4 |
| US-L1-P200 | 7.60 | 321 | 6.44 | 500 | 30 | 0.9 |
| US-L1-P225 | 7.70 | -20 | 5.52 | 770 | 1590 | 1.4 |
| L1 1.65-1.8 m | 7.60 | 93 | 5.24 | 288 | 35 | 34.8 |
| L1 1.8-1.95 m | 7.70 | 43 | 6.31 | 540 | 2650 | 22.3 |
| L1 2.25-2.4 m | 7.90 | 365 | 4.17 | 670 | | 12.4 |
| L1 2.4-2.55 m | 7.70 | -82 | 3.34 | 792 | 18550 | 7.0 |
| L1 2.55-2.7 m | 7.90 | -63 | 3.46 | 811 | 12850 | 7.7 |
| L2 0.95-1.15 m | 7.79 | 154 | 4.92 | 702 | | 8.5 |
| L2 1.15-1.35 m | 7.99 | 195 | 3.54 | 836 | 95 | 8.0 |
| L2 1.35-1.5 m | 7.83 | -6 | 3.82 | 452 | 5140 | 7.7 |
| L2 2.15-2.3 m | 7.88 | -54 | 3.30 | 930 | 13700 | 7.0 |
| L2 2.3-2.45 m | 7.91 | -41 | 3.39 | 1037 | 13380 | 7.4 |
| L2 2.45-2.6 m | 7.90 | -43 | 3.30 | 1033 | 15480 | 7.6 |
| L3 0.15-0.3 m | 8.08 | 351 | 6.75 | 613 | 10 | 9.5 |
| L3 0.3-0.45 m | 7.91 | 353 | 3.74 | 1010 | 24 | 8.7 |
| L3 0.45-0.6 m | 7.96 | 345 | 3.67 | 1108 | | 8.5 |
| L3 0.9-1.05 m | 8.00 | 346 | 5.13 | 1062 | | 7.1 |
| L3 1.05-1.2 m | 8.04 | 254 | 5.36 | 1262 | | 5.3 |

| Sample ID | pH | $E_h$ (mV) | EC (mS $cm^{-1}$) | [1]Alkalinity (mg $L^{-1}$) | $S^{2-}$ (µg $L^{-1}$) | $NH_3$-N (mg $L^{-1}$) |
|---|---|---|---|---|---|---|
| L3 1.2-1.35 m | 7.94 | 356 | 5.06 | 1181 | | 5.7 |
| US-L3-P300 | 7.25 | 345 | 4.39 | 1120 | 3 | 0.3 |
| US-L3-P300C | 7.33 | 374 | 6.42 | 1270 | 4 | 0.6 |
| US-L4-P050 | 7.52 | 298 | 4.87 | 310 | 5 | 0.5 |
| US-L4-P075 | 6.80 | 250 | 4.07 | 310 | 18 | 2.9 |
| US-L4-P100 | 7.28 | 387 | 5.38 | 670 | 1 | 15.4 |
| US-L4-P125 | 7.47 | 313 | 5.87 | 465 | 1.5 | 10.3 |
| US-L4-P150 | 7.67 | 269 | 5.96 | 890 | 377 | 25.8 |
| US-L4-P175 | 7.68 | -25 | 5.49 | 1050 | 1450 | 19.4 |
| L4 1.4-1.55 m | 7.79 | 127 | 5.30 | 851 | 250 | 17.0 |
| L4 1.55-1.7 m | 7.77 | 142 | 4.90 | 1245 | 170 | 6.8 |
| L4 1.7-1.85 m | 7.85 | 37 | 4.45 | 1308 | 1310 | 6.2 |
| L4 2.2-2.35 m | 7.74 | 52 | 4.96 | 1222 | 990 | 7.9 |
| L4 2.35-2.5 m | 7.88 | 286 | 5.08 | 1348 | | 6.9 |
| L4 2.5-2.65 m | 7.86 | -9 | 4.77 | 1179 | 2200 | 6.7 |
| US-L5-P050 | 7.51 | 231 | 11.61 | 420 | 4 | 1.0 |
| US-L5-P075 | 7.22 | 205 | 9.25 | 260 | 0 | 7.4 |
| US-L5-P100 | 7.41 | 138 | 7.68 | 500 | 360 | 32.6 |
| US-L5-P125 | 7.99 | -45 | 6.45 | 890 | 11200 | 15.4 |
| L5 0.95-1.1 m | 7.99 | 250 | 4.18 | 852 | | 8.8 |
| L5 1.1-1.25 m | 7.80 | 333 | 5.21 | 634 | | 12.2 |
| L5 1.25-1.4 m | 7.83 | 10 | 3.54 | 861 | 900 | 8.2 |
| L5 2.25-2.4 m | 7.92 | 118 | 3.47 | 354 | 10 | 7.4 |
| L5 2.4-2.55 m | 7.83 | -79 | 3.38 | 895 | 17800 | 7.1 |
| L5 2.55-2.7 m | 7.87 | -69 | 3.42 | 871 | 11000 | 7.8 |
| US-L6-P150 | 8.37 | 307 | 6.55 | 480 | 160 | 3.2 |
| US-L6-P175 | 8.00 | 57 | 10.39 | 400 | 380 | 2.8 |
| US-L6-P200 | 7.78 | -119 | 5.53 | 680 | 660 | 4.9 |
| US-L6-P225 | 7.81 | 353 | 3.63 | 1040 | 189 | 3.9 |
| US-L6-P250 | 7.20 | 218 | 0.87 | 1010 | 62 | 1.2 |
| US-L6-P275 | 7.17 | 233 | 0.85 | 860 | 25 | 1.6 |
| US-L6-P300 | 7.33 | 378 | 1.61 | 920 | 20 | 5.8 |
| US-L6-P300C | 7.40 | 363 | 5.13 | 920 | 53 | 6.8 |
| L6 0.4-0.55 m | 7.95 | 344 | 5.45 | 735 | | 9.5 |
| L6 0.55-0.7 m | 7.97 | | | 687 | | 9.1 |
| L6 0.7-0.85 m | 8.07 | 336 | 3.70 | 814 | | 8.6 |
| L6 0.85-1.0 m | 7.87 | 358 | 3.97 | 900 | | 10.7 |
| L6 1.0-1.15 m | 7.92 | 365 | 4.23 | | | 8.3 |
| L6 1.15-1.3 m | 7.91 | 284 | 3.82 | | | 8.3 |

**NOTES:**

Cores stored frozen (-20C) between sampling and squeezing

[1]Alkalinity reported in mg $L^{-1}$ as $CaCO_3$

ud - concentration below method detection limit

Table B-3: Results from naphthenic acid, isotopic, and IC analyses. "ud" identifies a measurement under the method detection limit when a detection limit was not provided.

| Sample ID | Naphthenic Acids | Isotopes of Water (‰) | | Anions by IC (mg $L^{-1}$) | | | | | | |
|---|---|---|---|---|---|---|---|---|---|---|
| | (mg $L^{-1}$) | $\delta^{18}O$ | $\delta^{2}H$ | F | Cl | $NO_2$ | $NO_3$ | $PO_4$ | $SO_4$ | Br |
| US-L1-P175 | 5.4 | -12.8 | -117.6 | 1.07 | 456.34 | ud | 7.67 | ud | 3686.51 | ud |
| US-L1-P200 | 10.3 | -12.7 | -115.9 | 1.27 | 548.24 | ud | 11.48 | ud | 3087.25 | ud |
| US-L1-P225 | 23.7 | -11.8 | -111.5 | 1.41 | 560.73 | ud | 7.22 | ud | 2174.73 | ud |
| L1 1.65-1.8 m | | -12.8 | -121.2 | 0.75 | 429.00 | <0.2 | 38.70 | <1 | 3290.00 | <0.4 |
| L1 1.8-1.95 m | | -13.2 | -120.1 | 1.28 | 528.00 | <0.2 | 40.00 | <1 | 2370.00 | <0.4 |
| L1 2.25-2.4 m | | -13.1 | -119.1 | 1.18 | 475.00 | <0.2 | 18.60 | <1 | 1720.00 | <0.4 |
| L1 2.4-2.55 m | | -12.8 | -115.4 | 1.01 | 602.00 | <0.2 | 1.83 | <1 | 89.90 | <0.4 |
| L1 2.55-2.7 m | | -11.8 | -114.1 | 1.38 | 608.00 | <0.2 | 1.58 | <1 | 83.40 | <0.4 |
| L2 0.95-1.15 m | | | | 0.77 | 475.00 | <0.2 | 0.50 | <1 | 2760.00 | <0.4 |
| L2 1.15-1.35 m | | -12.5 | -113.6 | 1.99 | 615.00 | <0.2 | <0.4 | <1 | 55.80 | <0.4 |
| L2 1.35-1.5 m | | -11.8 | -112.7 | 1.39 | 584.00 | <0.2 | 0.67 | <1 | 405.00 | <0.4 |
| L2 2.15-2.3 m | | -11.5 | -110.3 | 1.38 | 615.00 | <0.2 | <0.4 | <1 | 26.50 | <0.4 |
| L2 2.3-2.45 m | | -12.3 | -113.3 | 1.45 | 604.00 | <0.2 | <0.4 | <1 | 14.80 | <0.4 |
| L2 2.45-2.6 m | | -12.6 | -112.4 | 1.44 | 633.00 | <0.2 | 0.36 | <1 | 13.30 | <0.4 |
| L3 0.15-0.3 m | | -13.98 | -120 | 2.28 | 1460.00 | <0.2 | <0.4 | <1 | 1880.00 | <0.4 |
| L3 0.3-0.45 m | | -12.72 | -112.7 | 1.75 | 740.00 | <0.2 | <0.4 | <1 | 128.00 | 0.42 |
| L3 0.45-0.6 m | | -12.75 | -113.1 | 1.83 | 681.00 | <0.2 | 0.53 | <1 | 92.70 | 0.45 |
| L3 0.9-1.05 m | | | | 1.77 | 791.00 | <0.2 | 0.90 | <1 | 264.00 | <0.4 |
| L3 1.05-1.2 m | | | | 1.24 | 769.00 | <0.2 | 0.42 | <1 | 38.10 | 0.45 |
| L3 1.2-1.35 m | | | | 1.62 | 742.00 | <0.2 | <0.4 | <1 | 15.90 | 0.44 |
| US-L3-P300 | 39.8 | -12.36 | -113.3 | 1.01 | 740.64 | ud | 1.43 | ud | 448.99 | ud |
| US-L3-P300C | 75.1 | -13.28 | -119.45 | 1.13 | 1058.03 | ud | 1.24 | ud | 1114.47 | ud |
| US-L4-P050 | 17.6 | -13.86 | -122.5 | ud | 310.71 | ud | ud | ud | 2524.51 | ud |
| US-L4-P075 | 13.5 | -13.44 | -120.6 | 0.68 | 320.07 | ud | 0.25 | ud | 1962.84 | ud |
| US-L4-P100 | 6.1 | -13.73 | -121.6 | ud | 452.37 | ud | 1.27 | ud | 2401.26 | ud |
| US-L4-P125 | 8.15 | -12.885 | -116.95 | 1.03 | 407.07 | ud | 2.98 | ud | 2540.94 | ud |
| US-L4-P150 | 23.3 | -13.18 | -118.4 | 1.35 | 509.44 | ud | 1.71 | ud | 2060.72 | ud |
| US-L4-P175 | 47.3 | -13.05 | -116.8 | 1.57 | 580.41 | ud | 0.16 | ud | 1347.49 | ud |
| L4 1.4-1.55 m | | -13.3 | -117.6 | 1.48 | 714.00 | <0.2 | 0.42 | <1 | 552.00 | <0.4 |
| L4 1.55-1.7 m | | -13.04 | -114.7 | 1.54 | 745.00 | <0.2 | <0.4 | <1 | 21.90 | 0.47 |
| L4 1.7-1.85 m | | -12.52 | -113.2 | 1.59 | 775.00 | <0.2 | <0.4 | <1 | 17.80 | 0.49 |
| L4 2.2-2.35 m | | -13.04 | -114.6 | 1.11 | 704.00 | <0.2 | <0.4 | <1 | 592.00 | <0.4 |
| L4 2.35-2.5 m | | | | | | | | | | |
| L4 2.5-2.65 m | | -12.98 | -114.6 | 1.48 | 755.00 | <0.2 | <0.4 | <1 | 209.00 | 0.40 |
| US-L5-P050 | 5.4 | -11.58 | -112.8 | 0.96 | 1161.95 | ud | 6.60 | ud | 6755.55 | ud |
| US-L5-P075 | 3.5 | -12.33 | -116.9 | 1.01 | 784.15 | ud | 6.11 | ud | 4986.79 | ud |
| US-L5-P100 | 14.4 | -13.12 | -120 | 1.09 | 607.34 | ud | 0.73 | ud | 3575.29 | ud |
| US-L5-P125 | 29.95 | -12.55 | -113.45 | 1.25 | 561.36 | ud | 0.12 | ud | 2583.18 | ud |
| L5 0.95-1.1 m | | -12.48 | -113.2 | 1.67 | 656.00 | <0.2 | 1.29 | <1 | 227.00 | <0.4 |
| L5 1.1-1.25 m | | -12.98 | -117.4 | 1.10 | 580.00 | <0.2 | 6.06 | <1 | 1480.00 | <0.4 |
| L5 1.25-1.4 m | | -12.95 | -115.1 | 1.30 | 620.00 | <0.2 | 1.33 | <1 | 226.00 | <0.4 |
| L5 2.25-2.4 m | | -13.89 | -122 | 1.06 | 509.00 | <0.2 | 7.04 | <1 | 931.00 | <0.4 |
| L5 2.4-2.55 m | | -12.61 | -114.4 | 1.40 | 601.00 | <0.2 | 0.52 | <1 | 18.50 | <0.4 |
| L5 2.55-2.7 m | | -12.53 | -113.9 | 1.39 | 610.00 | <0.2 | 0.51 | <1 | 15.80 | <0.4 |

| Sample ID | Naphthenic Acids | Isotopes of Water (‰) | | Anions by IC (mg $L^{-1}$) | | | | | | |
|---|---|---|---|---|---|---|---|---|---|---|
| | (mg $L^{-1}$) | $\delta^{18}O$ | $\delta^{2}H$ | F | Cl | $NO_2$ | $NO_3$ | $PO_4$ | $SO_4$ | Br |
| US-L6-P150 | 165 | -11.3 | -108.6 | 2.00 | 2084.54 | ud | ud | ud | 3126.12 | ud |
| US-L6-P175 | 167 | -11.95 | -111.2 | 2.20 | 1772.99 | ud | ud | ud | 2629.58 | ud |
| US-L6-P200 | 127 | -12.21 | -111.8 | 1.75 | 1319.56 | ud | ud | ud | 1849.40 | ud |
| US-L6-P225 | 15.725 | -12.08 | -111.5 | 1.58 | 1212.37 | ud | ud | ud | 1534.63 | ud |
| US-L6-P250 | 60.3 | -12.84 | -114.3 | 1.21 | 645.56 | ud | ud | ud | 537.39 | ud |
| US-L6-P275 | 66.1 | -12.37 | -112.6 | 1.02 | 661.96 | ud | ud | ud | 621.69 | ud |
| US-L6-P300 | 50.1 | -12.37 | -111.2 | 1.31 | 664.00 | ud | ud | ud | 405.54 | ud |
| US-L6-P300C | 12.4 | -16.775 | -135.85 | 1.43 | 653.91 | ud | ud | ud | 359.91 | ud |
| L6 0.4-0.55 m | | | | 2.04 | 1000.00 | <0.2 | 0.49 | <1 | 706.00 | 0.45 |
| L6 0.55-0.7 m | | | | 2.02 | 816.00 | <0.2 | 0.58 | <1 | 295.00 | 0.41 |
| L6 0.7-0.85 m | | | | | | | | | | |
| L6 0.85-1.0 m | | -13.21 | -118.4 | 1.66 | 877.00 | <0.2 | 0.70 | <1 | 417.00 | 0.43 |
| L6 1.0-1.15 m | | -12.78 | -114.6 | 1.97 | 664.00 | <0.2 | <0.4 | <1 | 85.10 | 0.41 |
| L6 1.15-1.3 m | | | | 1.77 | 620.00 | <0.2 | <0.4 | <1 | 2.44 | 0.45 |

Table B-4: Results from ICP-OES analyses. “ud” identifies a measurement under the method detection limit when a detection limit was not provided.

| Sample ID | Major Cations by ICP-OES (mg $L^{-1}$) | | | | | |
|---|---|---|---|---|---|---|
| | Al | As | Ba | Ca | Cd | Fe |
| US-L1-P175 | ud | 0.05 | 0.03 | 398.08 | ud | 0.04 |
| US-L1-P200 | ud | 0.07 | 0.04 | 300.62 | ud | 0.01 |
| US-L1-P225 | ud | 0.11 | 0.07 | 179.74 | ud | 0.05 |
| L1 1.65-1.8 m | ud | 0.04 | 0.05 | 249.47 | ud | ud |
| L1 1.8-1.95 m | ud | 0.05 | 0.16 | 172.34 | ud | ud |
| L1 2.25-2.4 m | ud | ud | 0.34 | 174.88 | ud | ud |
| L1 2.4-2.55 m | ud | 0.06 | 0.38 | 18.44 | ud | ud |
| L1 2.55-2.7 m | ud | 0.05 | 0.44 | 20.91 | ud | ud |
| L2 0.95-1.15 m | ud | ud | 0.11 | 156.51 | ud | ud |
| L2 1.15-1.35 m | ud | 0.08 | 0.44 | 19.32 | ud | ud |
| L2 1.35-1.5 m | ud | 0.06 | 0.31 | 27.10 | ud | ud |
| L2 2.15-2.3 m | ud | 0.09 | 0.40 | 18.36 | ud | 0.03 |
| L2 2.3-2.45 m | ud | 0.08 | 0.40 | 18.27 | ud | ud |
| L2 2.45-2.6 m | ud | 0.07 | 0.35 | 16.60 | ud | ud |
| L3 0.15-0.3 m | ud | 0.05 | 0.06 | 69.88 | ud | ud |
| L3 0.3-0.45 m | ud | 0.06 | 0.12 | 20.62 | ud | ud |
| L3 0.45-0.6 m | ud | 0.08 | 0.17 | 22.09 | ud | ud |
| L3 0.9-1.05 m | ud | 0.08 | 0.32 | 18.86 | ud | ud |
| L3 1.05-1.2 m | ud | 0.07 | 0.28 | 13.52 | ud | ud |
| L3 1.2-1.35 m | ud | 0.03 | 0.32 | 13.91 | ud | ud |
| US-L3-P300 | ud | 0.16 | 0.05 | 57.44 | ud | 0.00 |
| US-L3-P300C | ud | 0.18 | 0.03 | 101.33 | 0.00 | 0.01 |
| US-L4-P050 | ud | 0.04 | 0.13 | 369.44 | ud | 1.47 |
| US-L4-P075 | 0.00 | 0.05 | 0.11 | 312.52 | ud | 4.42 |
| US-L4-P100 | ud | 0.05 | 0.05 | 276.95 | ud | 0.17 |
| US-L4-P125 | ud | 0.07 | 0.03 | 231.22 | ud | 0.01 |

| Sample ID | Major Cations by ICP-OES (mg $L^{-1}$) | | | | | |
|---|---|---|---|---|---|---|
| | Al | As | Ba | Ca | Cd | Fe |
| US-L4-P150 | ud | 0.11 | 0.07 | 157.88 | ud | 0.08 |
| US-L4-P175 | ud | 0.13 | 0.08 | 96.56 | ud | 0.04 |
| L4 1.4-1.55 m | ud | 0.02 | 0.39 | 35.56 | ud | ud |
| L4 1.55-1.7 m | ud | 0.02 | 0.39 | 17.46 | ud | ud |
| L4 1.7-1.85 m | ud | 0.03 | 0.45 | 18.54 | ud | ud |
| L4 2.2-2.35 m | ud | ud | 0.07 | 45.22 | ud | ud |
| L4 2.35-2.5 m | ud | ud | 0.02 | 24.94 | ud | ud |
| L4 2.5-2.65 m | ud | 0.02 | 0.16 | 28.82 | ud | ud |
| US-L5-P050 | ud | 0.02 | 0.02 | 460.32 | ud | 0.03 |
| US-L5-P075 | ud | 0.03 | 0.02 | 409.41 | ud | ud |
| US-L5-P100 | ud | 0.07 | 0.05 | 294.88 | ud | 0.28 |
| US-L5-P125 | ud | 0.09 | 0.09 | 162.14 | ud | 0.04 |
| L5 0.95-1.1 m | ud | 0.03 | 0.34 | 21.61 | ud | ud |
| L5 1.1-1.25 m | ud | 0.04 | 0.31 | 97.75 | ud | ud |
| L5 1.25-1.4 m | ud | 0.03 | 0.38 | 20.86 | ud | ud |
| L5 2.25-2.4 m | ud | 0.03 | 0.22 | 91.29 | ud | ud |
| L5 2.4-2.55 m | ud | 0.04 | 0.37 | 16.46 | ud | ud |
| L5 2.55-2.7 m | ud | 0.03 | 0.41 | 18.85 | ud | ud |
| US-L6-P150 | ud | 0.05 | 0.13 | 79.03 | ud | 0.01 |
| US-L6-P175 | ud | 0.04 | 0.30 | 56.85 | ud | 0.01 |
| US-L6-P200 | ud | 0.09 | 0.16 | 61.77 | ud | 0.06 |
| US-L6-P225 | ud | 0.11 | 0.18 | 85.59 | ud | 0.33 |
| US-L6-P250 | ud | 0.15 | 0.14 | 105.01 | ud | 0.89 |
| US-L6-P275 | ud | 0.12 | 0.08 | 134.10 | ud | 1.60 |
| US-L6-P300 | ud | 0.13 | 0.05 | 43.33 | ud | 0.31 |
| US-L6-P300C | ud | 0.11 | 0.05 | 36.66 | ud | 2.82 |
| L6 0.4-0.55 m | ud | 0.03 | 0.08 | 31.62 | ud | ud |
| L6 0.55-0.7 m | ud | 0.04 | 0.23 | 23.78 | ud | ud |
| L6 0.7-0.85 m | ud | 0.03 | 0.27 | 16.71 | ud | ud |
| L6 0.85-1.0 m | ud | ud | 0.50 | 30.18 | ud | ud |
| L6 1.0-1.15 m | ud | 0.03 | 0.37 | 15.80 | ud | ud |
| L6 1.15-1.3 m | 0.12 | ud | 0.29 | 11.70 | ud | ud |

Table B-4 continued.

| Sample ID | Major Cations by ICP-OES (mg $L^{-1}$) | | | | | | |
|---|---|---|---|---|---|---|---|
| | K | Mg | Mo | Na | P | S | Se |
| US-L1-P175 | 23.95 | 252.09 | 1.94 | 1078.17 | 0.08 | 1260.31 | 0.03 |
| US-L1-P200 | 22.94 | 176.95 | 0.98 | 1244.28 | 0.12 | 1086.23 | 0.02 |
| US-L1-P225 | 20.20 | 139.20 | 0.46 | 1194.02 | 0.19 | 763.94 | ud |
| L1 1.65-1.8 m | 36.15 | 195.25 | 0.32 | 1266.55 | 0.12 | 1113.86 | ud |
| L1 1.8-1.95 m | 29.28 | 115.32 | 0.10 | 1276.52 | 0.15 | 937.23 | ud |
| L1 2.25-2.4 m | 26.10 | 83.97 | 0.38 | 1003.69 | 0.10 | 632.56 | ud |
| L1 2.4-2.55 m | 10.75 | 8.57 | ud | 788.32 | 0.27 | 693.64 | ud |
| L1 2.55-2.7 m | 12.42 | 9.12 | ud | 827.31 | 0.29 | 299.24 | ud |
| L2 0.95-1.15 m | 26.93 | 103.65 | 0.58 | 1349.14 | 0.18 | 934.17 | ud |

| Sample ID | Major Cations by ICP-OES (mg $L^{-1}$) | | | | | | |
|---|---|---|---|---|---|---|---|
| | K | Mg | Mo | Na | P | S | Se |
| L2 1.15-1.35 m | 13.43 | 8.86 | 0.02 | 801.75 | 0.26 | 30.59 | ud |
| L2 1.35-1.5 m | 12.80 | 13.15 | 0.02 | 886.37 | 0.23 | 275.60 | ud |
| L2 2.15-2.3 m | 10.91 | 8.46 | ud | 777.90 | 0.28 | 807.78 | ud |
| L2 2.3-2.45 m | 11.88 | 8.25 | ud | 782.04 | 0.32 | 484.85 | ud |
| L2 2.45-2.6 m | 9.76 | 7.29 | ud | 786.25 | 0.26 | 410.13 | ud |
| L3 0.15-0.3 m | 34.60 | 36.77 | 0.21 | 1883.34 | 0.13 | 697.95 | ud |
| L3 0.3-0.45 m | 12.70 | 9.78 | 0.02 | 911.69 | 0.20 | 45.56 | ud |
| L3 0.45-0.6 m | 14.93 | 10.52 | 0.03 | 896.60 | 0.23 | 41.38 | ud |
| L3 0.9-1.05 m | 14.59 | 10.01 | 0.05 | 1017.28 | 0.20 | 81.67 | ud |
| L3 1.05-1.2 m | 9.90 | 7.04 | 0.04 | 1106.55 | 0.14 | 12.94 | ud |
| L3 1.2-1.35 m | 11.42 | 7.47 | ud | 1020.35 | 0.12 | 9.90 | ud |
| US-L3-P300 | 12.67 | 16.89 | ud | 1029.36 | 0.26 | 160.95 | ud |
| US-L3-P300C | 14.78 | 28.50 | 0.02 | 1476.88 | 0.30 | 400.93 | 0.01 |
| US-L4-P050 | 21.84 | 143.40 | 0.01 | 728.44 | 0.09 | 968.39 | ud |
| US-L4-P075 | 40.87 | 113.06 | 0.07 | 595.47 | 0.11 | 762.00 | ud |
| US-L4-P100 | 61.80 | 123.90 | 0.84 | 877.27 | 0.10 | 877.43 | ud |
| US-L4-P125 | 26.20 | 144.84 | 0.92 | 1040.33 | 0.12 | 929.83 | 0.01 |
| US-L4-P150 | 25.42 | 119.79 | 0.54 | 1115.55 | 0.19 | 733.35 | ud |
| US-L4-P175 | 87.26 | 73.76 | 0.04 | 1087.18 | 0.30 | 984.95 | ud |
| L4 1.4-1.55 m | 18.46 | 22.59 | 0.14 | 1120.15 | 0.18 | 194.33 | ud |
| L4 1.55-1.7 m | 10.97 | 8.66 | ud | 1064.33 | 0.25 | 11.48 | ud |
| L4 1.7-1.85 m | 12.21 | 9.21 | ud | 1098.28 | 0.27 | 13.82 | ud |
| L4 2.2-2.35 m | 17.94 | 20.17 | ud | 1278.17 | 0.24 | 209.87 | ud |
| L4 2.35-2.5 m | 7.72 | 10.14 | ud | 636.28 | 0.14 | 119.30 | ud |
| L4 2.5-2.65 m | 15.12 | 13.59 | ud | 1177.28 | 0.25 | 84.94 | ud |
| US-L5-P050 | 62.12 | 479.53 | 1.81 | 2414.55 | 0.04 | 2344.97 | 0.07 |
| US-L5-P075 | 46.65 | 337.70 | 1.27 | 1750.45 | 0.04 | 1735.98 | 0.03 |
| US-L5-P100 | 33.46 | 222.70 | 1.05 | 1332.24 | 0.13 | 1242.77 | ud |
| US-L5-P125 | 24.76 | 130.89 | 0.10 | 1271.89 | 0.23 | 951.30 | ud |
| L5 0.95-1.1 m | 14.63 | 10.85 | ud | 855.38 | 0.21 | 82.40 | ud |
| L5 1.1-1.25 m | 22.90 | 48.99 | 0.39 | 1126.50 | 0.13 | 529.69 | ud |
| L5 1.25-1.4 m | 13.17 | 10.06 | ud | 849.38 | 0.26 | 85.79 | ud |
| L5 2.25-2.4 m | 19.01 | 34.44 | 0.28 | 835.16 | 0.12 | 335.00 | ud |
| L5 2.4-2.55 m | 11.89 | 7.51 | ud | 768.41 | 0.28 | 81.55 | ud |
| L5 2.55-2.7 m | 12.41 | 8.22 | ud | 803.32 | 0.24 | 26.57 | ud |
| US-L6-P150 | 37.91 | 68.27 | 0.16 | 2465.02 | 0.09 | 1061.88 | ud |
| US-L6-P175 | 32.25 | 55.54 | 0.16 | 2142.65 | 0.09 | 909.98 | ud |
| US-L6-P200 | 24.33 | 43.35 | 0.10 | 1674.89 | 0.17 | 683.76 | ud |
| US-L6-P225 | 21.67 | 44.24 | 0.12 | 1517.73 | 0.19 | 566.61 | ud |
| US-L6-P250 | 37.37 | 35.96 | ud | 827.65 | 0.24 | 201.13 | ud |
| US-L6-P275 | 17.56 | 28.72 | ud | 832.34 | 0.19 | 236.15 | ud |
| US-L6-P300 | 12.93 | 7.52 | ud | 874.35 | 0.21 | 138.12 | ud |
| US-L6-P300C | 9.94 | 7.56 | ud | 856.95 | 0.17 | 135.87 | ud |
| L6 0.4-0.55 m | 18.75 | 16.43 | 0.10 | 1233.95 | 0.22 | 227.60 | ud |
| L6 0.55-0.7 m | 16.40 | 11.99 | 0.07 | 929.92 | 0.16 | 94.64 | ud |
| L6 0.7-0.85 m | 12.38 | 8.57 | 0.03 | 851.13 | 0.18 | 46.33 | ud |
| L6 0.85-1.0 m | 17.88 | 16.29 | ud | 1083.19 | 0.22 | 152.29 | ud |
| L6 1.0-1.15 m | 13.90 | 8.39 | 0.04 | 792.67 | 0.19 | 36.19 | ud |

| Sample ID | Major Cations by ICP-OES (mg $L^{-1}$) | | | | | | |
|---|---|---|---|---|---|---|---|
| | K | Mg | Mo | Na | P | S | Se |
| L6 1.15-1.3 m | 8.70 | 5.65 | ud | 827.42 | 0.24 | 4.56 | ud |

Table B-5: Results from ICP-MS analyses. "ud" identifies a measurement under the method detection limit when a detection limit was not provided.

| Sample ID | Trace Elements by ICP-MS (mg $L^{-1}$) | | | | | | | |
|---|---|---|---|---|---|---|---|---|
| | Ag | Al | As | B | Ba | Be | Ca | Cd |
| US-L1-P175 | ud | ud | ud | 1.7674 | ud | | 433.9389 | ud |
| US-L1-P200 | ud | ud | ud | 2.1055 | ud | | 314.2376 | ud |
| US-L1-P225 | ud | ud | ud | 2.2908 | ud | | 190.3881 | ud |
| L1 1.65-1.8 m | 0.1074 | <0.01 | 0.0059 | 2.3800 | 0.0890 | <0.002 | 300.2000 | 0.0040 |
| L1 1.8-1.95 m | 0.1074 | <0.01 | <0.002 | 2.4270 | 0.1558 | <0.002 | 188.4000 | <0.002 |
| L1 2.25-2.4 m | 0.1074 | <0.01 | 0.0039 | 2.3380 | 0.3059 | <0.002 | 168.6000 | <0.002 |
| L1 2.4-2.55 m | 0.1074 | <0.01 | <0.002 | 2.4050 | 0.3002 | <0.002 | 32.4200 | <0.002 |
| L1 2.55-2.7 m | 0.0970 | 0.0111 | 0.0025 | 3.2690 | 0.3976 | <0.002 | 23.4100 | <0.002 |
| L2 0.95-1.15 m | 0.1082 | <0.01 | 0.0072 | 2.2350 | 0.1219 | <0.002 | 160.1000 | 0.0021 |
| L2 1.15-1.35 m | 0.1078 | <0.01 | 0.0063 | 4.4655 | 0.4108 | <0.002 | 24.1300 | <0.002 |
| L2 1.35-1.5 m | 0.1083 | <0.01 | 0.0040 | 2.3235 | 0.2624 | <0.002 | 39.9300 | <0.002 |
| L2 2.15-2.3 m | 0.1078 | <0.01 | 0.0024 | 2.3020 | 0.3162 | <0.002 | 34.0700 | <0.002 |
| L2 2.3-2.45 m | 0.1084 | <0.01 | <0.002 | 4.3180 | 0.3114 | <0.002 | 34.6800 | <0.002 |
| L2 2.45-2.6 m | 0.1075 | <0.01 | 0.0022 | 4.2550 | 0.3320 | <0.002 | 39.2550 | <0.002 |
| L3 0.15-0.3 m | 0.1100 | <0.01 | 0.0169 | 4.3710 | 0.0889 | <0.002 | 79.1400 | <0.002 |
| L3 0.3-0.45 m | 0.1082 | <0.01 | 0.0093 | 4.2710 | 0.1443 | <0.002 | 26.5000 | <0.002 |
| L3 0.45-0.6 m | 0.1079 | <0.01 | 0.0094 | 4.5990 | 0.1623 | <0.002 | 25.0300 | <0.002 |
| L3 0.9-1.05 m | 0.1079 | <0.01 | 0.0115 | 4.6420 | 0.2658 | <0.002 | 23.8300 | 0.0033 |
| L3 1.05-1.2 m | 0.1077 | <0.01 | 0.0118 | 5.2890 | 0.3176 | <0.002 | 24.4700 | <0.002 |
| L3 1.2-1.35 m | 0.1077 | <0.01 | 0.0179 | 5.2610 | 0.3219 | <0.002 | 19.9800 | <0.002 |
| US-L3-P300 | ud | ud | ud | 2.1107 | ud | | 59.3673 | ud |
| US-L3-P300C | ud | ud | ud | 2.9546 | ud | | 105.9329 | ud |
| US-L4-P050 | ud | ud | ud | 0.9728 | 0.1089 | | 395.3770 | ud |
| US-L4-P075 | ud | ud | ud | 0.8096 | ud | | 310.3655 | ud |
| US-L4-P100 | ud | ud | ud | 1.6307 | ud | | 278.4966 | ud |
| US-L4-P125 | ud | ud | ud | 1.8109 | ud | | 235.2676 | ud |
| US-L4-P150 | ud | ud | ud | 1.8525 | ud | | 167.8043 | ud |
| US-L4-P175 | ud | ud | ud | 2.2177 | 0.1124 | | 100.9373 | ud |
| L4 1.4-1.55 m | 0.1682 | <0.01 | 0.0067 | 2.5860 | 0.1696 | <0.002 | 102.6000 | <0.002 |
| L4 1.55-1.7 m | 0.1660 | 0.0947 | <0.002 | 4.5850 | 0.2747 | <0.002 | 23.4200 | <0.002 |
| L4 1.7-1.85 m | 0.1657 | 0.0419 | 0.0059 | 3.5010 | 0.2043 | <0.002 | 58.2500 | <0.002 |
| L4 2.2-2.35 m | 0.1652 | <0.01 | 0.0022 | 4.5840 | 0.2834 | <0.002 | 26.2300 | <0.002 |
| L4 2.35-2.5 m | | | | | | | | |
| L4 2.5-2.65 m | 0.1652 | <0.01 | 0.0051 | 4.4740 | 0.0777 | <0.002 | 40.4900 | <0.002 |
| US-L5-P050 | ud | ud | ud | 3.7182 | ud | | 534.2441 | ud |
| US-L5-P075 | ud | ud | ud | 3.1191 | ud | | 477.2571 | ud |
| US-L5-P100 | ud | ud | ud | 3.0031 | ud | | 348.9849 | ud |
| US-L5-P125 | ud | ud | ud | 3.2495 | ud | | 202.2244 | ud |
| L5 0.95-1.1 m | 0.1652 | 0.0183 | 0.0056 | 3.2830 | 0.1724 | <0.002 | 26.6200 | <0.002 |
| L5 1.1-1.25 m | 0.1654 | 0.0221 | 0.0045 | 4.6440 | 0.2354 | <0.002 | 25.7600 | <0.002 |

| Sample ID | Trace Elements by ICP-MS (mg $L^{-1}$) | | | | | | | |
|---|---|---|---|---|---|---|---|---|
| | Ag | Al | As | B | Ba | Be | Ca | Cd |
| L5 1.25-1.4 m | 0.1654 | <0.01 | 0.0043 | 4.5690 | 0.4195 | <0.002 | 35.3000 | <0.002 |
| L5 2.25-2.4 m | 0.1652 | 0.1368 | 0.0077 | 3.9200 | 0.2681 | <0.002 | 21.3300 | <0.002 |
| L5 2.4-2.55 m | 0.1674 | 0.2092 | 0.0229 | 4.7550 | 0.3368 | <0.002 | 23.3300 | 0.0050 |
| L5 2.55-2.7 m | 0.1652 | <0.01 | 0.0022 | 4.5840 | 0.2834 | <0.002 | 26.2300 | <0.002 |
| US-L6-P150 | ud | ud | ud | 4.4000 | 0.1114 | | 86.5982 | ud |
| US-L6-P175 | ud | ud | ud | 4.8807 | 0.1377 | | 60.7456 | ud |
| US-L6-P200 | ud | ud | ud | 3.9735 | ud | | 70.2267 | ud |
| US-L6-P225 | ud | ud | ud | 2.9507 | 0.1542 | | 86.7167 | ud |
| US-L6-P250 | ud | ud | ud | 1.7283 | 0.1211 | | 111.4807 | ud |
| US-L6-P275 | ud | ud | ud | 1.5201 | ud | | 130.4000 | ud |
| US-L6-P300 | ud | ud | ud | 1.9115 | ud | | 44.7542 | ud |
| US-L6-P300C | ud | ud | ud | 1.9301 | ud | | 39.8780 | ud |
| L6 0.4-0.55 m | 0.1652 | <0.01 | 0.0051 | 4.4740 | 0.0777 | <0.002 | 40.4900 | <0.002 |
| L6 0.55-0.7 m | 0.1652 | 0.0183 | 0.0056 | 3.2830 | 0.1724 | <0.002 | 26.6200 | <0.002 |
| L6 0.7-0.85 m | 0.1654 | 0.0221 | 0.0045 | 4.6440 | 0.2354 | <0.002 | 25.7600 | <0.002 |
| L6 0.85-1.0 m | 0.1654 | <0.01 | 0.0043 | 4.5690 | 0.4195 | <0.002 | 35.3000 | <0.002 |
| L6 1.0-1.15 m | 0.1652 | 0.1368 | 0.0077 | 3.9200 | 0.2681 | <0.002 | 21.3300 | <0.002 |
| L6 1.15-1.3 m | 0.1674 | 0.2092 | 0.0229 | 4.7550 | 0.3368 | <0.002 | 23.3300 | 0.0050 |

Table B-5 continued.

| Sample ID | Trace Elements by ICP-MS (mg $L^{-1}$) | | | | | | | |
|---|---|---|---|---|---|---|---|---|
| | Co | Cr | Cu | Dy | Fe | Hg | K | Li |
| US-L1-P175 | ud | ud | ud | ud | ud | ud | 22.4015 | 0.2496 |
| US-L1-P200 | ud | ud | ud | ud | ud | ud | 21.1197 | 0.3016 |
| US-L1-P225 | ud | ud | ud | ud | ud | ud | 18.7363 | 0.3065 |
| L1 1.65-1.8 m | 0.0369 | <0.0004 | <0.003 | <0.002 | 1.9850 | <0.02 | 26.5800 | 0.2996 |
| L1 1.8-1.95 m | 0.2524 | <0.0004 | <0.003 | <0.002 | 1.2900 | <0.02 | 19.7000 | 0.2764 |
| L1 2.25-2.4 m | 0.2524 | <0.0004 | <0.003 | <0.002 | 1.2780 | <0.02 | 18.5500 | 0.2277 |
| L1 2.4-2.55 m | 0.0248 | <0.0004 | <0.003 | <0.002 | 0.1470 | <0.02 | 10.1100 | 0.1898 |
| L1 2.55-2.7 m | 0.0329 | <0.0004 | <0.003 | <0.002 | 0.1681 | <0.02 | 11.4400 | 0.1952 |
| L2 0.95-1.15 m | 0.0271 | <0.0004 | <0.003 | <0.002 | 1.2050 | <0.02 | 18.4000 | 0.2727 |
| L2 1.15-1.35 m | 0.0278 | <0.0004 | <0.003 | <0.002 | 0.1509 | <0.02 | 12.7000 | 0.2053 |
| L2 1.35-1.5 m | 0.0373 | <0.0004 | <0.003 | <0.002 | 0.1733 | <0.02 | 12.0150 | 0.2028 |
| L2 2.15-2.3 m | 0.0488 | <0.0004 | <0.003 | <0.002 | 0.1530 | <0.02 | 9.9530 | 0.1895 |
| L2 2.3-2.45 m | 0.0372 | <0.0004 | <0.003 | <0.002 | 0.1421 | <0.02 | 10.7700 | 0.1919 |
| L2 2.45-2.6 m | 0.0420 | <0.0004 | <0.003 | <0.002 | 0.1547 | <0.02 | 11.0200 | 0.1935 |
| L3 0.15-0.3 m | 0.0319 | <0.0004 | 0.0031 | <0.002 | 0.3445 | <0.02 | 21.5100 | 0.3344 |
| L3 0.3-0.45 m | 0.0261 | <0.0004 | <0.003 | <0.002 | 0.1622 | <0.02 | 10.5600 | 0.2211 |
| L3 0.45-0.6 m | 0.0428 | <0.0004 | <0.003 | <0.002 | 0.1563 | <0.02 | 10.6000 | 0.2211 |
| L3 0.9-1.05 m | 0.0257 | <0.0004 | <0.003 | <0.002 | 0.1539 | <0.02 | 13.5900 | 0.2291 |
| L3 1.05-1.2 m | 0.0343 | <0.0004 | 0.0130 | <0.002 | 0.1615 | <0.02 | 12.9100 | 0.2377 |
| L3 1.2-1.35 m | 0.0207 | <0.0004 | <0.003 | <0.002 | 0.1449 | <0.02 | 12.7300 | 0.2219 |
| US-L3-P300 | ud | ud | ud | ud | ud | ud | 11.7225 | 0.2361 |
| US-L3-P300C | ud | ud | ud | ud | ud | ud | 13.3597 | 0.3538 |
| US-L4-P050 | ud | ud | ud | ud | ud | ud | 20.0022 | 0.1694 |
| US-L4-P075 | ud | ud | ud | ud | 3.9275 | ud | 32.5396 | 0.1487 |

| Sample ID | Trace Elements by ICP-MS (mg $L^{-1}$) | | | | | | | |
|---|---|---|---|---|---|---|---|---|
| | Co | Cr | Cu | Dy | Fe | Hg | K | Li |
| US-L4-P100 | ud | ud | ud | ud | ud | ud | 60.4026 | 0.2119 |
| US-L4-P125 | ud | ud | ud | ud | ud | ud | 25.6367 | 0.2695 |
| US-L4-P150 | ud | ud | ud | ud | ud | ud | 24.4919 | 0.2903 |
| US-L4-P175 | ud | ud | ud | ud | ud | ud | 95.0929 | 0.2691 |
| L4 1.4-1.55 m | 0.0207 | <0.0004 | 0.0042 | <0.002 | 0.5521 | <0.02 | 17.4500 | 0.2523 |
| L4 1.55-1.7 m | 0.0481 | <0.0004 | <0.003 | <0.002 | 0.2037 | <0.02 | 10.7700 | 0.2164 |
| L4 1.7-1.85 m | 0.0427 | <0.0004 | <0.003 | <0.002 | 0.3434 | <0.02 | 12.8150 | 0.1972 |
| L4 2.2-2.35 m | 0.0277 | <0.0004 | <0.003 | <0.002 | 0.1918 | <0.02 | 11.0700 | 0.2007 |
| L4 2.35-2.5 m | | | | | | | | |
| L4 2.5-2.65 m | 0.2647 | <0.0004 | <0.003 | <0.002 | 0.2684 | <0.02 | 16.0100 | 0.2625 |
| US-L5-P050 | ud | ud | ud | ud | ud | ud | 84.3098 | 0.5341 |
| US-L5-P075 | ud | ud | ud | ud | ud | ud | 58.1650 | 0.3990 |
| US-L5-P100 | ud | ud | ud | ud | ud | ud | 38.9301 | 0.3898 |
| US-L5-P125 | ud | ud | ud | ud | ud | ud | 31.2074 | 0.3833 |
| L5 0.95-1.1 m | 0.0477 | <0.0004 | <0.003 | <0.002 | 0.2020 | <0.02 | 12.5300 | 0.2322 |
| L5 1.1-1.25 m | 0.0171 | <0.0004 | <0.003 | <0.002 | 0.3008 | <0.02 | 11.9700 | 0.2274 |
| L5 1.25-1.4 m | 0.0306 | <0.0004 | <0.003 | <0.002 | 0.2400 | <0.02 | 13.6600 | 0.2564 |
| L5 2.25-2.4 m | 0.2640 | <0.0004 | <0.003 | <0.002 | 0.1842 | <0.02 | 11.1100 | 0.2179 |
| L5 2.4-2.55 m | 0.0498 | 0.0017 | 0.0062 | <0.002 | 0.1930 | <0.02 | 10.5800 | 0.2180 |
| L5 2.55-2.7 m | 0.0277 | <0.0004 | <0.003 | <0.002 | 0.1918 | <0.02 | 11.0700 | 0.2007 |
| US-L6-P150 | ud | ud | ud | ud | ud | ud | 42.2231 | 0.6484 |
| US-L6-P175 | ud | ud | ud | ud | ud | ud | 10.4299 | 0.5981 |
| US-L6-P200 | ud | ud | ud | ud | ud | ud | 27.8051 | 0.4754 |
| US-L6-P225 | ud | ud | ud | ud | ud | ud | 15.9620 | 0.3993 |
| US-L6-P250 | ud | ud | ud | ud | ud | ud | 14.1709 | 0.2333 |
| US-L6-P275 | ud | ud | ud | ud | ud | ud | 12.0083 | 0.2187 |
| US-L6-P300 | ud | ud | ud | ud | ud | ud | 11.5488 | 0.1985 |
| US-L6-P300C | ud | ud | ud | ud | 6.1698 | ud | 10.3718 | 0.2031 |
| L6 0.4-0.55 m | 0.2647 | <0.0004 | <0.003 | <0.002 | 0.2684 | <0.02 | 16.0100 | 0.2625 |
| L6 0.55-0.7 m | 0.0477 | <0.0004 | <0.003 | <0.002 | 0.2020 | <0.02 | 12.5300 | 0.2322 |
| L6 0.7-0.85 m | 0.0171 | <0.0004 | <0.003 | <0.002 | 0.3008 | <0.02 | 11.9700 | 0.2274 |
| L6 0.85-1.0 m | 0.0306 | <0.0004 | <0.003 | <0.002 | 0.2400 | <0.02 | 13.6600 | 0.2564 |
| L6 1.0-1.15 m | 0.2640 | <0.0004 | <0.003 | <0.002 | 0.1842 | <0.02 | 11.1100 | 0.2179 |
| L6 1.15-1.3 m | 0.0498 | 0.0017 | 0.0062 | <0.002 | 0.1930 | <0.02 | 10.5800 | 0.2180 |

Table B-5 continued.

| Sample ID | Trace Elements by ICP-MS (mg $L^{-1}$) | | | | | | | |
|---|---|---|---|---|---|---|---|---|
| | Mg | Mn | Mo | Na | Ni | P | Pb | Rb |
| US-L1-P175 | 248.7687 | 0.6775 | 1.6222 | 1141.7640 | 0.0548 | ud | ud | 0.0321 |
| US-L1-P200 | 185.2419 | 0.3558 | 0.8124 | 1257.3955 | ud | ud | ud | 0.0307 |
| US-L1-P225 | 139.6532 | 0.2612 | 0.3776 | 1129.4746 | ud | ud | ud | 0.0272 |
| L1 1.65-1.8 m | 181.2000 | 0.4945 | 0.3021 | 1145.0000 | 0.0161 | 0.1138 | 0.0024 | 0.1221 |
| L1 1.8-1.95 m | 99.4400 | 0.2327 | 0.0565 | 1151.0000 | 0.0075 | 0.1518 | 0.0030 | 0.0404 |
| L1 2.25-2.4 m | 74.8600 | 0.2461 | 0.3114 | 1054.0000 | 0.0121 | 0.1334 | 0.0031 | 0.0362 |
| L1 2.4-2.55 m | 8.2330 | 0.0090 | 0.0017 | 824.2000 | 0.0040 | 0.2212 | 0.0038 | 0.0148 |
| L1 2.55-2.7 m | 8.6320 | 0.0106 | 0.0042 | 875.9000 | 0.0040 | <0.02 | <0.001 | 0.0172 |

| Sample ID | Trace Elements by ICP-MS (mg $L^{-1}$) | | | | | | | |
|---|---|---|---|---|---|---|---|---|
| | Mg | Mn | Mo | Na | Ni | P | Pb | Rb |
| L2 0.95-1.15 m | 88.3100 | 0.1569 | 0.5017 | 1210.0000 | 0.0126 | 0.1478 | 0.0062 | 0.0346 |
| L2 1.15-1.35 m | 8.5050 | 0.0146 | 0.0210 | 873.6500 | 0.0063 | 0.2150 | 0.0030 | 0.0204 |
| L2 1.35-1.5 m | 11.7250 | 0.0177 | 0.0193 | 923.4500 | 0.0055 | 0.1961 | 0.0043 | 0.0183 |
| L2 2.15-2.3 m | 7.8350 | 0.0090 | 0.0013 | 808.6000 | 0.0047 | 0.2170 | 0.0062 | 0.0150 |
| L2 2.3-2.45 m | 7.7590 | 0.0106 | 0.0011 | 827.4000 | 0.0051 | 0.2375 | 0.0052 | 0.0166 |
| L2 2.45-2.6 m | 8.2345 | 0.0116 | 0.0008 | 846.7500 | 0.0050 | 0.2329 | 0.0049 | 0.0166 |
| L3 0.15-0.3 m | 31.4600 | 0.1196 | 0.2027 | 1686.0000 | 0.0192 | 0.1167 | 0.0047 | 0.0461 |
| L3 0.3-0.45 m | 10.2500 | 0.0425 | 0.0254 | 934.1000 | 0.0051 | 0.1847 | 0.0042 | 0.0218 |
| L3 0.45-0.6 m | 9.7730 | 0.0385 | 0.0336 | 954.0000 | 0.0056 | 0.1881 | 0.0032 | 0.0221 |
| L3 0.9-1.05 m | 9.4240 | 0.0371 | 0.0492 | 1073.0000 | 0.0074 | 0.1580 | 0.0035 | 0.0200 |
| L3 1.05-1.2 m | 9.3270 | 0.0557 | 0.0626 | 1154.0000 | 0.0104 | 0.1440 | 0.0033 | 0.0160 |
| L3 1.2-1.35 m | 8.8180 | 0.0371 | 0.0437 | 1069.0000 | 0.0057 | 0.1571 | 0.0031 | 0.0167 |
| US-L3-P300 | 17.3821 | 0.5245 | ud | 994.2075 | ud | ud | ud | 0.0209 |
| US-L3-P300C | 32.2327 | 0.9242 | ud | 1415.3771 | ud | ud | ud | 0.0242 |
| US-L4-P050 | 148.6916 | 2.7005 | ud | 790.6548 | ud | ud | ud | 0.0110 |
| US-L4-P075 | 99.1726 | 1.5486 | 0.0566 | 529.4689 | ud | ud | ud | 0.0169 |
| US-L4-P100 | 128.3388 | 0.8187 | 0.6789 | 997.5437 | ud | ud | ud | 0.0408 |
| US-L4-P125 | 151.7795 | 0.5367 | 0.7364 | 1100.8817 | ud | ud | ud | 0.0460 |
| US-L4-P150 | 135.6309 | 0.4444 | 0.4368 | 1182.5720 | ud | ud | ud | 0.0451 |
| US-L4-P175 | 70.7871 | 0.1275 | ud | 1280.1437 | ud | ud | ud | 0.0377 |
| L4 1.4-1.55 m | 45.2000 | 0.1840 | 0.4428 | 1081.0000 | 0.0121 | 0.1242 | 0.0028 | 0.0321 |
| L4 1.55-1.7 m | 9.1190 | 0.0273 | 0.0069 | 865.9000 | 0.0060 | 0.2458 | <0.001 | 0.0183 |
| L4 1.7-1.85 m | 19.0530 | 0.0345 | 0.1922 | 783.7500 | 0.0079 | 0.1782 | <0.001 | 0.0213 |
| L4 2.2-2.35 m | 7.3390 | 0.0118 | 0.0036 | 776.1000 | 0.0056 | 0.2335 | 0.0027 | 0.0173 |
| L4 2.35-2.5 m | | | | | | | | |
| L4 2.5-2.65 m | 16.8600 | 0.0651 | 0.2948 | 1177.0000 | 0.0098 | 0.1216 | <0.001 | 0.0275 |
| US-L5-P050 | 462.1700 | 0.6808 | 1.4880 | 3380.9973 | 0.0726 | ud | ud | 0.0535 |
| US-L5-P075 | 306.2508 | 0.8986 | 1.0329 | 2140.9444 | 0.0546 | ud | ud | 0.0631 |
| US-L5-P100 | 210.7385 | 0.9292 | 0.8367 | 1590.9287 | ud | ud | ud | 0.0541 |
| US-L5-P125 | 130.2379 | 0.4182 | 0.0953 | 1635.9322 | ud | ud | ud | 0.0351 |
| L5 0.95-1.1 m | 10.9800 | 0.0487 | 0.2684 | 922.8000 | 0.0064 | 0.1530 | <0.001 | 0.0216 |
| L5 1.1-1.25 m | 9.1520 | 0.0463 | 0.0457 | 870.7000 | 0.0067 | 0.2055 | 0.0015 | 0.0203 |
| L5 1.25-1.4 m | 14.7000 | 0.0659 | 0.0269 | 1062.0000 | 0.0064 | 0.1876 | <0.001 | 0.0241 |
| L5 2.25-2.4 m | 7.7630 | 0.0343 | 0.0469 | 800.5000 | 0.0073 | 0.1735 | 0.0011 | 0.0197 |
| L5 2.4-2.55 m | 7.8960 | 0.0312 | 0.0280 | 787.2000 | 0.0091 | 0.2023 | 0.0014 | 0.0188 |
| L5 2.55-2.7 m | 7.3390 | 0.0118 | 0.0036 | 776.1000 | 0.0056 | 0.2335 | 0.0027 | 0.0173 |
| US-L6-P150 | 65.6413 | 0.2584 | 0.1333 | 2778.7602 | ud | ud | ud | 0.0355 |
| US-L6-P175 | 49.6956 | 0.1307 | 0.1372 | 815.4228 | ud | ud | ud | 0.0379 |
| US-L6-P200 | 48.0654 | 0.4857 | 0.0945 | 1860.6867 | ud | ud | ud | 0.0282 |
| US-L6-P225 | 43.6146 | 0.8700 | 0.0979 | 1186.0284 | ud | ud | ud | 0.0235 |
| US-L6-P250 | 36.6372 | 1.1952 | ud | 817.8648 | ud | ud | ud | 0.0138 |
| US-L6-P275 | 25.7481 | 2.4555 | ud | 828.8528 | ud | ud | ud | 0.0155 |
| US-L6-P300 | 7.7466 | 1.8423 | ud | 865.2072 | ud | ud | ud | 0.0214 |
| US-L6-P300C | 7.5572 | 1.2521 | ud | 1051.1560 | ud | ud | ud | 0.0205 |
| L6 0.4-0.55 m | 16.8600 | 0.0651 | 0.2948 | 1177.0000 | 0.0098 | 0.1216 | <0.001 | 0.0275 |
| L6 0.55-0.7 m | 10.9800 | 0.0487 | 0.2684 | 922.8000 | 0.0064 | 0.1530 | <0.001 | 0.0216 |
| L6 0.7-0.85 m | 9.1520 | 0.0463 | 0.0457 | 870.7000 | 0.0067 | 0.2055 | 0.0015 | 0.0203 |
| L6 0.85-1.0 m | 14.7000 | 0.0659 | 0.0269 | 1062.0000 | 0.0064 | 0.1876 | <0.001 | 0.0241 |

| Sample ID | Trace Elements by ICP-MS (mg $L^{-1}$) | | | | | | | |
|---|---|---|---|---|---|---|---|---|
| | Mg | Mn | Mo | Na | Ni | P | Pb | Rb |
| L6 1.0-1.15 m | 7.7630 | 0.0343 | 0.0469 | 800.5000 | 0.0073 | 0.1735 | 0.0011 | 0.0197 |
| L6 1.15-1.3 m | 7.8960 | 0.0312 | 0.0280 | 787.2000 | 0.0091 | 0.2023 | 0.0014 | 0.0188 |

Table B-5 continued.

| Sample ID | Trace Elements by ICP-MS (mg $L^{-1}$) | | | | | | | |
|---|---|---|---|---|---|---|---|---|
| | Sb | Se | Si | Sn | Sr | Th | Ti | Tl |
| US-L1-P175 | ud | 0.0245 | ud | ud | 4.9753 | ud | ud | ud |
| US-L1-P200 | ud | 0.0199 | ud | ud | 4.0766 | ud | ud | ud |
| US-L1-P225 | ud | 0.0093 | ud | ud | 3.2670 | ud | ud | ud |
| L1 1.65-1.8 m | 0.0014 | <0.004 | 2.7770 | <0.0003 | 4.9720 | <0.004 | <0.1 | <0.0007 |
| L1 1.8-1.95 m | 0.0005 | <0.004 | 3.1680 | <0.0003 | 3.2700 | <0.004 | <0.1 | <0.0007 |
| L1 2.25-2.4 m | 0.0021 | 0.0049 | 2.5380 | <0.0003 | 2.1850 | <0.004 | <0.1 | <0.0007 |
| L1 2.4-2.55 m | 0.0005 | <0.004 | 3.2100 | <0.0003 | 0.4995 | <0.004 | <0.1 | <0.0007 |
| L1 2.55-2.7 m | 0.0034 | <0.004 | 3.2910 | <0.0003 | 0.5291 | <0.004 | <0.1 | <0.0007 |
| L2 0.95-1.15 m | 0.0015 | <0.004 | 2.6590 | <0.0003 | 3.4320 | <0.004 | <0.1 | <0.0007 |
| L2 1.15-1.35 m | 0.0014 | <0.004 | 3.4835 | <0.0003 | 0.6174 | <0.004 | <0.1 | <0.0007 |
| L2 1.35-1.5 m | 0.0042 | <0.004 | 2.8825 | <0.0003 | 0.7697 | <0.004 | <0.1 | <0.0007 |
| L2 2.15-2.3 m | 0.0013 | <0.004 | 3.0290 | <0.0003 | 0.5012 | <0.004 | <0.1 | <0.0007 |
| L2 2.3-2.45 m | 0.0011 | <0.004 | 3.6230 | <0.0003 | 0.4951 | <0.004 | <0.1 | <0.0007 |
| L2 2.45-2.6 m | 0.0009 | <0.004 | 3.4585 | <0.0003 | 0.5718 | <0.004 | <0.1 | <0.0007 |
| L3 0.15-0.3 m | 0.0074 | <0.004 | 1.7420 | <0.0003 | 1.9200 | <0.004 | <0.1 | <0.0007 |
| L3 0.3-0.45 m | 0.0030 | <0.004 | 3.6070 | <0.0003 | 0.7060 | <0.004 | <0.1 | <0.0007 |
| L3 0.45-0.6 m | 0.0031 | <0.004 | 3.5950 | <0.0003 | 0.6848 | <0.004 | <0.1 | <0.0007 |
| L3 0.9-1.05 m | 0.0046 | <0.004 | 2.7710 | <0.0003 | 0.7833 | <0.004 | <0.1 | <0.0007 |
| L3 1.05-1.2 m | 0.0067 | <0.004 | 2.8810 | <0.0003 | 0.9090 | <0.004 | <0.1 | <0.0007 |
| L3 1.2-1.35 m | 0.0064 | <0.004 | 3.0950 | <0.0003 | 0.8295 | <0.004 | <0.1 | <0.0007 |
| US-L3-P300 | ud | 0.0052 | ud | ud | 0.7401 | ud | ud | ud |
| US-L3-P300C | ud | 0.0171 | ud | ud | 1.2385 | ud | ud | ud |
| US-L4-P050 | ud | 0.0037 | ud | ud | 3.4714 | ud | ud | ud |
| US-L4-P075 | ud | 0.0036 | ud | ud | 3.0204 | ud | ud | ud |
| US-L4-P100 | ud | 0.0048 | ud | ud | 3.4828 | ud | ud | ud |
| US-L4-P125 | ud | 0.0093 | ud | ud | 3.8641 | ud | ud | ud |
| US-L4-P150 | ud | 0.0065 | ud | ud | 2.9236 | ud | ud | ud |
| US-L4-P175 | ud | 0.0035 | ud | ud | 2.4775 | ud | ud | ud |
| L4 1.4-1.55 m | 0.0046 | <0.004 | 2.7150 | <0.0003 | 1.6700 | <0.004 | <0.1 | <0.0007 |
| L4 1.55-1.7 m | 0.0015 | <0.004 | 3.3080 | <0.0003 | 0.5739 | <0.004 | <0.1 | <0.0007 |
| L4 1.7-1.85 m | 0.0019 | <0.004 | 2.5620 | <0.0003 | 0.8462 | <0.004 | <0.1 | <0.0007 |
| L4 2.2-2.35 m | 0.0007 | <0.004 | 3.1600 | <0.0003 | 0.4476 | <0.004 | <0.1 | <0.0007 |
| L4 2.35-2.5 m | | | | | | | | |
| L4 2.5-2.65 m | 0.0030 | <0.004 | 2.3260 | <0.0003 | 0.9971 | <0.004 | <0.1 | <0.0007 |
| US-L5-P050 | ud | 0.0525 | ud | ud | 10.5046 | ud | ud | ud |
| US-L5-P075 | ud | 0.0275 | ud | ud | 8.6534 | ud | ud | ud |
| US-L5-P100 | ud | 0.0080 | ud | ud | 5.8763 | ud | ud | ud |
| US-L5-P125 | ud | 0.0090 | ud | ud | 4.1732 | ud | ud | ud |
| L5 0.95-1.1 m | 0.0019 | <0.004 | 2.7790 | <0.0003 | 0.6668 | <0.004 | <0.1 | <0.0007 |
| L5 1.1-1.25 m | 0.0017 | <0.004 | 3.2880 | <0.0003 | 0.5280 | <0.004 | <0.1 | <0.0007 |

| Sample ID | Trace Elements by ICP-MS (mg $L^{-1}$) | | | | | | | |
|---|---|---|---|---|---|---|---|---|
| | Sb | Se | Si | Sn | Sr | Th | Ti | Tl |
| L5 1.25-1.4 m | 0.0012 | <0.004 | 3.3780 | <0.0003 | 0.8819 | <0.004 | <0.1 | <0.0007 |
| L5 2.25-2.4 m | 0.0026 | <0.004 | 2.8700 | <0.0003 | 0.4162 | <0.004 | <0.1 | <0.0007 |
| L5 2.4-2.55 m | 0.0051 | <0.004 | 3.3150 | <0.0003 | 0.4493 | <0.004 | <0.1 | <0.0007 |
| L5 2.55-2.7 m | 0.0007 | <0.004 | 3.1600 | <0.0003 | 0.4476 | <0.004 | <0.1 | <0.0007 |
| US-L6-P150 | ud | 0.0138 | ud | ud | 2.6855 | ud | ud | ud |
| US-L6-P175 | ud | 0.0116 | ud | ud | 1.9155 | ud | ud | ud |
| US-L6-P200 | ud | 0.0097 | ud | ud | 1.6657 | ud | ud | ud |
| US-L6-P225 | ud | 0.0069 | ud | ud | 2.0450 | ud | ud | ud |
| US-L6-P250 | ud | 0.0031 | ud | ud | 1.8247 | ud | ud | ud |
| US-L6-P275 | ud | 0.0017 | ud | ud | 1.2409 | ud | ud | ud |
| US-L6-P300 | ud | 0.0022 | ud | ud | 0.4315 | ud | ud | ud |
| US-L6-P300C | ud | ud | ud | ud | 0.3963 | ud | ud | ud |
| L6 0.4-0.55 m | 0.0030 | <0.004 | 2.3260 | <0.0003 | 0.9971 | <0.004 | <0.1 | <0.0007 |
| L6 0.55-0.7 m | 0.0019 | <0.004 | 2.7790 | <0.0003 | 0.6668 | <0.004 | <0.1 | <0.0007 |
| L6 0.7-0.85 m | 0.0017 | <0.004 | 3.2880 | <0.0003 | 0.5280 | <0.004 | <0.1 | <0.0007 |
| L6 0.85-1.0 m | 0.0012 | <0.004 | 3.3780 | <0.0003 | 0.8819 | <0.004 | <0.1 | <0.0007 |
| L6 1.0-1.15 m | 0.0026 | <0.004 | 2.8700 | <0.0003 | 0.4162 | <0.004 | <0.1 | <0.0007 |
| L6 1.15-1.3 m | 0.0051 | <0.004 | 3.3150 | <0.0003 | 0.4493 | <0.004 | <0.1 | <0.0007 |

Table B-5 continued.

| Sample ID | Trace Elements by ICP-MS (mg $L^{-1}$) | | | | | |
|---|---|---|---|---|---|---|
| | U | V | W | Y | Zn | Zr |
| US-L1-P175 | ud | 1.0562 | ud | ud | ud | ud |
| US-L1-P200 | 0.0112 | 0.6127 | ud | ud | ud | ud |
| US-L1-P225 | ud | 0.2975 | ud | ud | ud | ud |
| L1 1.65-1.8 m | 0.0036 | 0.2281 | 0.0012 | 0.0003 | <0.008 | 0.0049 |
| L1 1.8-1.95 m | 0.0036 | 0.0351 | 0.0060 | 0.0004 | <0.008 | 0.0076 |
| L1 2.25-2.4 m | 0.0086 | 0.2453 | 0.0051 | 0.0005 | <0.008 | 0.0062 |
| L1 2.4-2.55 m | <0.002 | 0.0150 | 0.0017 | 0.0004 | <0.008 | 0.0155 |
| L1 2.55-2.7 m | <0.002 | 0.0063 | 0.0024 | 0.0005 | <0.008 | 0.0237 |
| L2 0.95-1.15 m | 0.0041 | 0.3638 | 0.0030 | 0.0004 | 0.0173 | 0.0131 |
| L2 1.15-1.35 m | 0.0045 | 0.0262 | 0.0026 | 0.0005 | <0.008 | 0.0162 |
| L2 1.35-1.5 m | 0.0029 | 0.2385 | 0.0021 | 0.0004 | <0.008 | 0.0153 |
| L2 2.15-2.3 m | 0.0029 | 0.0185 | 0.0019 | 0.0006 | <0.008 | 0.0164 |
| L2 2.3-2.45 m | 0.0028 | 0.0181 | 0.0022 | 0.0004 | <0.008 | 0.0173 |
| L2 2.45-2.6 m | 0.0036 | 0.0205 | 0.0020 | 0.0005 | <0.008 | 0.0176 |
| L3 0.15-0.3 m | 0.0181 | 0.0246 | 0.0108 | 0.0002 | <0.008 | 0.0109 |
| L3 0.3-0.45 m | 0.0036 | 0.0216 | 0.0021 | 0.0003 | <0.008 | 0.0146 |
| L3 0.45-0.6 m | 0.0055 | 0.0378 | 0.0024 | 0.0003 | <0.008 | 0.0182 |
| L3 0.9-1.05 m | 0.0107 | 0.0340 | 0.0032 | 0.0004 | <0.008 | 0.0216 |
| L3 1.05-1.2 m | 0.0120 | 0.0190 | 0.0013 | 0.0002 | 0.0082 | 0.0268 |
| L3 1.2-1.35 m | 0.0107 | 0.0266 | 0.0016 | 0.0003 | <0.008 | 0.0250 |
| US-L3-P300 | ud | ud | ud | ud | ud | ud |
| US-L3-P300C | 0.0116 | ud | ud | ud | ud | ud |
| US-L4-P050 | ud | ud | ud | ud | ud | ud |
| US-L4-P075 | ud | ud | ud | ud | ud | ud |

| Sample ID | Trace Elements by ICP-MS (mg $L^{-1}$) | | | | | |
|---|---|---|---|---|---|---|
| | U | V | W | Y | Zn | Zr |
| US-L4-P100 | ud | 0.4692 | ud | ud | ud | ud |
| US-L4-P125 | ud | 0.6912 | ud | ud | ud | ud |
| US-L4-P150 | ud | 0.5182 | ud | ud | ud | ud |
| US-L4-P175 | ud | 0.0637 | ud | ud | ud | ud |
| L4 1.4-1.55 m | 0.0045 | 0.2622 | 0.0024 | 0.0005 | 0.0359 | 0.0083 |
| L4 1.55-1.7 m | <0.002 | 0.0095 | 0.0017 | 0.0006 | 0.0213 | 0.0200 |
| L4 1.7-1.85 m | 0.0053 | 0.1394 | 0.0053 | 0.0005 | 0.0147 | 0.0126 |
| L4 2.2-2.35 m | <0.002 | 0.0133 | 0.0031 | 0.0005 | 0.0093 | 0.0190 |
| L4 2.35-2.5 m | | | | | | |
| L4 2.5-2.65 m | 0.0055 | 0.0181 | 0.0048 | 0.0004 | 0.0096 | 0.0120 |
| US-L5-P050 | ud | 0.1160 | ud | ud | ud | ud |
| US-L5-P075 | ud | 0.2474 | ud | ud | ud | ud |
| US-L5-P100 | ud | 0.1402 | ud | ud | ud | ud |
| US-L5-P125 | ud | ud | ud | ud | ud | ud |
| L5 0.95-1.1 m | 0.0038 | 0.0262 | 0.0038 | 0.0004 | 0.0099 | 0.0125 |
| L5 1.1-1.25 m | 0.0023 | 0.0198 | 0.0031 | 0.0005 | 0.0178 | 0.0125 |
| L5 1.25-1.4 m | 0.0024 | 0.0178 | 0.0022 | 0.0004 | <0.008 | 0.0131 |
| L5 2.25-2.4 m | 0.0055 | 0.0353 | 0.0026 | 0.0004 | 0.0271 | 0.0162 |
| L5 2.4-2.55 m | 0.0031 | 0.0219 | 0.0021 | 0.0005 | 0.0130 | 0.0166 |
| L5 2.55-2.7 m | <0.002 | 0.0133 | 0.0031 | 0.0005 | 0.0093 | 0.0190 |
| US-L6-P150 | ud | ud | ud | ud | ud | ud |
| US-L6-P175 | ud | ud | 0.0425 | ud | ud | ud |
| US-L6-P200 | ud | ud | 0.0312 | ud | ud | ud |
| US-L6-P225 | ud | ud | ud | ud | ud | ud |
| US-L6-P250 | 0.0136 | ud | ud | ud | ud | ud |
| US-L6-P275 | 0.0105 | ud | ud | ud | ud | ud |
| US-L6-P300 | ud | ud | ud | ud | ud | ud |
| US-L6-P300C | ud | ud | ud | ud | ud | ud |
| L6 0.4-0.55 m | 0.0055 | 0.0181 | 0.0048 | 0.0004 | 0.0096 | 0.0120 |
| L6 0.55-0.7 m | 0.0038 | 0.0262 | 0.0038 | 0.0004 | 0.0099 | 0.0125 |
| L6 0.7-0.85 m | 0.0023 | 0.0198 | 0.0031 | 0.0005 | 0.0178 | 0.0125 |
| L6 0.85-1.0 m | 0.0024 | 0.0178 | 0.0022 | 0.0004 | <0.008 | 0.0131 |
| L6 1.0-1.15 m | 0.0055 | 0.0353 | 0.0026 | 0.0004 | 0.0271 | 0.0162 |
| L6 1.15-1.3 m | 0.0031 | 0.0219 | 0.0021 | 0.0005 | 0.0130 | 0.0166 |

## APPENDIX C GEOLOGICAL SETTING

Table C-1: Generalized stratigraphy in the Athabasca Oil Sands Region (adapted from Carrigy, 1959; McPherson and Kathol, 1977).

| Age | Group | Formation | Member | Lithology |
|---|---|---|---|---|
| Pliestocene, Recent | | | | Till, sand, silt and gravel surficial deposits |
| Erosional Unconformity | | | | |
| Cretaceous | Colorado | La Biche<br>Pelican<br>Joli Fou | | Shale and sandstone |
| | Mannville | Grand Rapids | | Lithic sands and sandstones |
| | | Clearwater | | Shale and sandstone |
| | | | Wabiskaw | Glauconitic sandstone |
| | | McMurray | | Fine- to coarse-grained sand with heavy oil |
| Erosional Unconformity | | | | |
| Devonian | Woodbend | Grosmont<br>Ireton<br>Duvernay<br>Cooking Lake | | Limestone |
| | Beaverhill Lake | Waterways | Mildred<br>Moberly<br>Christina<br>Calumet<br>Firebag | Argillaceous and clastic limestones |
| | Paraconformity | | | |
| | | Slave Point | | Limestone and dolomite |
| | Paraconformity | | | |
| | | Dawson Bay | | Siltstone interbedded by dolomite and anhydrite |
| | Elk Point | Prairie Evaporite | | Halite, anhydrite, gypsum and dolomite |
| | | Methy | | Limestone and dolomite |
| | | McLean | | Dolomite, claystone and evaporite |
| | | LaLoche | | Claystone and arkosic sandstone |
| Erosional Unconformity | | | | |
| Precambrian | | | | Metasedimentary rocks and granite |